Design and Testing of a Linearly Actuated Pulsatile Pump for Ventricular Assist

A Dissertation

Presented to

the Faculty of the Department of Mechanical Engineering

University of Houston

In Partial Fulfillment

of the Requirements for the Degree

Doctor of Philosophy

in Mechanical Engineering

by

Holley Carole Love

May 2013

Design and Testing of a Linearly Actuated Pulsatile Pump for Ventricular Assist

Holley Love

Approved:

Committee Chairman
Stanley Kleis, Associate Professor
Mechanical Engineering

Committee Members:

William Cohn, Associate Professor
Baylor College of Medicine

Dong Liu, Assistant Professor
Mechanical Engineering

Ralph Metcalfe, Professor
Mechanical and Biomedical Engineering
and Mathematics

Keh-Han Wang, Professor
Civil and Environmental Engineering

Suresh Khator, Associate Dean,
Cullen College of Engineering

Pradeep Sharma, Professor and Chair
Mechanical Engineering

ACKNOWLEDGEMENTS

I give my deepest thanks to Dr. Stan Kleis. I can never thank him enough for guiding me these last seven years. His infinite patience and unwavering, realistic encouragement kept me moving forward, despite my own insecurities and hesitations. I could not have accomplished this work without him. His mentoring has extended far beyond academics, and I feel truly lucky to have been part of his lab family. I wish him the best as he begins to enjoy his retirement!

Special thanks must also be given to Dr. Billy Cohn for sharing the secret of the LAPP with us and for helping us to bring it to life. Thanks also to Dr. Ralph Metcalfe for introducing me to the Texas Heart Institute and for all the interesting discussions and digressions at our meetings. I look forward to continuing my affiliation with Drs. Kleis, Cohn, and Metcalfe as we continue to develop the LAPP.

I would be remiss not to acknowledge the dedicated research team in the THI Cardiovascular Research Labs, especially Jeff Conger. We could not have completed our hemolysis studies without his insights and ideas. Thanks also to Manuel Hurtado, Aaron Palmer, and Nathan Taylor for their assistance during the studies. Though he was not involved with this project, I must thank Jesse Rios for his encouragement and interesting discussions, as well as providing the aortic casting photographed in this document. Sharon Williams, Dawn Thomas, and Kim Hubbard have been indispensible for their help with scheduling, purchasing, and support at the Texas Heart Institute.

At the University of Houston, I owe great thanks to Trina Johnson for her help in keeping up with all of the details of my graduate career from start to finish. Her empathy, kindness, and support brightened my time here. Thanks to Tammy Engelbosch and Emily Marin for their support and for making sure I got paid! Thanks to the faculty involved in the GK12 program—Drs. Chiappetta, Claydon, Long, Sharma, and Rifai—for giving me an opportunity to venture into secondary science education. Dr. Fritz Claydon, in particular, has long been a mentor and

champion of mine, and I give him many thanks for his encouragement. Thanks also to Janice Quiroz for her support and conversations from CougarPaw and beyond. I thank Gene Webster for his support and electronic supplies and Dr. Matt Franchek for accepting me in the inaugural biomedical engineering undergraduate class. I would like to acknowledge the encouragement of Drs. Amina Qutub and Byron Long at Rice University.

Thanks also to Drs. Dong Liu and Keh-Han Wang for their comments on the manuscript and service on the defense committee. I also thank Irene Abercrombie for her diligence in refining the formatting and grammar of this final document.

I must thank my friends—especially Wasy Akhtar, Sandra Moore, Monica Ortega, Krutina Patel, Aritra Sur, and Leyuan Yu—for their belief and unwavering support. The lengths they went through to get me through this long educational process leave me touched and lucky to have such great friends. I appreciate them letting me borrow their families when mine were far away.

Lastly and most importantly, I give my heartfelt thanks to my family, above all my parents. My parents have loved and encouraged and supported me even before I was born. They have been with me every step of my journey, and I hope that I have been able to make them proud. With love and best wishes, I present the following document.

Design and Testing of a Linearly Actuated Pulsatile Pump for Ventricular Assist

An Abstract

of a

Dissertation

Presented to

the Faculty of the Department of Mechanical Engineering

at the University of Houston

In Partial Fulfillment

of the Requirements for the Degree

Doctor of Philosophy

in Mechanical Engineering

by

Holley Carole Love

May 2013

ABSTRACT

The prevalence of heart failure around the world has led clinicians and engineers to develop mechanical circulatory support systems. Most heart assist technology today is classified as continuous flow because blood is pumped in a steady stream. Though well tolerated in general, some patients experience complications that appear to stem from the loss of pulsation. To investigate the role of pulsatility, a linearly actuated pulsatile pump (LAPP) has been designed. Unlike early pulsatile devices that lacked robustness, the LAPP has a single translating part plus two prosthetic valves. To aid in the design process, numerical models were developed using the commercial software packages COMSOL and FLUENT. Bench-top testing loops were also developed. The LAPP has been shown to be capable of providing pulsatile flow at physiologically relevant pressures, and preliminary studies have been conducted to assess its damage to blood. A major outstanding concern is the excessive heat generation requiring external cooling in the present prototype. Despite the heating, the LAPP has potential to become a clinical research tool for studying pulsatility, if not as an approved ventricular assist device.

TABLE OF CONTENTS

ACKNOWLEDGEMENTS v

ABSTRACT viii

TABLE OF CONTENTS ix

LIST OF FIGURES xii

LIST OF TABLES 1

CHAPTER 1: Overview 2

Heart Failure Causes and Treatments 2

Ventricular Assist Devices 5

LAPP Overview 7

Operating Principle 8

Advantages/Disadvantages 9

Current Level of Development 10

CHAPTER 2: LAPP Models 11

Model Development 11

Bench-Top Models 13

Mock Circulatory Loop 13

Hemolysis Testing Loop 21

COMSOL Model 24

Finite Element Method 25

Model Set-up 25

FLUENT Model 33

Finite Volume Method 33

Model Set-up 34

CHAPTER 3: Model Verification 43
Flow Loops 43
Mock Circulatory Loop 43
Hemolysis Testing Loop 46
FLUENT Model 49
Time Step Convergence 50
Mesh Convergence 52
Pressure Comparison 54
COMSOL Model 56
Magnet Comparison 56
Force Comparison 57
Time Step Convergence 64
Mesh Convergence 66
CHAPTER 4: Numerical Results and Discussion 69
Fluid Mechanics and Heat Transfer 69
Gap Estimation 69
Shape of Shuttle 70
Heating 71
Electromagnetics 76
Full COMSOL Model 76
Back EMF Estimation 79
High Permeability Shielding 82
CHAPTER 5: Hemolysis Testing 85
CHAPTER 6: Future Work and Conclusions 93
Linearly Actuated Pulsatile Pump 93
Mock Circulatory Loop 94

Hemolysis Testing Loop 95
FLEUNT Model 95
COMSOL Model 96
Conclusion 96
REFERENCES 97
APPENDIX 99

LIST OF FIGURES

Figure 1: Schematic of LAPP ejecting blood (a) and resetting to start a new cycle (b) 8

Figure 2: Proof-of-concept LAPP 9

Figure 3: Schematic of the Mock Circulatory Loop 14

Figure 4: (a) Close-up view of the LDV measurement section and (b) an overview of the LDV measurement system 15

Figure 5: (a) Close-Up view of the mock ventricle with no liquid in the optical corrector and (b) side-view of the mock ventricle with appropriately filled optical corrector (note: a Jarvik 2000 is inserted at the apex rather than the LAPP) 16

Figure 6: Close-up picture of valves, connective tubing, and balloon attachment. Aortic compliance chamber removed for clarity 16

Figure 7: Actuator-piston assembly 17

Figure 8: Aortic compliance chamber 18

Figure 9: (a) Photos of the LAPP showing windings, PVC spacer rings, and titanium tube and (b) the LAPP with protective coverings and attached to the loop 19

Figure 10: (a) Mock loop overview and (b) a close-up of the resistance and compliance elements 20

Figure 11: LabView VI front panel 21

Figure 12: (a) ASTM recommended loop and (b) modified Hemolysis Testing Loop 23

Figure 13: Physics modules available in COMSOL 26

Figure 14: Typical LAPP geometry in COMSOL 29

Figure 15: Final model tree 32

Figure 16: LAPP geometry in Gambit/FLUENT 34

Figure 17: Boundary and Continuum Type dialogue boxes 36

Figure 18: FLEUNT main window 37

Figure 19: Solver window 38

Figure 20: Dynamic Mesh Model window 39

Figure 21: Dynamic Mesh Zones window 40

Figure 22: (a) Ventricular and aortic pressure in the Mock Circulatory Loop and (b) a normal human 44

Figure 23: Addition of aortic compliance reduces ventricular pressure spikes 45

Figure 24: Compliance reduces pressure variation in hemolysis testing loop 47

Figure 25: Compliance chambers (first hemolysis test configuration) and pressure infusion bag 47

Figure 26: Comparison of hemolysis loop and healthy human pressure levels 48

Figure 27: Multiple cycles of the LAPP pressure rise overlaid 49

Figure 28: FLUENT data appears independent of time step size 51

Figure 29: Meshes used in FLUENT grid convergence study 52

Figure 30: FLUENT data appears to be independent of grid spacing 53

Figure 31: Comparison of aortic pressure in FLUENT and the Mock Circulatory Loop 55

Figure 32: axial (a) and radial (b) magnetic flux density fields from Hall probe 57

Figure 33: axial (a) and radial (b) magnetic flux density fields from COMSOL 57

Figure 34: (a) a shuttle is attached to an actuator, while (b) the LAPP is coupled to a cantilever beam 59

Figure 35: Axial force for several shuttle positions 60

Figure 36: Comparison of the COMSOL model force and the experimental data 61

Figure 37: The offset parameter controls the peak force timing in the COMSOL model 63

Figure 38: After a few time steps, the shuttle comes to an equilibrium position 64

Figure 39: COMSOL data appears independent of time step size 65

Figure 40: Three computational meshes used to check for grid independence 66

Figure 41: COMSOL data appears to be independent of grid spacing 68

Figure 42: Photographs of the prototype shuttle (a) before and (b) after assembly 71

Figure 43: Temperatures increase in time on the titanium surface 72

Figure 44: Temperature rise comparison for old and new LAPP geometries and currents 74

Figure 45: Contours of static temperature at 46.75 *sec* 75

Figure 46: The square of the current is higher overall in the odd windings 75

Figure 47: Shuttle position and velocity computed by COMSOL 77

Figure 48: Forces in the COMSOL model with Moving Mesh 77

Figure 49: Specially made shuttle is attached to the linear actuator to gather EMF data 79

Figure 50: Schematic illustrating the LAPP winding diagram 80

Figure 51: Comparison of EMF vs time (a) and vs velocity (b) for COMSOL simulated and experimental data 81

Figure 52: Addition of shielding can increase the shuttle force 83

Figure 53: μ-metal causes the magnetic flux density to be flattened into the radial direction (note arrows) 84

Figure 54: Flowloop and MIH data for the mechanically actuated LAPP 88

Figure 55: Blood is cyclically squeezed between the silicone tubing and the PVC framework ... 88

Figure 56: Flowloop and MIH data for the HeartMate-IP 89

Figure 57: Flow loop and MIH data for the first electrically actuated LAPP 90

Figure 58: Flow loop and MIH data for the second electrically actuated LAPP 91

Figure 59: Two views of a cast of the aortic root showing the cusps and coronary arteries 95

LIST OF TABLES

Table 1: Items specified in ASTM Standard F1841-97 (2005)..... 23

Table 2: FLUENT Mesh Statistics..... 52

Table 3: COMSOL Mesh Statistics 67

CHAPTER 1: Overview

Based on American Heart Association data from 2009, cardiovascular disease (CVD) was accountable for roughly one in three deaths in the United States (Go et al., 2013). Even more sobering, more than 2150 Americans die from CVD each day (ibid). CVD accounts for more healthcare cost than any other diagnostic group. Specifically, the estimated total direct and indirect cost of cardiovascular disease and stroke in the United States for 2009 was $312.6 billion, compared to the $228 billion estimated cost of cancer and benign neoplasms (tissue masses caused by abnormal cell growth) in 2008 (ibid). Out of the larger group of patients with CVD, an estimated 5.1 million adults are classified as being in heart failure.

Heart Failure Causes and Treatments

Conceptual models describing heart failure have evolved dramatically in the past half century. What was once believed to be a fluid build-up from improper flow through the kidneys, congestive heart failure has proved to be a more complicated problem (Bozkurt and Mann, 2013). The aforementioned "cardiorenal model" was revised and amended when evidence was gathered that the diuretics being used to reduce the perceived water retention did not in fact alter the progression of heart failure (ibid). Next it was proposed that high peripheral vascular resistance led to changes in the heart's output capabilities that eventually led to heart failure. Drugs that alter the muscular contractility of the heart and relax the vascular tone (inotropes and vasodilators, respectively) were able to increase cardiac output but could not alter the disease progression; thus the "cardiocirculatory model" was retired (ibid). Additional research linked the over-expression of certain biologically derived molecules to damage in the heart and vascular system. This "neurohormonal model" has had some success facilitating the design of drugs that promote the remodeling of failing hearts. However, it does not yet fully explain or predict the observed disease progression. The newest model—the "biomechanical model"—builds upon the

neurohormonal model by focusing treatments on redressing the *consequences* of neurohormonal activation and interrupting ventricular remodeling and heart muscle cell dysfunction (ibid).

Though the details differ from one case to another and the underlying mechanisms remain elusive, the progression toward end-stage heart failure can be viewed as an iterative spiral because of the interaction of several "pathophysiological derangements" (Renlund and Kfoury, 2006). An initial insult to the heart muscle, such as hormonal or pharmaceutical stimulation or possibly oxygen or nutrient deprivation, triggers myocardial dysfunction. The dysfunction alters the chemical signals released from the cells, leading to apoptosis, chemical cascades, and altered gene expression, which act to further insult the myocardium and exacerbate dysfunction. The abnormal cellular responses cause adverse ventricular "remodeling" wherein the healthy left ventricle geometry is transformed from a tight ellipsoid to an enlarged, thin-walled sphere. Since the heart muscle cells have become less capable of strong contractions, the ventricle must grow in size to achieve a comparable ejection fraction. Additionally, the patient may become intolerant to previously beneficial medications. Eventually, functionality decreases until the heart is no longer able to meet a patient's minimal blood flow requirements, and a transplant may be warranted.

For many patients, diet and exercise changes are sufficient to check the progression of cardiovascular disease. When these are not, doctors begin prescribing pharmaceuticals. Unfortunately, as with all medications, side effects, increased dosage tolerance, and patient noncompliance hinder the medications' effectiveness. As a patient progresses through the spiral of heart failure, additional treatments options are explored, namely, transplantation and mechanical circulatory support (Hunt et al., 2001).

Since the first heart transplantations in December 1967, the survival rates have increased steadily, if slowly. As of 2009, the projected half-life for heart transplant is eleven years (Taylor et al., 2009), meaning that fifty percent of patients will live at least this long after transplantation. Surprisingly, since 1982, the largest improvement in patient survival occurs during the first six

months post-transplantation, after which time, the survival curves drop linearly at roughly the same slope (ibid); this slope is steeper than that for the "normal" healthy population.

The annual number of heart transplants performed in North America has stayed between 2000 and 2500 from 1990 through 2007, despite an ever increasing demand for donor hearts and improvement in transplant outcome (Taylor et al., 2009). Some attribute the stagnation in the United States (and marked decline in Europe) of heart availability to the reduction in traumatic deaths in young persons (Birks, 2010), largely due to increased highway safety regulations—mandatory helmet and seatbelt laws, in addition to improved vehicle crash response.

Even if a donor heart is made available, the recipient must still face issues related to organ rejection, such as a lifetime of immune suppression and the worry that their new heart will become diseased as well (Taylor et al., 2009). Depending on what other complications may be present, a patient may not even be eligible to be placed on the waiting list. In response to these issues, clinicians and engineers have turned to mechanical circulatory support systems to improve the quality of life for greater numbers of individuals.

Over the last forty years, considerable progress has been made toward finding a viable alternative to transplantation. A mechanical circulatory support device of sorts was introduced by Gibbon in 1953—it was a cardiopulmonary bypass machine for use during cardiac surgery to reduce chances of pulmonary embolism (Baughman and Jarcho, 2007). The first true mechanical support device to assist the pumping action of the heart was the intra-aortic balloon pump developed by Moulopoulos in 1963 (Helman and Rose, 2000). Akutsu and Kolff reported the first total artificial heart success in a dog in 1958; the animal was supported for about 90 minutes (Helman and Rose, 2000). It was not until 1969 that Cooley began to use the total artificial heart as a bridge to transplantation (Helman and Rose, 2000). As computer technology, manufacturing processes, biological understanding, and fluid mechanical knowledge have improved, the size of circulatory support devices has decreased while their biocompatibility and reliability have increased.

One of the most promising avenues of mechanical support is a range of pumps broadly classified as "left ventricle assist devices" or LVADs. It was DeBakey who was one of the earliest champions of the LVAD. Since the National Heart Lung and Blood Institute began calling for proposals to develop LVADs in 1977 and 1980, numerous types of pumps have become available for research use and several have FDA approval as “bridge-to-transplant” devices while patients await donor hearts (Helman and Rose, 2000). The duration of patient support with these devices continues to increase. In fact, on January 20th of 2010, the FDA granted approved for the HeartMate II Left Ventricular Assist System to be used as a permanently implantable device—“destination therapy”—in patients not eligible for transplantation. The use of LVADs as destination therapy was not always (and to a lesser degree, still is not) embraced by all physicians. In an article published in 2008, Rizzieri et al. implore clinicians to thoroughly and clearly discuss quality of life and caregiver burden before implanting an LVAD as a permanent device (Rizzieri et al., 2008).

Generally, LVADs are connected at the apex, or base, of the left ventricle and act to remove some of the pumping load from the heart. Blood can either follow its natural path, flowing from ventricle to aorta through the aortic valve, or it can pass through the ventricle into the LVAD before being pumped directly into the ascending or descending aorta; the proportion of blood travelling through the aortic valve depends on the ventricle's native pulsatility and the flow setting of the LVAD. Because it handles most of the load, the left ventricle is typically in need of assistance during heart failure, but some right ventricular and bi ventricular assist pumps have been developed and successfully tested.

Ventricular Assist Devices

LVADs grew in popularity as the far more complicated total artificial hearts struggled in the mid-twentieth century. Early assist devices were pulsatile. Evolution has shaped the human heart to eject blood in discrete pulses, so it was natural for the first forays into VAD design to try and emulate the successes for the healthy native heart. These devices like the HeartMate-IP were

large and noisy but performed well over the short term, giving patients who would be bedridden or barely clinging to life the strength to move about the hospital and, in some cases to go home. Then, as now, pulsatile VADs are considered "volume displacement" pumps. A diaphragm driven by compressed air or a pusher-plate driven by cams/linkages moves back and forth within a rigid case pulling blood in and pushing it out. Prostheic valves—procine bioprosthetic trileaflet valves, in the case of the HeratMate-IP—are used at the pump inlet and exit to ensure unidirectional flow through the pump.

The large size of the pumps meant that the implantation operation was invasive and reserved almost exclusively for large males, as they had the required chest space. Nevertheless, research has continued on these devices, and the Thoratec XVE remains a popularly implanted (and FDA approved for destination therapy) device. Syncardia and AbioMed make pulsatile total artificial hearts that resemble a combination of two pulsatile VADs.

The greatest downfall of the pulsatile pumps, however, has been the fact that they tend to fail within twelve to eighteen months. The flexible diaphragms tend to rupture, or the delicate linkages driving the pusher plate break—a pump of this type is after all ejecting at least once per second for every minute of every day. In a year, the pump will have cycled more than 31,536,000 times, so it is not surprising that these pumps fail. A new paradigm was needed.

To borrow an analogy from Dr. W. E. Cohn, just as man's dreams of heavier-than-air flight did not take off until the development of the propeller and jet engine, the VAD did not come into its own until the development of the first continuous flow devices. Inspired by a trip to Egypt, Dr. R. K. Wampler adapted the ancient Archimedes screw into a small device for pumping blood. The idea of supplying blood to the body in a continuous stream was met with disbelief by most of the medical community at the time. Dr. O. H. Frazier encouraged the idea, however, and the first use of the pump as a peripheral arterial assist was published in 1988 (Wampler et al., 1988). Work continued from that early study, and today many companies are producing continuous flow assist devices in axial flow types (like the HeartMate II from Thoratec,

MicroMed from Debakey) and centrifugal flow types (like the Thoratec HeartWare). Advances in the technology continue: pumps are now made with one single moving part and the use of magnetic or hydrodynamic suspension has eliminated the bearings. Total artificial hearts are now being developed on the continuous flow platform.

As continuous flow devices are implanted in greater numbers and for longer durations, however, complications are being observed. Some patients develop gastrointestinal hemorrhages. Others develop aortic insufficiency (where the aortic valve does not close completely). As a patient's heart weakens, his pulse may no longer be palpable, so general physicians cannot easily monitor his blood pressure. Flow in the lymphatic system is driven by the pulsation of the arterial system, so some continuous flow LVAD patients develop edema, or fluid build-up in their extremities. The body has evolved under pulsatile conditions, and though continuous flow is well tolerated, questions about the physiological role of pulsatility remain.

LAPP Overview

Despite the progress and successes of existing commercialized mechanical assist devices, their designs have left room for improvement. Specifically, it seems there is merit in crafting a pump that blends the advantages of the continuous flow pumps' simplicity and robustness with the pulsatile pumps' discrete ejection volumes. Therefore, an entirely new device was created rather than trying to adapt an existing one.

The current design of the linearly actuated pulsatile pump (LAPP) was first conceived by Dr. William E. "Billy" Cohn during his general surgery residency at Baylor College of Medicine in the early 1990s. Patents on related devices were filed in the mid-1900s and early-2000s by several inventors. Many, if not all, of these devices could not have worked as described at the time due to the weakness of magnetic materials. With advances in rare earth magnets and prosthetic heart valves, the time seemed right to revisit the LAPP concept in hopes of developing a working prototype suitable for use as a research device and ultimately as a fully implantable heart assist pump.

Operating Principle

The LAPP generates flow by using a magnetically driven piston-like mechanism. A short plastic cylinder is fitted with a strong rare-earth magnet and a one-way valve—this assembly is refered to as a "shuttle." The shuttle is sized to fit inside a tube that has a second one-way valve fixed firmly at the LAPP inlet end. The shuttle valve and the fixed valve open in the same direction. A narrow gap between the outside of the shuttle and inside of the tube reduces friction and wear, but allows minimal leakage. The operation of the LAPP is shown schematically in Figure 1 below.

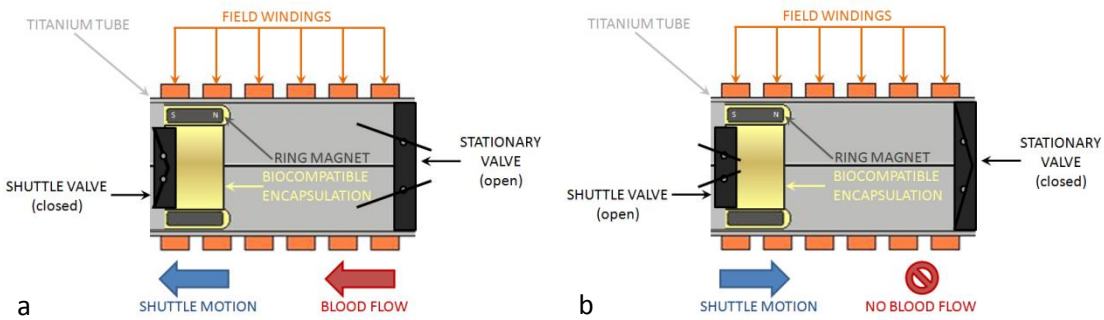

Figure 1: Schematic of LAPP ejecting blood (a) and resetting to start a new cycle (b)

When a magnetic field is applied along the axis on the outer surface of the tube, the shuttle inside will move axially to position itself within the magnetic field and be pushed toward or away from the fixed valve, depending on the motion of the external field. The field motion is achieved by varying the phase relationship of the applied current in the multiple sets of windings. The applied field spacing is such that the magnet is locked in a repulsive magnetic well, which (along with hydrodynamic lubrication) tends to keep the shuttle centered during its motion back and forth along the length of the tube. As the shuttle moves away from the fixed valve, the fixed valve will be open and the shuttle valve will close. Blood will be pushed down the tube. As the shuttle reaches its end of stroke, the fluid inertia will cause the shuttle valve to open and the flow to continue until the adverse pressure gradient causes the flow to decelerate to zero flow. During

this time, the shuttle will begin to return toward the fixed valve. When the flow begins to reverse, due to the high systemic pressure, the fixed valve will close (much like a normal aortic valve) and the blood between the fixed valve and shuttle will flow through the shuttle valve. As the shuttle reaches full withdrawal and begins to move away from the fixed valve, the shuttle valve closes while the fixed valve opens and the cycle begins again.

A photograph of an early proof-of-concept LAPP is shown in the figure below (Figure 2); the LAPP tube is made of clear plastic to show the shuttle and valves. Note that the external drive source has been removed. The design has been updated with a larger tube (now made of titanium) and shuttle, more powerful shuttle magnets, and external field windings to drive the shuttle motion. A single board computer and a microstepping Superior Electric Slo-Syn stepper motor driver are used to send step and direction signals to the windings, allowing fine control of the shuttle motion. A prototype LAPP has been constructed and operated in two flow loops to obtain pressure and flow data analogous to implantation in a heart failure patient and to compare blood damage done by the LAPP to that done by other VADs.

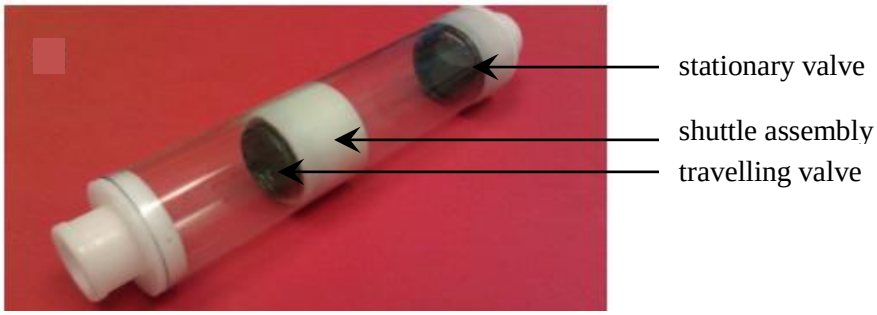

Figure 2: Proof-of-concept LAPP

Advantages/Disadvantages

Unlike the commercialized pulsatile pumps described above, the LAPP contains neither flexible membranes nor complex linkages, both of which have limited the life of other devices. By using "off-the-shelf" prosthetic valves and a single electro-hydrodynamically centered traveling shuttle, the LAPP's robustness could be comparable to continuous flow VADs. The

LAPP should, in fact, be more tolerant of circulating clots than continuous flow VADs. However, in order to develop physiological pressures and flows, the LAPP can produce a significant amount of resistive heating.

Current Level of Development

Currently, the LAPP has been advanced sufficiently to perform hemolysis testing, a way to verify that the pump is doing minimal damage to red blood cells. The remainder of this document describes the bench-top and numerical models developed to improve the LAPP's design. It includes the results of the hemolysis tests and concludes with a discussion of future studies to optimize performance.

Specifically, Chapter 2 describes in detail the various LAPP prototypes constructed, as well as the bench-top and numerical models used to characterize and refine the prototypes. The Mock Circulatory Loop was used to study the LAPP's pressure and flow relationship, while the Hemolysis Testing Loop was used to assess the blood cell damage caused by the pump. The numerical models constructed in the FLUENT and COMSOL modeling packages were used to predict heat transfer and electromagnetic interactions, respectively. Chapter 3 summarizes the verification of each of the models, including comparisons between experimental data and numerical predictions and grid and time-step independence checks.

Chapter 4 presents selected data from the numerical models. A discussion of the flow through the gap between the LAPP shuttle and titanium tube is provided, followed by brief remarks regarding the shape of the shuttle. The heat generated by the windings is explored. Additionally, the interaction of the winding current and shuttle magnets is explored. Results from four hemolysis tests are summarized in Chapter 5 before conclusions and some possibilities for future work are given in Chapter 6.

CHAPTER 2: LAPP Models

Because of the complexities of the problem, the design and refinement of the LAPP is best guided by both physical and numerical models. Each model can give results at different levels of detail—from bracketing a range of expected force outputs to capturing the time-varying inlet and outlet pressure levels. Also, the LAPP models can be used in a loose iterative loop, facilitating design improvement. For instance, the hand-operated proof-of-concept LAPP led to a version with large external magnets that could be moved by a linear actuator in a manner similar to the way the electrical windings would couple to the shuttle. As confidence increased that the LAPP could generate the necessary pressure and flow waveforms, numerical models were developed to aid in the winding and shuttle design. These numerical models were split into an electromagnetic (COMSOL) and fluid mechanic/heat transfer (FLUENT) portion to take advantage of the strengths of the packages available. Ultimately a pump was constructed with a shuttle and external field windings to begin hemolysis testing. What follows is a recounting of the model development and detailed descriptions of the finalized mock circulatory loop, hemolysis testing loop, COMSOL model, and FLUENT model.

Model Development

The short-comings of and open questions surrounding ventricular assist devices became apparent during the construction of a mock circulatory system to evaluate LVAD performance. Because of the relatively short lifetime of the early pulsatile pumps (roughly twelve to eighteen months), the field had turned to continuous flow devices. These devices, though far more mechanically robust, have been associated with pathologies not seen during pulsatile support. As discussed above, gastrointestinal bleeding, aortic insufficiency, and fluid build-up in the extremities (edema) seem to be associated with continuous flow support but not pulsatile support due to some as yet unknown mechanisms, though elevated fluid shearing is a likely component.

Further, some have posited that without some degree of cyclic blood pulses, regions of the vasculature may not be properly washed out, leading to thrombus or aneurysm formation.

This leads one to consider the possibilities of designing a new type of assist device. Once Dr. Cohn shared the LAPP concept drawings he created in the 1990s, it seemed to be one promising direction that had remained unexplored by previous innovators. A small proof-of-concept model was built from a Tenite™ tube and small prosthetic vales set in a Delrin™ shuttle. Using weak permanent magnets set in the shuttle and in an external Delrin™ slider, the pump could be actuated by hand. This model indicated that the concept was sound, that the pump could be self-priming, and that larger and stronger magnets were crucial to give the flows necessary to improve quality of life. It also suggested that there would be a need to balance the overall size with stroke length and frequency.

The next model was a larger Tenite™ one that could be run in a flow loop. A linear actuator attached to the external slider provided the moving magnetic field to operate the pump. Having a clear tube body was helpful in indentifying when the shuttle and slider would uncouple. The magnets still needed to be stronger. Also, having larger inner diameters on the tube and fittings attaching the pump to the flow loop would allow greater accelerations before decoupling; larger diameters would also reduce the stroke required to give a particular volume displacement.

Next, 28AWG enameled, solderable copper magnet wire was wound around a 1.33 inch (ID) titanium tube with the aid of a CNC milling machine. This LAPP has twelve windings of two hundred turns each that are driven ninety degrees out of phase from their neighbors by a stepper motor driver. Unfortunately, when sufficient current was applied to give the necessary force, the LAPP would overheat and the shuttle would seize in the tube.

Another titanium model was wound with larger diameter wire, with the thought that it would generate less heat and yield the same force. For this model, 22AWG magnet wire was used, but the anticipated gain in performance did not occur. At this point it became clear that

numerical modeling would be the most efficient way to determine the best combination of wire gauge, current, number of turns, etc. to give sufficient force.

While the numerical models were developed, the LAPP could be run in the mock circulatory loop with the addition of large, powerful magnets and a top-of-the-line linear motor to drive the LAPP mechanically as was done in the first prototypes. Pressure and flow data were gathered without uncoupling the shuttle and external magnets. A preliminary hemolysis test was also run with this LAPP.

After performing numerical studies in COMSOL, the 28AWG electrically actuated LAPP was revisited, this time with a magnet at both ends of the shuttle. Now the LAPP could be run in the hemolysis testing loop using a sine-wave motion profile. An air cooling jacket was added and hemolysis testing was performed.

Bench-Top Models

Two separate flow loops were developed to evaluate the LAPP's performance: one designed to mimic the pressure-flow relationship in a heart failure patient and one to quantify the amount of damage done to circulating red blood cells (hemolysis). The Mock Circulatory Loop, though capable of matching heart failure flow conditions is not appropriate for performing hemolysis testing. The volume of blood required, as well as the logistics of cleaning the system before and after testing, makes the Mock Circulatory Loop an impractical choice. A Hemolysis Testing Loop of simple geometry maximizing the use of disposable materials is ideal for tests involving blood.

Mock Circulatory Loop

The Mock Circulatory Loop is a five-element Windkessel model, meaning that the body's systemic resistance and compliance, the ventricular compliance, and the aortic inertance and compliance are each captured in discrete elements—a needle valve, glass bottle, balloon bladder, and length of flexible tubing, respectively. A schematic of the loop is included as Figure

3 below; each component will be discussed in detail below. A 35% glycerol solution is used as a blood analog.

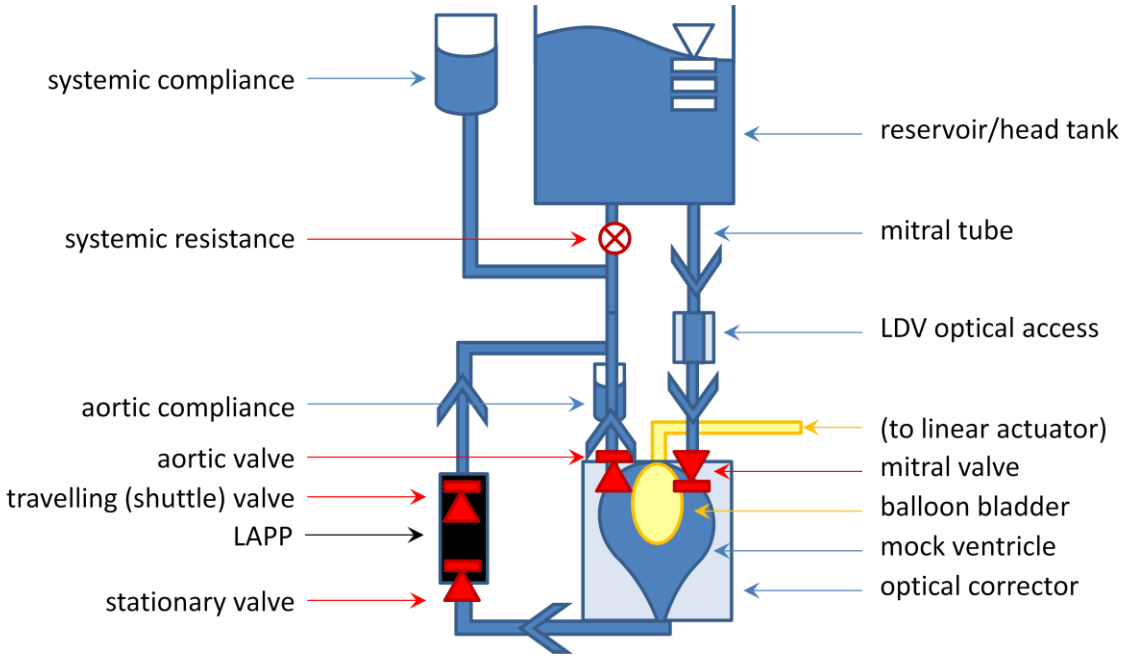

Figure 3: Schematic of the Mock Circulatory Loop

Fluid enters the flow loop from a large reservoir through a "mitral tube." A section of the flexible vinyl tube is fitted with a rigid acrylic tube and optical corrector, so that laser Doppler velocimetry (LDV) can be used to measure the fluid flowrate within the mock loop. Briefly, LDV takes advantage of the Doppler shift to calculate the speed of minute particles suspended in the fluid. A dilute suspension of titanium dioxide particles is added to the working fluid; these particles do not alter the fluid properties but serve as reflectors that scatter light from a HeNe laser (Model 124b; Spectra Physics; Santa Clara, CA) to a photodetector. The shift in the light's frequency is analyzed and output (after filtering and amplification) as an analog voltage, which is read by a National Instruments analog-to-digital converter board and recorded in a text file. This measurement technique provides excellent temporal resolution of the flowrate and has a Bragg

cell, making it capable of handling flow reversal. A box filled with the working fluid has been added to mitigate the lens effect caused by the curved tube walls and refractive index mismatch between air and the working fluid. A close-up picture of the LDV measurement section is given in Figure 4.

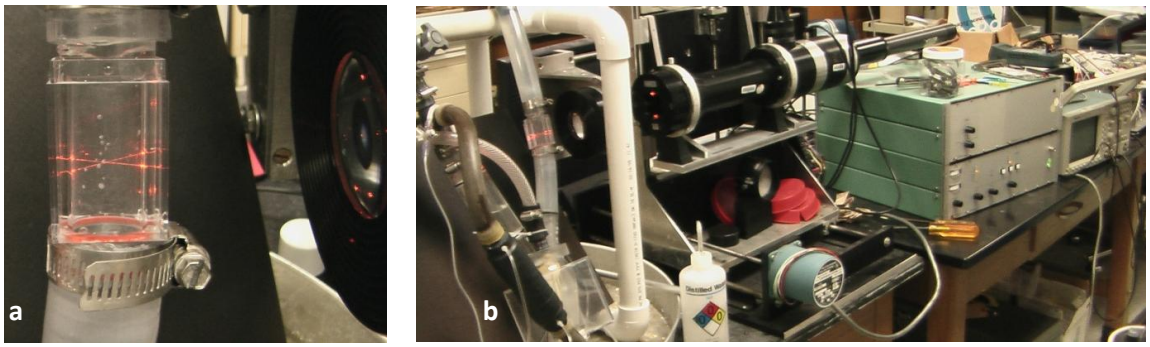

Figure 4: (a) Close-up view of the LDV measurement section and (b) an overview of the LDV measurement system

After passing through the mitral tube, fluid reaches the inlet of the mock ventricle. Photographs of the mock ventricle are presented in Figure 5 and Figure 6. Nineteen-millimeter pyrolitic carbon bileaflet valves (On-X Life Technologies, Inc; Austin, TX) are used as mitral and aortic valves to allow flow into and out of the mock ventricle. Because it is often the most diseased of patients that will be given LVADs, the mock ventricle is greatly enlarged and semi-rigid. As a patient's heart weakens, it tends to grow larger (so that a smaller change in circumference during contraction results in the same volume displacement) and more spherical; in some cases only one wall of the heart shows much contractility. Hence the mock ventricle was fashioned from a rigid plastic bottle (Method; San Francisco CA) with prolate ellipsoidal geometry and volume of roughly 350mL.

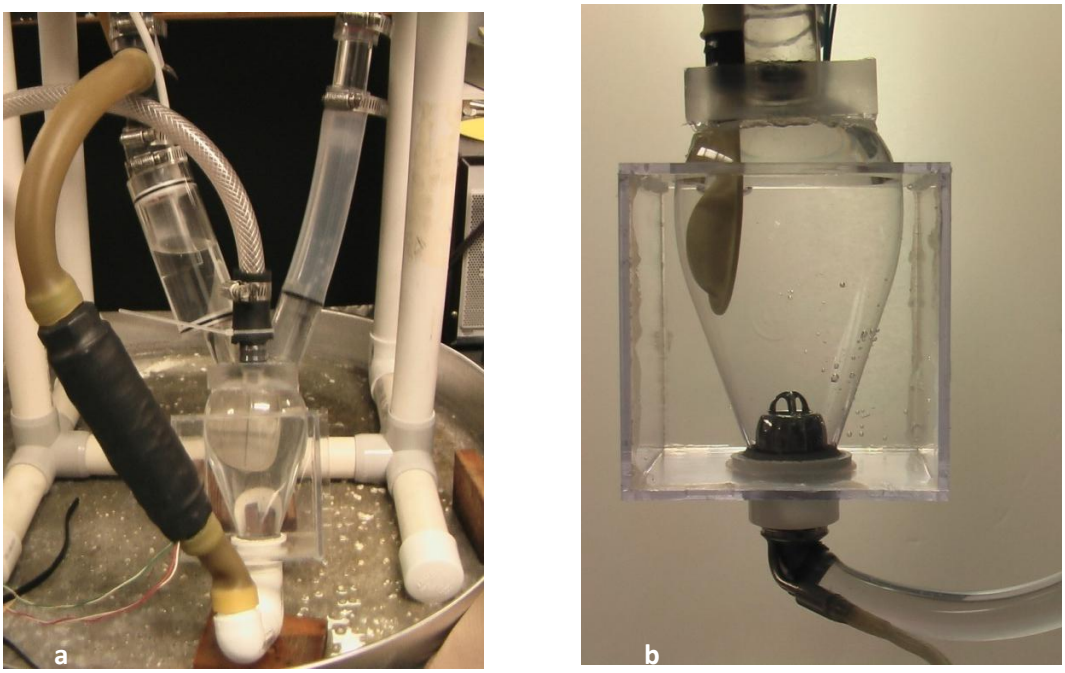

Figure 5: (a) Close-Up view of the mock ventricle with no liquid in the optical corrector and (b) side-view of the mock ventricle with appropriately filled optical corrector (note: a Jarvik 2000 is inserted at the apex rather than the LAPP)

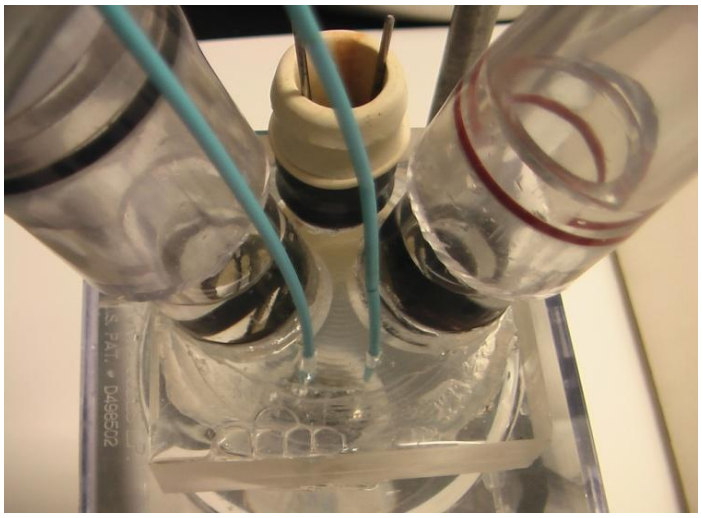

Figure 6: Close-up picture of valves, connective tubing, and balloon attachment. Aortic compliance chamber removed for clarity

A balloon bladder is inserted into the rigid vessel, and stretched over a plastic skeleton to prevent it from inflating spherically and to keep it near the ventricular wall. Air is driven in and out of the balloon by a linear actuator/piston assembly shown in Figure 7 (EC2 Series Linear Actuator, EC2-BK23-15-16B-150-MF1-FT1E; Kollmorgen; Radford, VA). As the balloon is

filled, there is less volume for fluid in the rest of the ventricle and the pressure rises. This is directly analogous to systole where the volume of the ventricle decreases and the intraventricular pressure increases. When fluid is removed from the balloon, the pressure inside the ventricle decreases while its effective volume increases, as in diastole. The intraventricular balloon bladder's expansion and contraction lends ventricular compliance, which is necessary to have a physiological pressure-flow relationship; mimics the ventricular volume change that occurs in some LVAD patients; and allows optical access for flow visualization techniques (specifically, dye injection can be used to observe flow patterns within the ventricle).

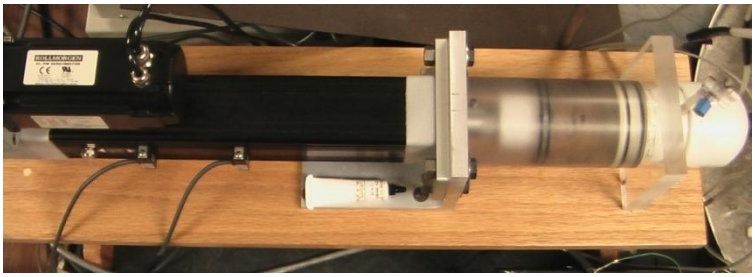

Figure 7: Actuator-piston assembly

Fluid ejected from the mock ventricle can flow through one of two paths. When the LAPP is not present, all working fluid exits the ventricle through an aortic valve and enters the aortic compliance chamber (shown in Figure 8). This chamber, partially filled with air, mimics the elastance of the human aorta and reduces "ringing" in the recorded pressure signals caused by the stiffness of the vinyl aortic tubing. Having compliance as close as possible to the aortic valve helps reduce the inertial spikes by reducing the length of the fluid column that must be accelerated.

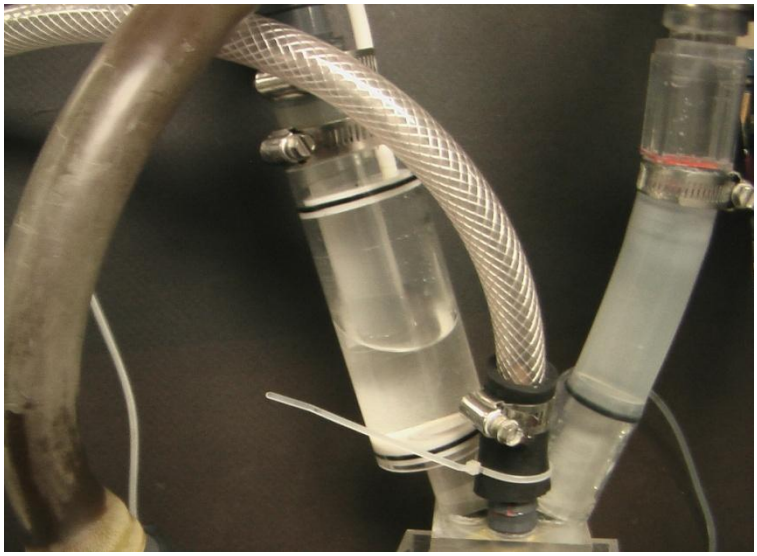

Figure 8: Aortic compliance chamber

When the LAPP is connected to the apex of the ventricle, some fluid still leaves through the aortic valve and follows the path described above; the rest of the fluid flows through the LAPP through a length of natural rubber tubing. The LAPP houses two more of the 19 [mm] On-X pyrolitic carbon bi-leaflet valves; one fixed and the other mounted onto a shuttle. The shuttle is driven along the axis of a titanium tube by an encapsulated, annular, axially poled rare earth magnet surfing an externally applied magnetic field (all permanent magnets: neodymium-iron-boron grade N52; K & J Magnetics; Pipersville, PA). The external magnetic field is generated either by winding copper magnet wire around the outside of the titanium tube (as shown in the figure below) or by using large permanent magnets coaxial to the shuttle that can be moved mechanically by a linear motor or actuator. Regardless, the shuttle is thus pushed along by a repulsive force gradient, much like a DC stepper motor. Photographs of the LAPP are shown in Figure 9, and details related to the shuttle and windings are given in separate subsections below.

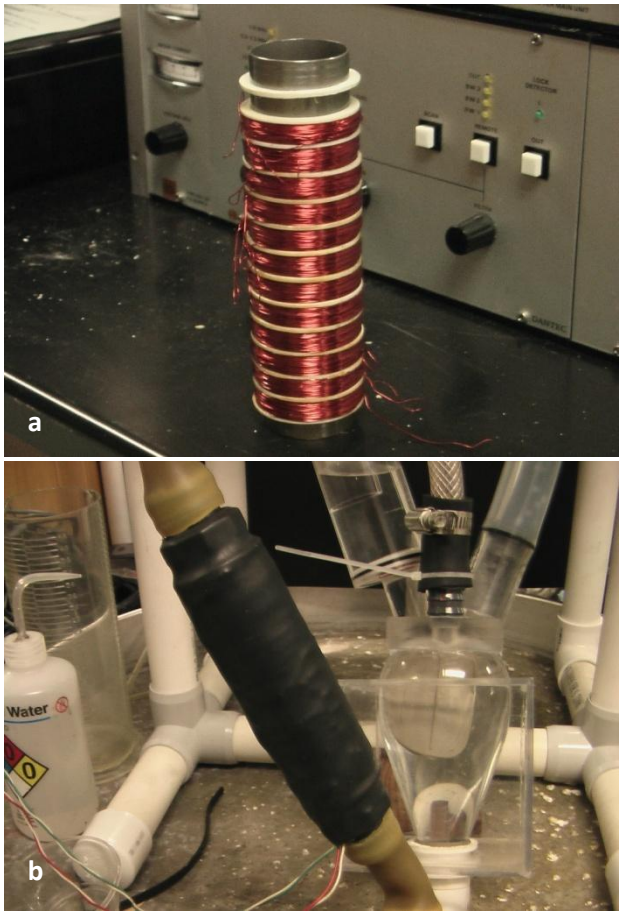

Figure 9: (a) Photos of the LAPP showing windings, PVC spacer rings, and titanium tube and (b) the LAPP with protective coverings and attached to the loop

The LAPP outflow connects to the aorta just before the needle valve (ThrottleMaster; Marquest Scientific; Costa Mesa, CA). The needle valve is opened and closed to adjust the systemic resistance. A rigid glass bottle upstream of the needle valve is used to mimic the systemic compliance. The bottle can be partially filled to adjust the compliance level. After passing the needle valve, fluid is returned to the reservoir and can cycle through the flow loop again. Figure 10 shows a photograph of the complete mock circulatory loop. Pressure taps are placed to monitor static pressure inside the ventricle, at the inlet and outlet of the LAPP, and inside the aortic compliance chamber.

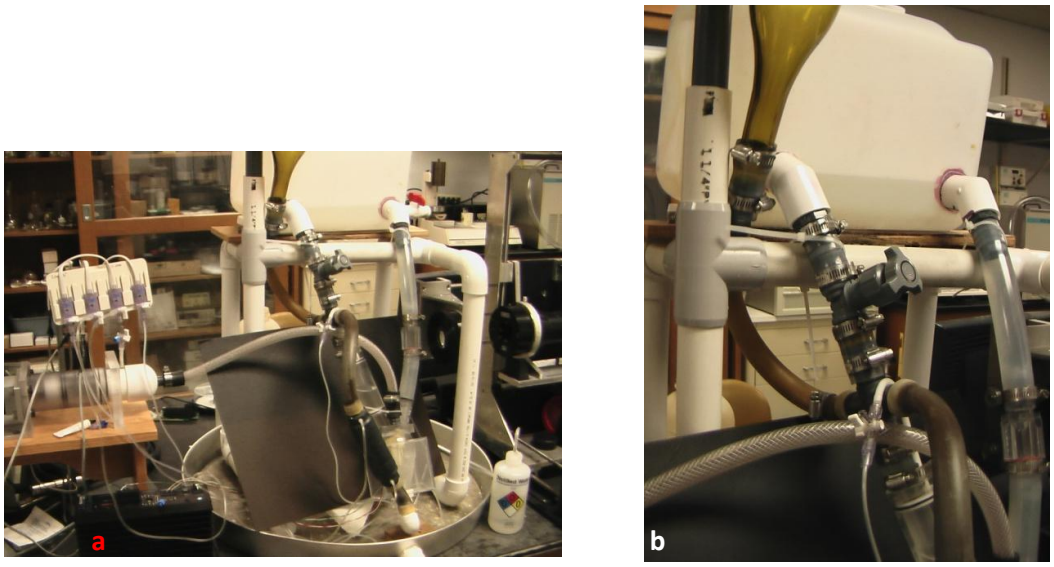

Figure 10: (a) Mock loop overview and (b) a close-up of the resistance and compliance elements

In order to monitor and record the pressure, flowrate, and temperature signals, a custom LabView virtual instrument, or VI, was created. Not only does the VI enable measurement of the aforementioned signals through data acquisition boards, but it enables a user to control the ejection volume of the balloon bladder, the relative phasing between the LAPP and the bladder, the beat rate, and the number of beats or cycles. Though not used in the LAPP studies, the VI can also control a dye injection system for visualizing flow patterns within the mock ventricle. A screenshot of the VI is shown below in Figure 11.

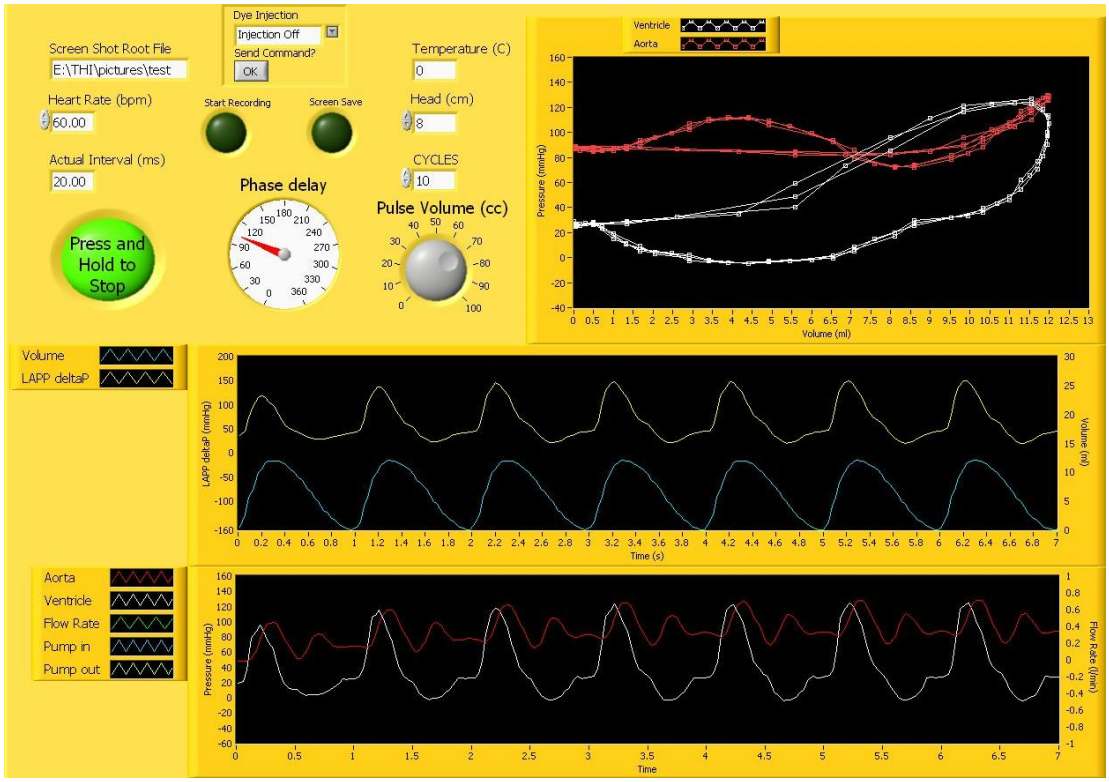

Figure 11: LabView VI front panel

Hemolysis Testing Loop

As mentioned above, the Mock Circulatory Loop is an unreasonable choice for performing studies with blood because of the large volume of fluid required and the difficulties inherent in taking it apart to thoroughly clean before and after blood is added.

In an effort to standardize hemolysis testing so clinicians and researchers could better compare the performance of different pumps, the American Society of Testing and Measurement (now ASTM International) published Standard F 1841-97: "Standard Practice for Assessment of Hemolysis in Continuous Flow Blood Pumps," which first appeared in 1997 and was reapproved for use in 2005. The standard specifies the lengths and diameters of tubing that must be included, as well as the total loop volume, operating temperature range, pressure drop across the VAD, flow rate, and blood properties. While this framework may be acceptable for continuous flow

devices, it is not appropriate for pulsatile devices where capacitance must be added to damp out the inertial effects which arise because of the non-constant flow rate.

Since hemolysis testing is standardized for continuous flow pumps, the LAPP hemolysis testing loop was designed to remain as true as possible to the standard. Six feet of ⅜ inch inner diameter vinyl tubing were used and the temperature, pressure, and flow guidelines were matched as closely as possible; blood was selected according to ASTM Standard F-1830: "Practice for Selection of Blood for In Vitro Evaluation of Blood Pumps" and handled according to ASTM Standard F-1841-97. Table 1 below summarizes the specified flow loop parameters and the experimental values of the same, while Figure 12 shows a recommended continuous flow loop and the Hemolysis Testing Loop; photographs of the actual Hemolysis testing loop are provided in the Hemolysis Testing chapter.

It should be noted that in a continuous flow pump, the total pressure head should remain constant. For a volume displacement pump like the LAPP and Heart Mate I (used as a control), the pressure developed by the pump changes throughout each ejection cycle. Therefore, it is not clear which pressure rise should be maintained at 100 *mmHg*—one could argue this should be the maximum difference between the inlet and outlet pressure or the difference between the average inlet and outlet pressures or perhaps even the difference between the maximum outlet and minimum inlet pressures. An effort was made to keep the average difference between inlet and outlet pressure close to 100 *mmHg*, while keeping the maximum pressure below 150 *mmHg*, which is at the high end of physiologically acceptable levels. As discussed in the results presentation, this requirement could not always be met.

Table 1: Items specified in ASTM Standard F1841-97 (2005)

Criterion	Value in Standard	Values Used
Circuit Volume	450 ± 45 *mL*	~800, ~1100, ~1300 *mL*
Loop Tubing (PVC)	6.6 *ft* of ⅜ *in* inner diameter	6.6 *ft* of ⅜ *in* inner diameter
Pump Flow Rate	5 ± 0.25 *L/min*	5, ~4.75, ~4.71 *L/min*
Total Pressure Head	100 ± 3 *mmHg*	
Circulating Blood Temperature	37 ± 1 ˚*C*	37, ~41, ~34 ˚*C*

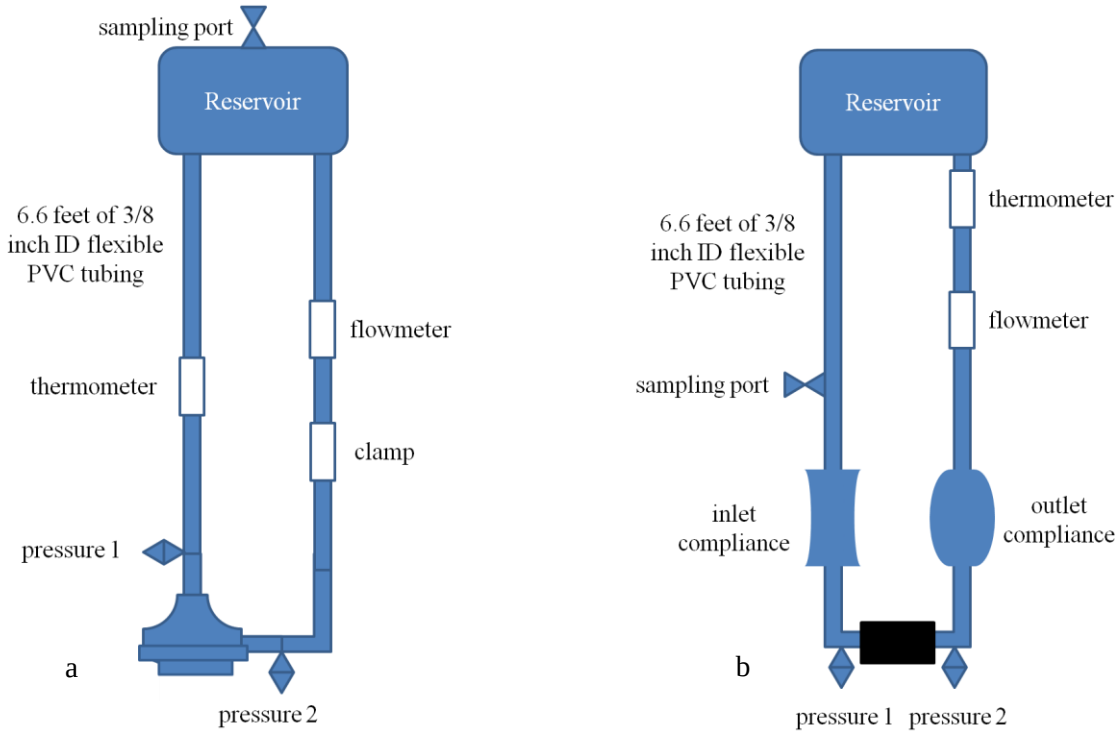

Figure 12: (a) ASTM recommended loop and (b) modified Hemolysis Testing Loop

To accomodate the pulsatile pumps, compliance chambers made from thin-wall silicone rubber tubing and modified PVC pipe fittings were added to the required components at the inlet and outlet of the LAPP; the compliance chambers have a resting volume of roughly 200 *mL*. These elastic structures are necessary to reduce pressure spikes caused by accelerating flow

through tubes with negligible circumferential stretch. Due to the long length of small diameter tubing, no clamp was necessary to reach the recommended pressure head.

A Transonic TS410 400-Series Flowmeter Module with 9PXL probe quantified blood flowrate. To capture pressure data, Edwards TruWave pressure transducers were connected to wall taps at the inlet and outlet of the LAPP. Pressure and flow probe signals were recorded by ADInstruments LabChart Pro Data Acquisition Software. Temperature was monitored by an RTD mounted in the reservoir bag connective tubing. A water bath was used to keep blood within the recommended temperature range.

The loop volume is higher than recommended by the standard because of the need for compliance elements to reduce inertial forces. The hemolysis calculations include a correction for volume, so there should be no complications with using whatever volume is sufficient to keep the pressure levels near physiological.

It should be noted that the hemolysis test loop maintained the recommended flow loop lengths and geometry used for continuous flow pump testing. The additional volume and loop length associated with the compliance chambers present additional fluid shear. Thus, the modifications represent a worst case situation for the pulsatile pumps when compared with continuous flow test results. This was one reason for evaluating the LAPP by comparing the hemolysis results with the proven HeartMate Internal Pneumatic (IP).

COMSOL Model

To study the interaction of the permanent magnet and the moving electromagnetic field within the windings, the commercial software package was used—COMSOL Multiphysics version 4.3, a finite element code developed in Sweden in the early 1980s. This model is semi-empirical because the measured fluid pressure from the bench-top flow loop was used as a retarding force acting on the shuttle in opposition to the magnetic force generated by the current in the coils.

The COMSOL model does not include the titanium tube or any blood. An incompatibility was found between the ODEs Interface and the Fluids Interface, which would not allow implementation of the appropriate boundary conditions. Since the flow field could not be calculated, there was no need to include the titanium or liquid; the permeability of these materials is not significantly different from air.

Finite Element Method

The finite element method is a technique to discretize the continuous governing equations and spatial domain. First, the geometry is subdivided into a grid or mesh made up of ideally uniform equilateral triangles or squares. In practice, grids are often irregular because the boundaries of the domain are curved or the dimensions do not allow perfect filling with squares or triangles. At times, a modeler may wish to intentionally have regions with relatively more or fewer grid points to gain refinement in areas of interest or save computational resources in regions that have less impact on the solution.

Each grid point is combined with a set of shape functions and appropriate degrees of freedom; this grouping is referred to as a finite element. These shape or basis functions are used to approximate the value of the unknown variable at each grid point. Basis functions are typically low-order polynomials. The basis functions can be rearranged and converted to a matrix form, which is then solved by linear algebra techniques to ultimately give values of the unknown at each grid point.

Model Set-up

The first step in creating a COMSOL model is to select the appropriate space dimension for the problem of interest. As a first approximation, the LAPP can be viewed as two-dimensional axisymmetric. By selecting an axisymmetric geometry, COMSOL will solve two-dimensional forms of the governing equations written for a cylindrical coordinate system (properties are considered uniform in the azimuthal direction). Though torques on the shuttle

may be an interesting future study, the length of time and level of complexity required to perform full three-dimensional simulations is not appropriate at this stage of LAPP development.

Next, one must select the "physics" that COMSOL is to model. Because it is specifically designed to study the interaction of different types of phenomena, COMSOL has a wide range of physics modules for purchase. Those available for use through collaboration with Dr. Philippe Mason are shown in Figure 13; note that the ACDC and Mathematics modules were used in the LAPP model and have been expanded in the figure below.

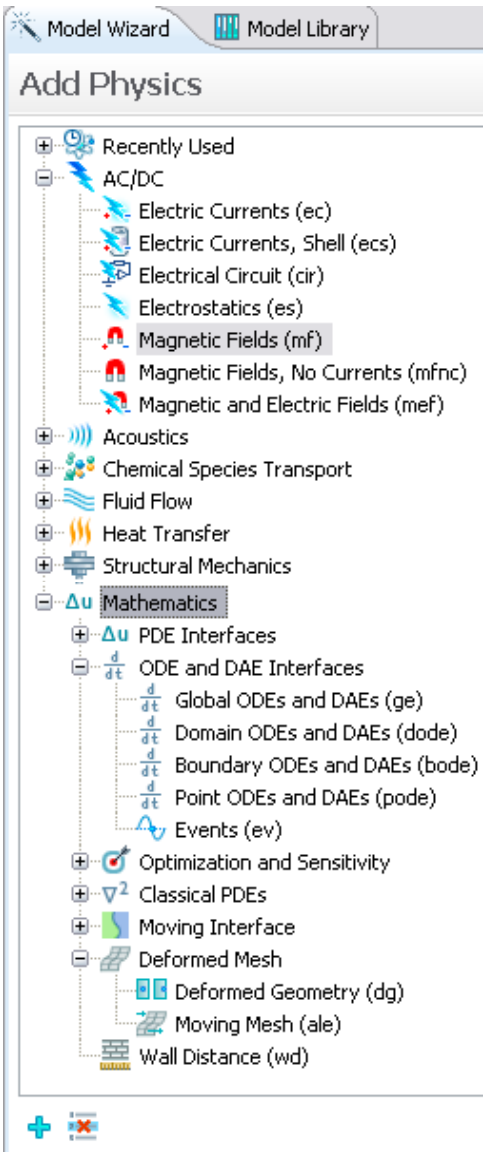

Figure 13: Physics modules available in COMSOL

The Magnetic Fields Interface in the AC/DC Module will solve the axisymmetric form of Ampere's Circuital Law, which relates the integrated magnetic field around a closed loop to the electric current passing through the loop. Ampere's Law with Maxwell's correction can be written

$$\nabla \times \boldsymbol{B} = \mu_0 \left(\boldsymbol{J} + \varepsilon_0 \frac{\partial \boldsymbol{E}}{\partial t} \right) , \qquad \text{Eq. 1}$$

where $\boldsymbol{B}$ is the magnetic flux density, μ_0 is the permeability of free space ($\mu_0 = 4\pi \times 10^{-7}$ $V{\cdot}s/(A{\cdot}m)$), $\boldsymbol{J}$ is the total current density (including external, polarization, and magnetization current densities), ε_0 is the permittivity of free space ($\varepsilon_0 = \mu_0^{-1} c^{-2}$, where c is the speed of light in a vacuum; $\varepsilon_0 \approx 8.854 \times 10^{-12}$ $A^2{\cdot}s^4/(kg^1{\cdot}m^3)$), and $\frac{\partial \boldsymbol{E}}{\partial t}$ is the time rate of change of the electric field.

To investigate the coupling between the shuttle magnet and the changing electric field in the windings, the shuttle must be allowed to move in response to the forces it experiences. To accomplish this, interfaces from the Mathematics Module must be added to the COMSOL model: Moving Mesh and Global ODEs and DAEs. Specifically, coupled ordinary differential equations (ODEs) were written and solved for the shuttle position and velocity in terms of an experimentally determined fluid force fit equation and the magnetic force being calculated simultaneously by COMSOL. Using the Moving Mesh Interface, the shuttle position is adjusted to match the solution of the ODE at each time point.

The moving mesh relies on an arbitrary Lagrangian-Eulerian (ALE) framework to allow the finite elements to move in ways not possible in purely Lagrangian or Eulerian formulations. From an Eulerian viewpoint a computational mesh would be fixed in space relative to a given coordinate system, while from a Lagrangian viewpoint the mesh would track the material motion relative to a reference (initial) configuration. From an ALE viewpoint the mesh is able to move and does not necessarily have to follow a material.

COMSOL differentiates between three types of reference frames: the spatial (Eulerian), material (Lagrangian), and mesh. Without the Moving Mesh Interface activated, all three frames

coincide. When active, the spatial and material frames are separated and Eulerian and Lagrangian physics will behave differently. COMSOL also provides a Deformed Geometry Interface, which separates the mesh and material frames so that geometrical changes can be studied without remeshing; this was not used in the LAPP model.

Once all of the desired interfaces are added, the study type must be specified—stationary, time-dependent, frequency domain, etc. The LAPP studies were generally time-dependent, but a few steady state cases were investigated.

After selecting the study type, COMSOL closes the model wizard dialogue and displays the model tree view. It is now time to draw the geometry, select material properties, create a computational mesh, specify boundary conditions, and choose a solution method. A representative geometry is shown in Figure 14. This particular model includes a mu-metal shield in addition to the shuttle magnets and field windings. A large air domain is included so that field lines will not be artificially constrained. Again, this is an axisymmetric model, to the red dash-dotted line at the left indicates the centerline of the geometry and the axis of revolution that would yield the correct three-dimensional LAPP. Values given are distances in centimeters. Though it does not have much effect on the physics, the shuttle body is included to aid in meshing and mesh movement. The titanium and working fluids are not included because they have little effect on the electromagnetic fields and this would make meshing the model unnecessarily difficult.

For air, copper, and Delrin®, COMSOL's built-in properties were used—each of these has a permittivity and permeability of unity. The electrical conductivity of copper, used in the multiturn coil domain set-up, is 5.998×10^{7}[S/m]. New materials were created for the neodymium iron boron magnet and the mu-metal shielding; the permeability of these materials is 1.05 and 8×10^{4}, respectively.

A triangular grid was used for computations. The spacing is necessarily small in the mu-metal and near the corners of the coils and magnets, but near the domain boundaries, the cells are

allowed to become much larger. Initial minimum mesh quality is 0.5278 and is not supposed to fall below 0.3 during the simulation. When this threshold is reached, COMSOL should automatically remesh the domain and map the solution from the original to the deformed configuration.

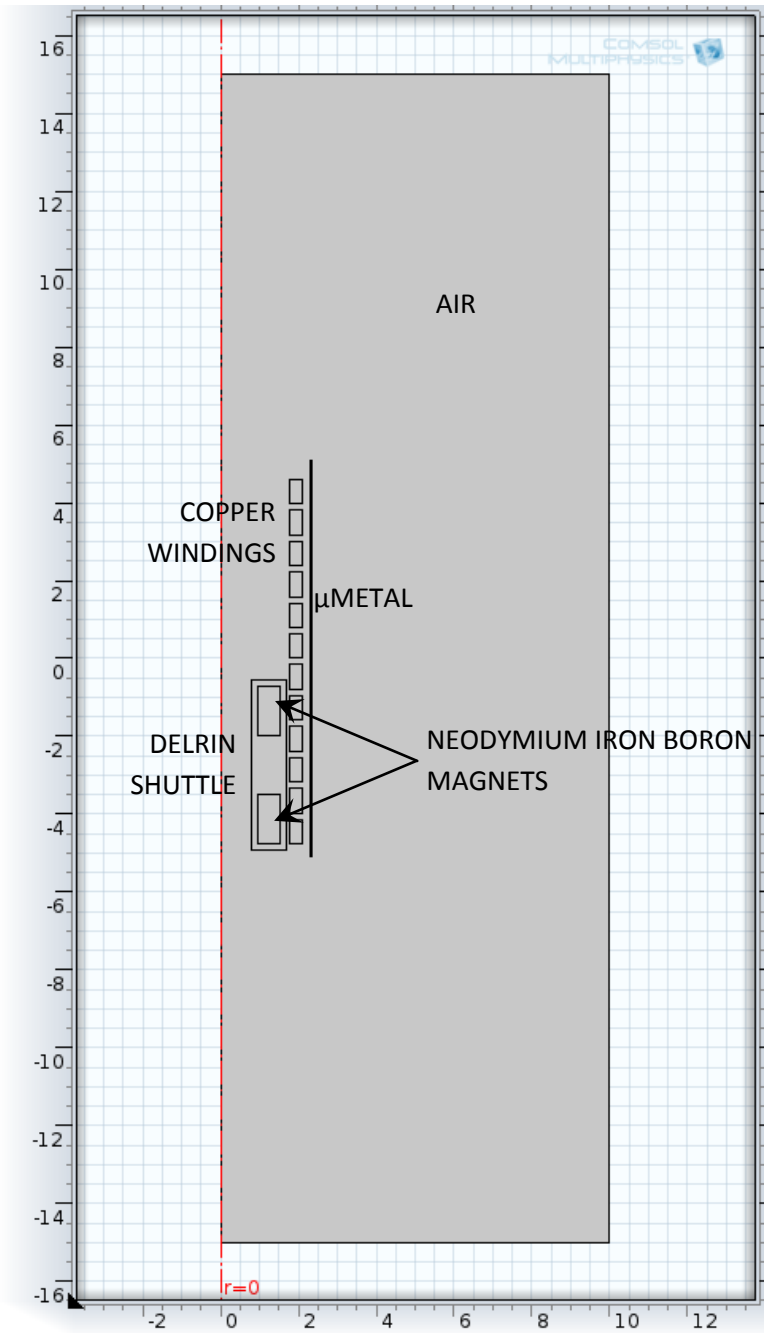

Figure 14: Typical LAPP geometry in COMSOL

Boundary conditions, parameters, and variables can now be added. For ease, stroke, ejection frequency, and winding current are defined as parameters so that all formulations on which they depend will be updated simultaneously. As mentioned above, the COMSOL model is a semi-empirical one, so the fit to pressure data is included as a variable—COMSOL will update its value at each new time point.

The ODEs being solved describe the motion of the shuttle. Specifically they are

$$0 = \frac{dz_s}{dt} - v_s + offset \quad \text{subject to } \frac{dz_s}{dt} = 0 \text{ at } t = 0 \quad , \qquad \text{Eq. 2}$$

$$\text{and } 0 = \frac{dv_s}{dt} + \frac{f_f + f_m}{M_{eq}} + 250.0 v_s \quad \text{subject to } \frac{dv_s}{dt} = v_s = 0 \text{ at } t = 0 \quad , \qquad \text{Eq. 3}$$

where t is time, z_s is the position of the inner corner of the bottom of the shuttle, v_s is the shuttle velocity, *offset* is a parameter based on the stroke to ensure the shuttle oscillates about the center of the LAPP, f_f is an equation for fluid force based on bench-top pressure waveforms, f_m is the force generated by the coil current (obtained by integrating the Maxwell stress tensor), M_{eq} is an equivalent mass of fluid and shuttle being accelerated by the forces, and 250.0 is a damping parameter.

In the Moving Mesh Interface, the shuttle region (magnet plus Delrin®) and its boundaries are set to be displaced by z_s ("prescribed deformation"). The surrounding air is allowed to deform freely ("free deformation"), but the windings (and shielding material, if present) and their boundaries are kept fixed in the original layout ("fixed mesh").

To solve for electromagnetic variables, Ampere's Law is solved for the air and Delrin® regions with the constitutive relation $\mathbf{B}=\mu_0\mu_r\mathbf{H}$ and separately in the magnet with $\mathbf{B}=\mu_0\mu_r\mathbf{H}+\mathbf{B_r}$ and remanent flux density B_r of 14.1 *kG* in the axial direction (note that **B** is the magnetic flux density, μ_0 is the permeability of free space, μ_r is the permeability of a material relative to μ_0, and **H** is the magnetic field). The outer boundaries of the air are treated as magnetically insulated.

The copper coils are treated as multiturn coil domains. Each coil is made of two-hundred turns of wire with a diameter of 0.0125 *in*. The current flowing through each coil varies in time. The variation can be viewed as a sinusoidally travelling sine wave and is written as

$$I(t) = I_{set}\, c\, \frac{stroke}{2}\left(sin\left(z_{os} + \frac{n\pi}{2} + 1 - \frac{stroke}{\lambda} sin\left(2\pi t_{sin} - \frac{\pi}{2}\right)\right)\right) , \qquad \text{Eq. 4}$$

where n is the winding number (lowest winding is number zero, highest winding is number eleven), I_n is the current in the nth winding, I_{set} is the maximum current, c controls whether the current is boosted, reduced, or normal, z_{os} is an offset controlling the starting location of the wave-front, λ is the wavelength of the windings, *stroke* is the amplitude of the wave-front's displacement, hr is the rate, and t_{sin} is a time such that $t_{sin} = \begin{Bmatrix} (t - int(t))\ if\ t \times hr \leq 0.5 \\ \left(hr - (t - int(t))\right)\ otherwise \end{Bmatrix}$ with t being simulation time and *int( )* designating the floor (or integer part) of t.

Now that the model is fully defined, it is time to set-up the solver. The start and end times must be specified, as well as the output time interval. COMSOL allows a user to take smaller time steps computationally to increase accuracy but can output (or interpolate) solutions at coarser intervals to save memory. Careful setting of maximum and initial time steps can reduce the wait-time for computations.

Though it provides artificial damping, based on the types of physics modules used, the backward difference formulation (BDF) solver gave the best stability. The BDF order was allowed to increase to five, but again for stability reasons, the order was generally lower—one or two. The spurious diffusion tends to smooth out gradients, but the quality of the results appeared acceptable.

Because of the long distances the shuttle must travel (much farther than one or two grid points), the mesh must be regenerated to prevent grid points from overlapping and disrupting ordering of the system of equations being solved. COMSOL provides an Automatic Remeshing tool in the Study node that will create a new grid when the quality drops below a threshold value

(0.3 for these simulations), map the solution from the deformed grid to the newly remeshed grid, and continue computing.

Figure 15 shows a screenshot of the finalized model tree used for some LAPP simulations.

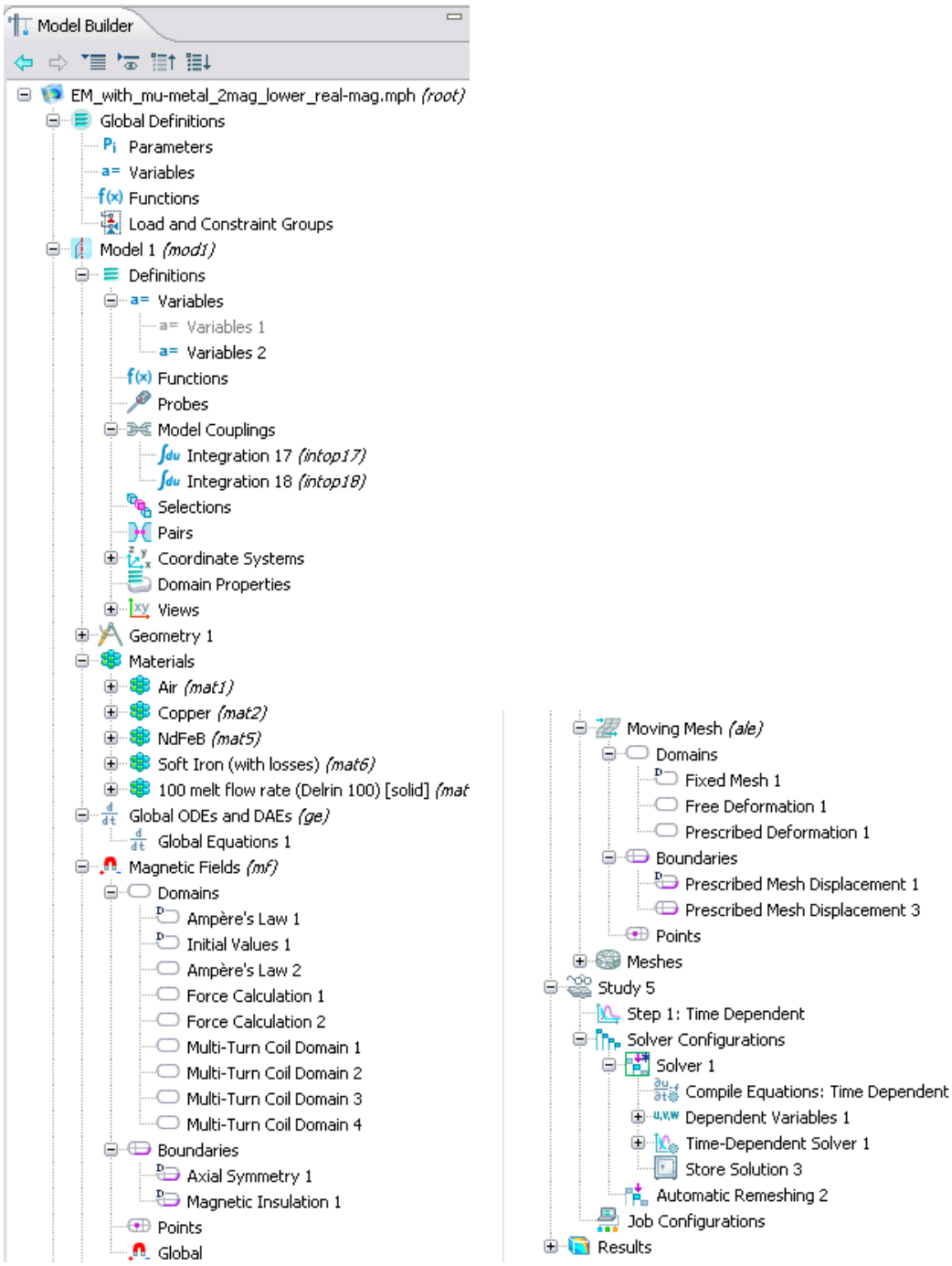

Figure 15: Final model tree

FLUENT Model

Although COMSOL is designed as a multiphysics package, an incompatibility between the Fluids Module and the ODE Module was encountered. The shuttle velocity needs to be applied to the shuttle walls and valve so that the wall motion will cause the fluid in contact with the wall to move (no slip condition). The shuttle velocity must be calculated through the ODE interface, since COMSOL will not give a user access to the simulation time during computations. When the velocity from the ODE is used as a no-slip boundary condition in the Laminar Flow Interface, COMSOL forces the value of the ODE to be zero rather than imparting the velocity to the wall. Forcing the ODE to be zero means that the shuttle will not move. If one writes a deterministic (but still time varying) expression for the velocity, the shuttle and flow field respond as expected, but the shuttle is no longer moving as directed by the interplay of the magnetic and electric fields.

COMSOL's Heat Transfer Module will allow a user to specify convective coefficients (*h* values) rather than calculating heat transfer using the flow field, but determining appropriate coefficients for the time-varying flow field would be difficult. Rather than trying to develop a work-around solution (perhaps using COMSOL's LiveLink for MATLAB) to break the one-way forcing of the no-slip condition, the decision was made to take advantage of previous experience with the FLUENT package to model the fluid mechanical and heat transfer aspects of the LAPP separately from the electromagnetic.

Finite Volume Method

In contrast to COMSOL's finite element method, FLUENT is based on the finite volume method. A solution domain is divided into a computational grid and conservative forms of the integral equations are applied at the center of each grid square or triangle—each control volume. Surface values are interpolated from the centers of neighboring control volumes. No basis functions or degrees of freedom are necessary, and the scheme is inherently conservative.

Integrals are approximated by quadrature formulas, which lead to a system of algebraic equations that can be solved with linear algebra techniques to give the flowfield variables.

Model Set-up

The geometry and computational grid are created in a separated software package, such as Gambit. Figure 16 shows the geometry used in FLUENT calculations. As in COMSOL, this LAPP model will be axisymmetric once loaded into FLUENT. Note again that a large region of air is included so that results will be analogous to the bench-top LAPP without any spurious effects due to a truncated computational domain.

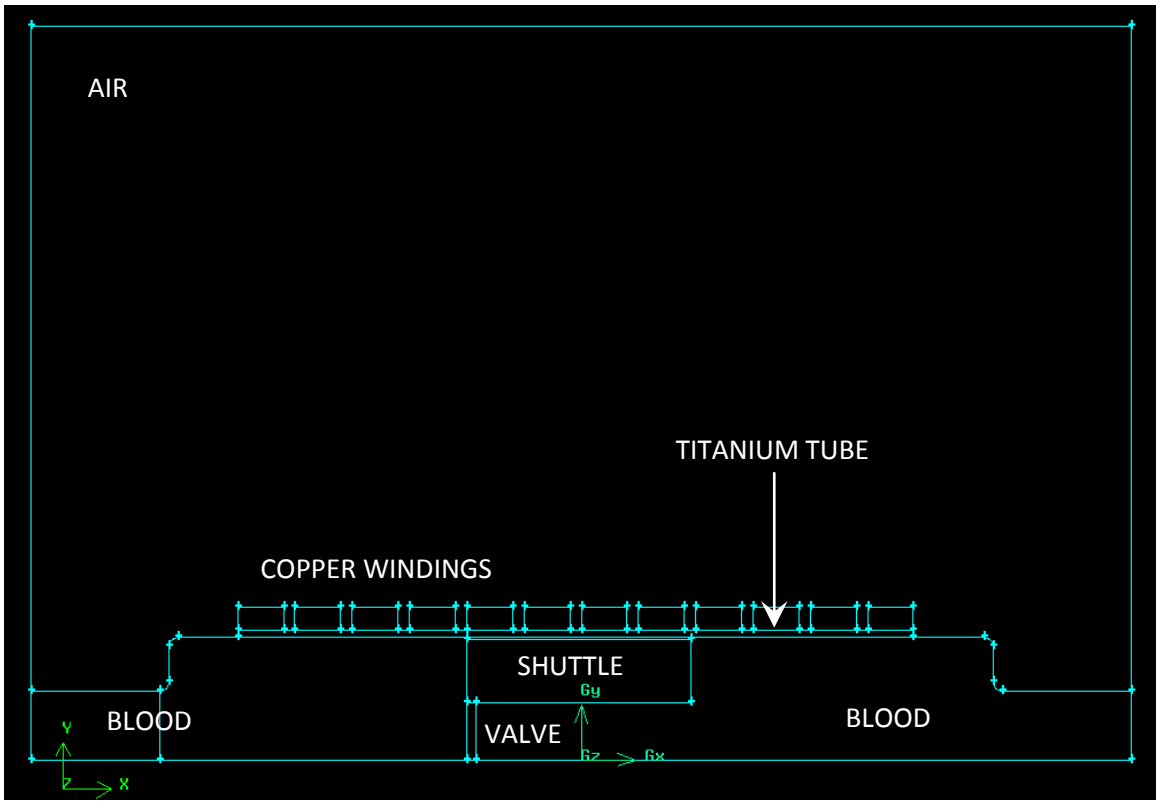

Figure 16: LAPP geometry in Gambit/FLUENT

It should also be noted that a narrow gap is included between the shuttle and the inner surface of the titanium. Because of the way the Dynamic Mesh is implemented, FLUENT is unable to have sliding solid-solid contact—the mesh does not remain continuous across the solid-

solid boundary. The thickness of the gap is larger than in the experimental LAPP, but as shown in the estimates of flow through the gap below (see Numerical Model Results chapter), this size of gap has little effect on the flow field. It should be noted that having a gap that is the same size as in the physical LAPP is not practical from a computational point of view—the small cells in the gap region would require taking unreasonably small time steps so as not to over step the mesh.

A triangular mesh, though a source of numerical diffusion, was generated because FLUENT's Dynamic Mesh Model responds better to that than to quadrilateral meshes. The mesh is fine near the gap and throughout the LAPP, but grows near the outer boundaries of the air domain. There is only one row of cells through the gap, so the flow through it is not resolved, but the gap is estimated to have little effect on the flow field. The initial skewness for the mesh was 0.52.

The boundaries and domains are named and given "types" in Gambit, but some changes can be made in FLUENT. The boundary and continuum specification dialogue boxes are shown in Figure 17. There are many options for boundary conditions, but continuum regions can only be fluid or solid. Every line and area of the geometry must be assigned to one of the boundary or continuum types.

Once the geometry and mesh has been finalized in Gambit, they can be exported to FLUENT and read as case files. After reading it is good practice to perform a grid check to make sure the cell volumes are positive and the file read properly. Next the grid must be scaled to ensure the dimensions are accurate (FLUENT takes dimensions to be in meters by default).

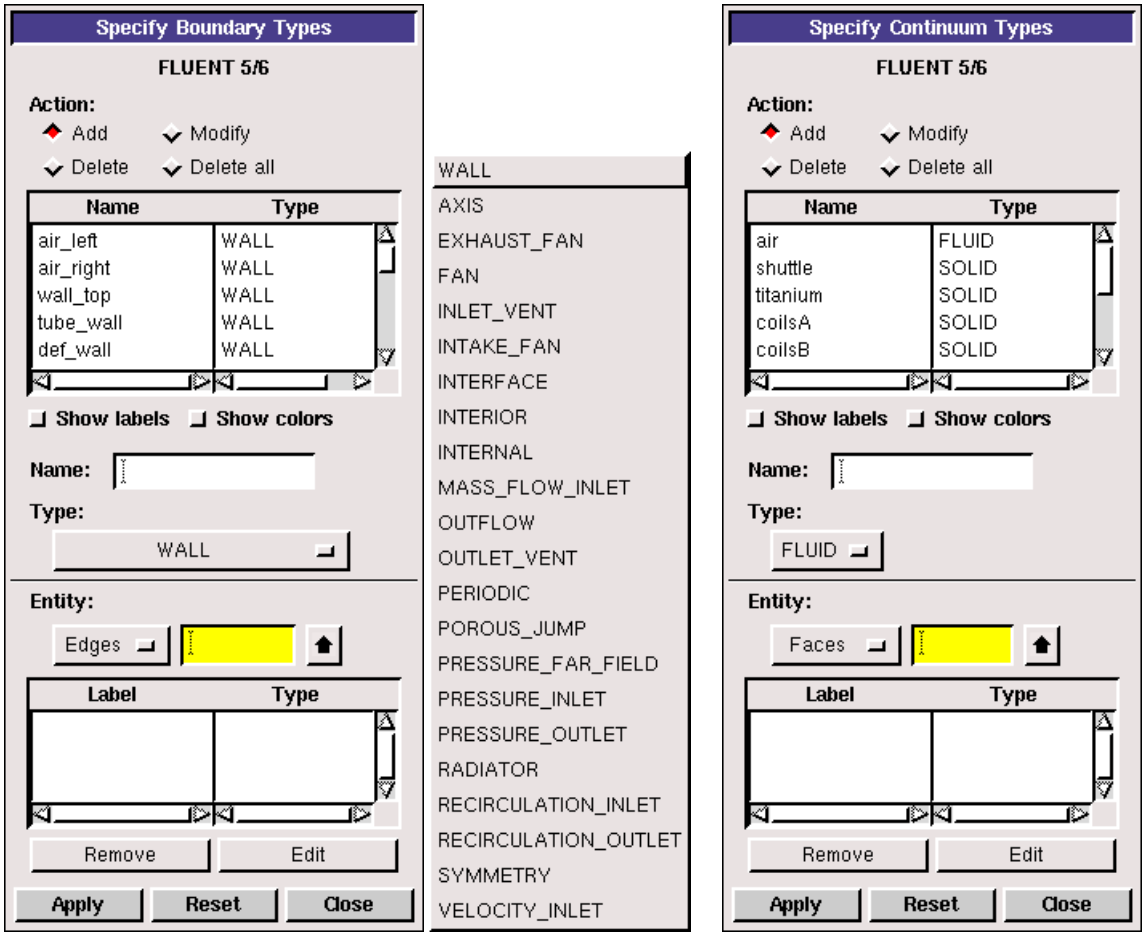

Figure 17: Boundary and Continuum Type dialogue boxes

Now that the grid is ready, the models, materials, and operating and boundary conditions must be specified. Unlike COMSOL with its model tree, FLUENT's options are nested in menus and dialogue boxes (see Figure 18 for a screenshot of the main FLUENT window).

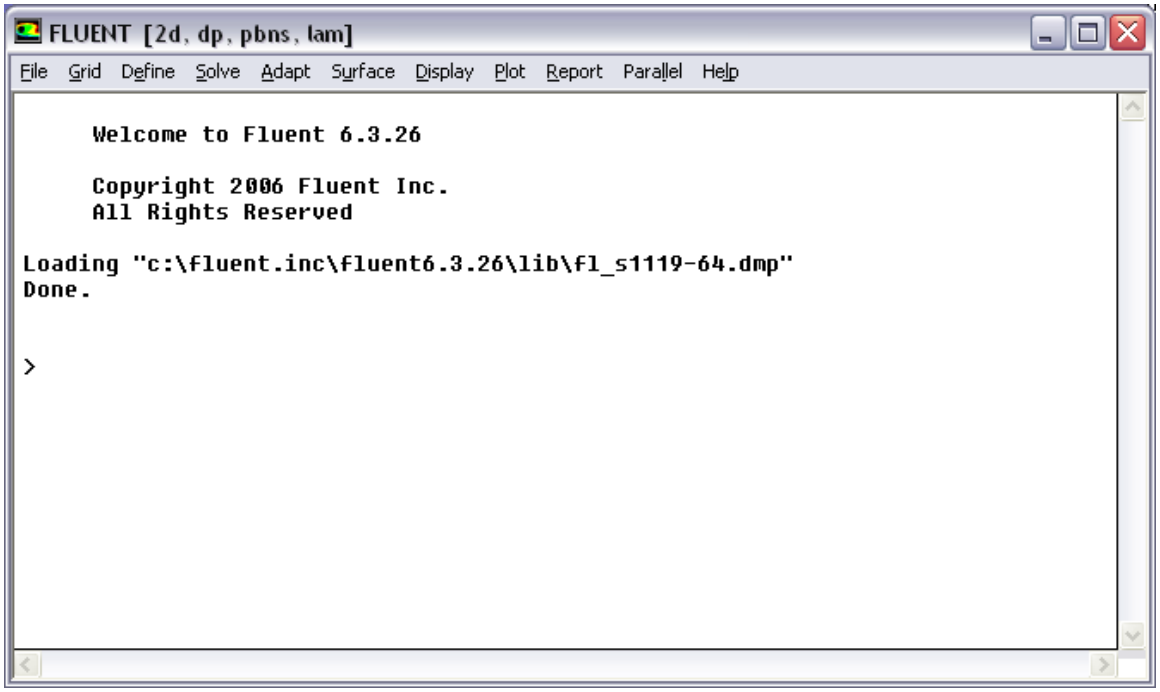

Figure 18: FLEUNT main window

The solver (dialogue box shown in Figure 19) can be set up first under Models in the Define menu. The solver was set to pressure based with an implicit axisymmetric formulation. The implicit solver computes a given unknown with a relation including already computed and unknown values from neighboring cells. These equations must then be solved simultaneously, since the same unknowns appear in (possibly) several equations. According to FLUENT documentation and help files, each coupled governing equation is "linearized implicitly with respect to all variables in the set." This set is then solved by a block Gauss-Seidel method with an algebraic multigrid. An absolute velocity formulation and the Green-Gauss node based gradient option were also employed, so nodal values of parameters are an arithmetic average of values at neighboring nodes. The scheme preserves second-order spatial accuracy and is more accurate than cell-based schemes for unstructured, triangular meshes like the one used here. The unsteady formulation was first-order implicit.

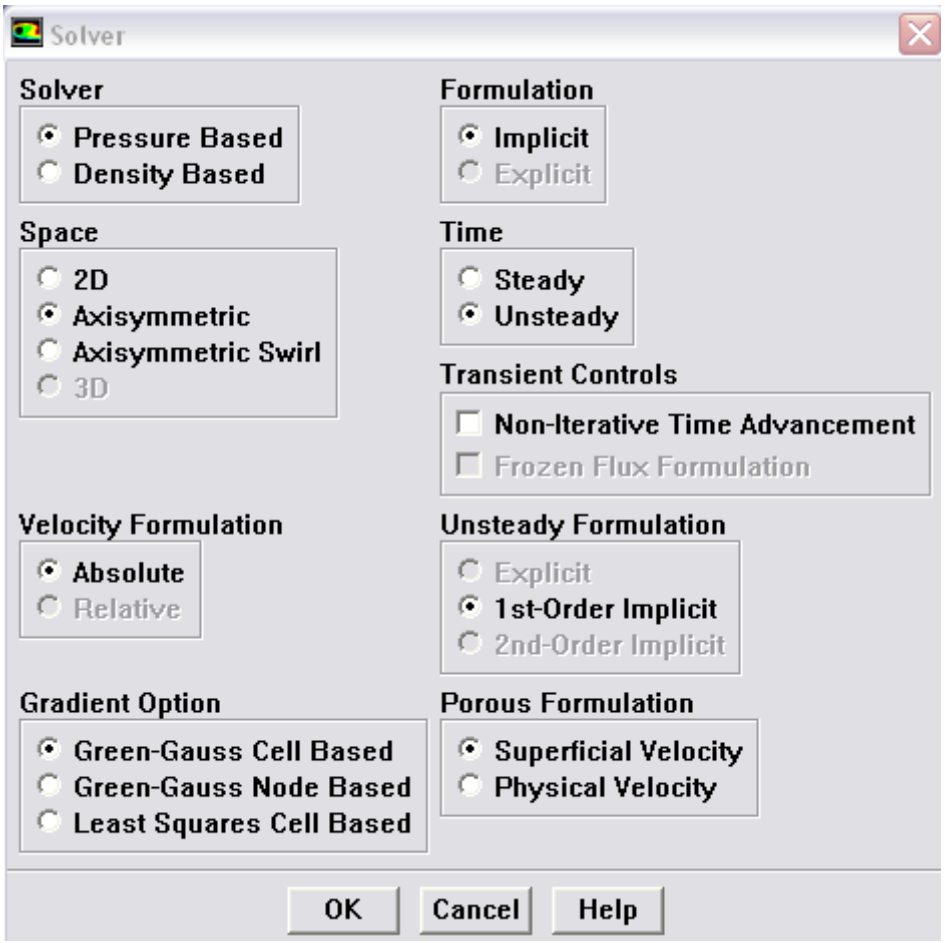

Figure 19: Solver window

The energy equation must be turned on to allow heat transfer calculations. The laminar model was picked for the viscous formulation, since turbulence does not have a chance to become fully developed; FLUENT does not have any preprogrammed turbulence models for developing flows.

Properties for a 35% glycerol solution were used in the FLUENT model in place of blood. Viscosity and density of a fluid sample from the bench-top model were measured as 0.0046045 *kg/m-s* and 1122.5 *kg/m3*, respectively. The default properties were used for FLUENT's built-in air, copper, and titanium materials. The shuttle body was given wood

properties. Density was kept constant for all materials and gravity was turned off so that no natural convention would occur.

Again, because of the need to model the shuttle travelling over long distances, some scheme for moving the mesh must be implemented. In FLUENT, one way of accomplishing this is to activate the Dynamic Mesh Model and write a user-defined function to describe the motion of the region. Adjoining regions are able to deform freely, and parameters can be set to control how the mesh is updated. The settings used in the model are shown below in Figure 20.

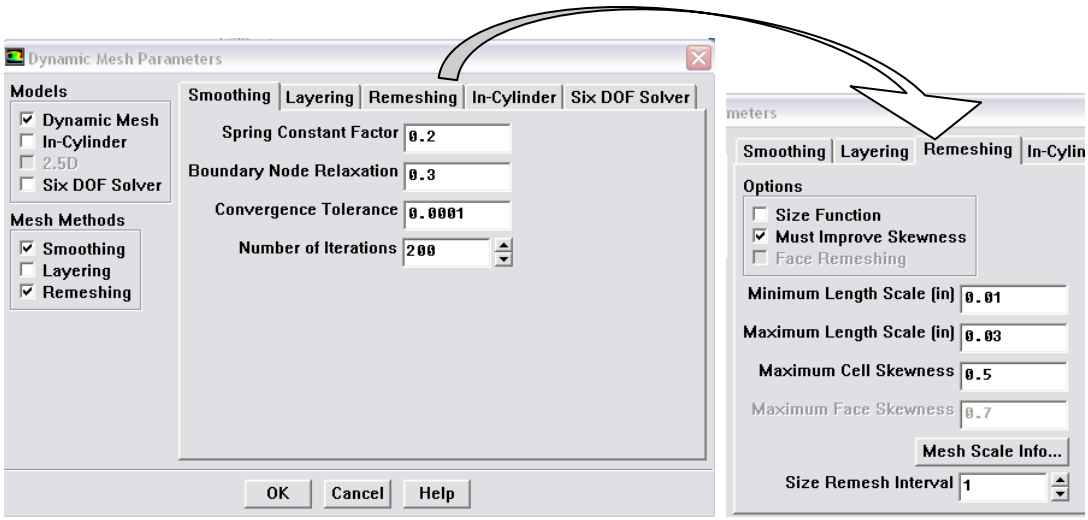

Figure 20: Dynamic Mesh Model window

After the Dynamic Mesh Model is turned on, the individual dynamic zones must be selected. These zones are anything whose length, shape, or type will change, such as the shuttle, the fluid region the shuttle moves through, the valves, etc. To make the remeshing easier, the shuttle, travelling valve (v2), and a tight region of fluid (mid) will move together in a rigid body translation; this way the small cells in the gap will not need to be remeshed. The Zones set-up window is shown in Figure 21. With the exception of "int_1" and the rigid body translators discussed above, the remaining zones are purely deforming. The deforming lines will only lengthen/shorten—they will not gain any curvature. The stationary valve (int_1) does not move, but it is included as a dynamic zone because, like the shuttle valve (v2), it switches between being

an interior face and a wall. It is important to remember that the action and geometry of the valves is not modeled. The flow through the valves is controlled in an on/off manner by switching between wall and interior boundary condition types, so there is no gradual flow stopping or starting nor any secondary flow created by fluid motion past the valves as occurs in the bench-top model.

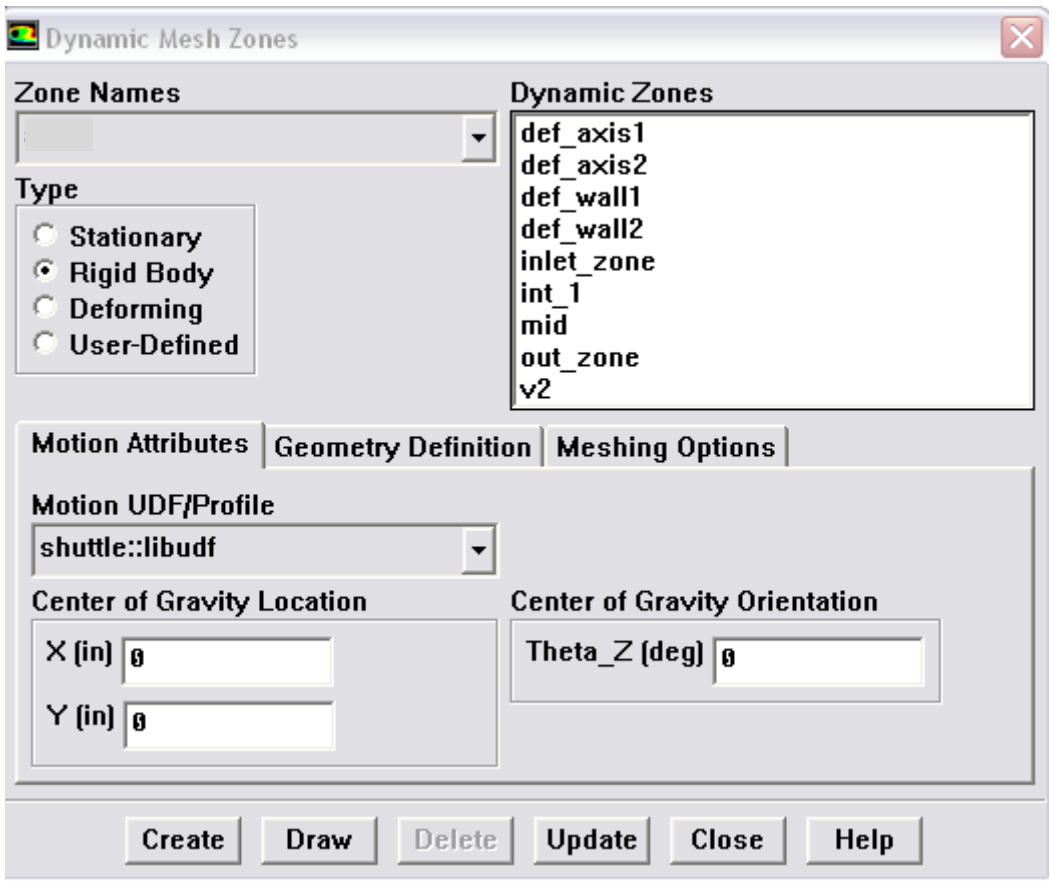

Figure 21: Dynamic Mesh Zones window

In addition to the Dynamic Mesh Motion, several boundary conditions are necessary to form a well-posed problem. The LAPP inlet is a pressure inlet set to a constant 2000 *Pa*, while the LAPP outlet is a pressure outlet controlled by a user defined function. The outlet pressure is set by resistance and compliance elements that were patterned after their analogues in the Mock Circulatory Loop. A user defined heat source is applied to the copper coils using a Joule heating

model ($Q = I_n^2R$, where the current I_n is the same as that in the COMSOL model and the R is calculated from the length and resistivity of the copper wire used). It is possible for the air outside of the LAPP to be circulated, although the simulations presented below were run for stagnant air to give a worst-case estimate of heating; the outer boundaries of the air are adiabatic.

In FLUENT the "standard" scheme for pressure and a second-order upwind scheme for momentum and energy discretization were selected. The "standard" scheme works well as long as pressure varies smoothly across a region and large body forces are not present. First order schemes would amplify the numerical diffusion already present from the use of tetrahedral elements. The QUICK scheme in FLUENT is really designed for quadrilateral, regular grids; when triangular or irregular patches are encountered, FLUENT automatically uses the regular second-order differencing scheme. Since the given mesh has very few quadrilateral elements, no advantage is gained over the plain second-order formulation. A third order MUSCL scheme could have been selected to further reduce numerical diffusion, but the relatively noncomplex flow field did not seem to merit such treatment.

Pressure-velocity coupling was specified as SIMPLE (semi-implicit method for pressure linked equations) while the pressure, density, body force, and momentum under-relaxation factors were changed to

Pressure:	0.7
Density:	1.0
Body Forces:	1.0
Momentum:	0.5
Energy:	0.98

to adjust the stability and speed of numerical convergence. The under-relaxation factors are used to adjust the changes in parameters from one iteration to the next. The coupled solver solves the continuity and momentum equations simultaneously and any other equations for scalars are

solved separately and sequentially. Because the grid becomes somewhat skewed during the shuttle's travel, the SIMPLEC coupling was avoided as it has a propensity to become unstable. The absolute convergence criteria were set one order of magnitude stricter for continuity, r- and z- momentum, and energy.

CHAPTER 3: Model Verification

In order to ensure that data generated is relevant and representative of the LAPP or the conditions it would experience in patients, the numerical and bench-top models must be checked and compared to measurements taken from the LAPP or from patient observation. Additionally, numerical models must be constructed and solved under conditions that allow a converged solution to be computed in a reasonable period of time.

Flow Loops

Current healthcare privacy considerations and hospital regulations make it difficult to obtain data from actual heart-failure patients. Furthermore, the variety of heart-failure modes and complicating conditions create a diverse and complex array of individual pressure tracings. Thus rather than attempt to duplicate the pressure levels of a single patient or group of patients, a general wave shape and amplitude were selected. It is important to remember that the LAPP is designed to pump blood within physiological constraints, but because its method of operation is fundamentally different from the human heart, it is unlikely that the LAPP's and heart's pressure-flow relationship will be the same. Ultimately, the LAPP could be tuned to match the native heart, but at this stage of development such refinement is not necessary. In fact, the physiological role of pulsatility and the optimal pulse waveform are open questions and are becoming important issues as "pulseless," continuous flow assist and total replacement devices increase in popularity.

Mock Circulatory Loop

The development and a detailed analysis of the Mock Circulatory Loop can be found in the 2009 Thesis *Hydrodynamic Effects of Left Ventricular Assist Device Implantation: a numerical and experimental approach* (Holley Love, University of Houston). Figure 22 shows pressure signals measured within the ventricle and after the aortic valve for a 25 *cc* stroke at 0.83 *Hz*. Included to the right is a sample waveform for a normal, healthy individual (adapted

from Wiggers_Diagram.png on the WikiMedia Commons). As the ventricular wall contracts (or the balloon bladder fills with air), the pressure within the ventricle builds rapidly because of the bloods incompressibility. When the intraventricular pressure exceeds the aortic pressure, the aortic valve will open. Blood will then flow into the aorta until the intraventricular pressure drops below the aortic level and the valve closes; the valve closure is driven by a reversal in pressure gradient across and reversal of flow through the valve. After valve closure, there is a small up-tick in the aortic pressure trace called the dichrotic notch (or incisure), which is caused by the valve cusps (or mechanical leaflets) snapping shut. The ventricle refills at nearly constant pressure with a slight increase as atrium contracts; nearly 80% of blood passes directly through the atrium into the ventricle without any atrial contraction (Guyton and Hall, 2006).

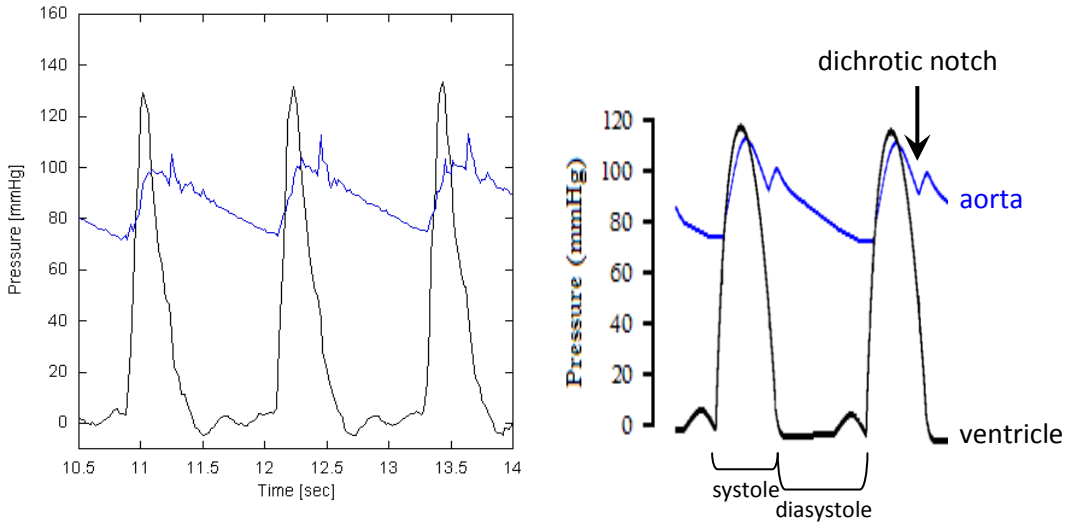

Figure 22: (a) Ventricular and aortic pressure in the Mock Circulatory Loop and (b) a normal human

In comparing (a) and (b) in Figure 22, the magnitudes and wave shapes are very similar. Because there is no left atrium in the flow loop, the diastolic pressure in the ventricular pressure is slightly different; the waves in the flow loop are most likely due to motion of the balloon bladder. A more important and undesirable difference is that the ventricular pressure rises higher above the aortic pressure in the model than it does in a healthy person. This is a consequence of using rigid tubing in the flow loop. The aorta is highly distensible and is able to accommodate

the sudden in rush of blood by expanding, thereby reducing the linear acceleration of the blood and thus the pressure gradient required to perform the acceleration.

An air chamber was added after the aortic valve to mimic the aortic compliance and reduce the inertial spike in ventricular pressure, as shown in Figure 23. In this final version of the Mock Circulatory Loop, the relative magnitudes of the aortic and ventricular pressures are even closer to the textbook case. The frequency of the ringing in the aortic pressure is much lower than in the previous model (Figure 22 (a)) because the tubing is a much stiffer system than the air chamber.

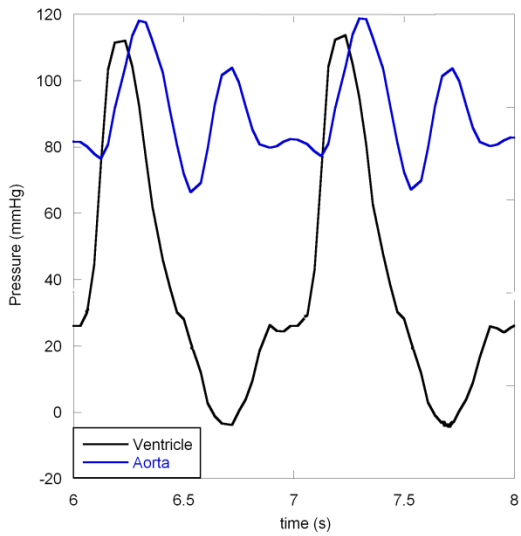

Figure 23: Addition of aortic compliance reduces ventricular pressure spikes

The above tests show that Mock Circulatory Loop is an acceptable environment for testing the LAPP. The resistance and compliance levels are tuned so that when the balloon bladder is operating within the mock ventricle, physiological pressure waveforms with physiological amplitudes are produced. The LAPP can then be added to study the effect of phasing between the native ejection (balloon) and LAPP ejection or to study dye washout in the ventricle and aorta; the importance of these studies is outlined in the Future Work (Chapter 6).

Hemolysis Testing Loop

The Mock Circulatory Loop is a valuable tool for studying the hydrodynamic impact of the LAPP, but it cannot be used to study blood damage. A simple loop that can be cleaned or disposed of is called for. As discussed in the preceding chapter, a hemolysis testing standard has been developed by ASTM International for evaluating continuous flow ventricular assist devices. Unfortunately, the rigidity and long length of small bore tubing required by the Hemolysis Testing Standard (Standard F 1841-97: "Standard Practice for Assessment of Hemolysis in Continuous Flow Blood Pumps") introduces large pressure spikes during operation of a pulsatile pump due to inertia—a long column of fluid must be cyclically accelerated and decelerated through the flow loop. The resulting pressure levels then fall outside the limits set by the standard unless compliance elements are added at the pump inlet and outlet. The addition of compliance chambers in turn increases the total volume of the flow loop above the 450±45 *mL*, so testing a pulsatile pump demands relaxation of the conditions set forth for continuous flow VADs.

The data below (Figure 24) show the effects of adding compliance chambers to the hemolysis testing loop. The pressures are measured using wall taps placed before both the inlet and outlet compliance chambers; the LAPP was driven mechanically in a sine wave profile of 60 *cc* per stroke at 1.5 *Hz*. The data in the left panel was obtained using two reservoir bags in series (CAPIOX Flexible Venous Reservoir (500 *cc*), Terumo Cardiovascular Systems Corporation, Ann Arbor, MI). Note the large amplitude of both inlet and outlet pressures.

The data in the right panel was taken with a single reservoir bag after the addition of an inlet and outlet compliance chamber, each with a resting volume of approximately 200 *cc*. These chambers were assembled by stretching 1.5 *inch* inner diameter, $^{1}/_{32}$ *inch* thick silicone tubing (Argon Masking USA, Monrovia, CA) over custom tapered 1 *inch* to 0.5 *inch* slip-slip Schedule 40 PVC reducer fittings, see Figure 25. Thin rings cut from PVC pipe are slid over the outside of the silicone to secure the tubing and form a liquid-tight seal. In order to keep the inlet chamber

from collapsing, the reservoir must be pressurized either by placing a weight on top of it or using a pressure infusion bag (shown in right side of Figure 25; image taken from LabMarketInc.com).

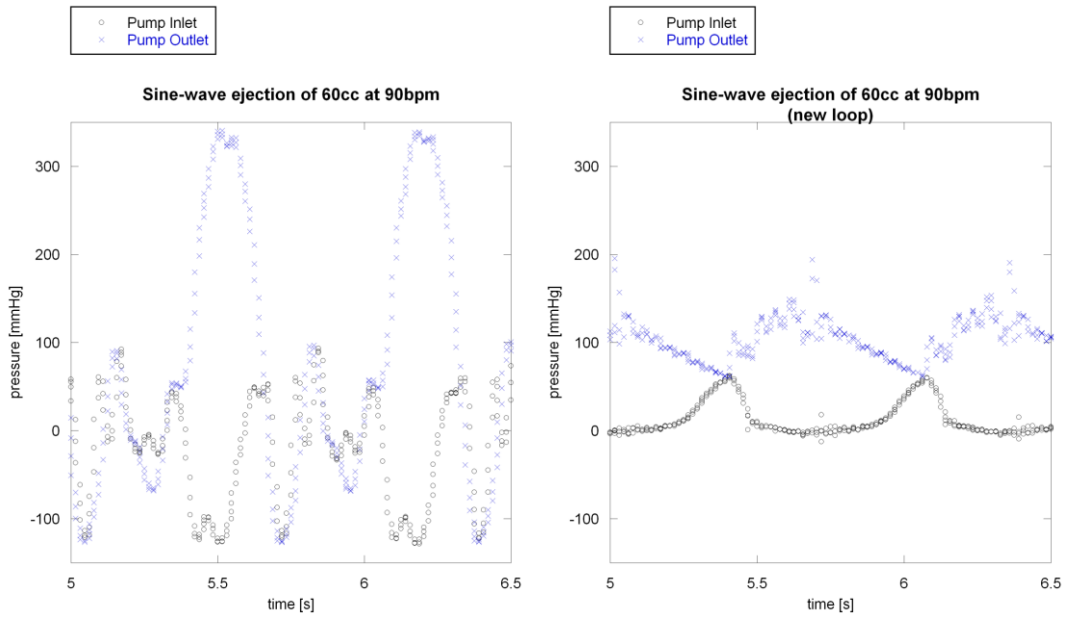

Figure 24: Compliance reduces pressure variation in hemolysis testing loop

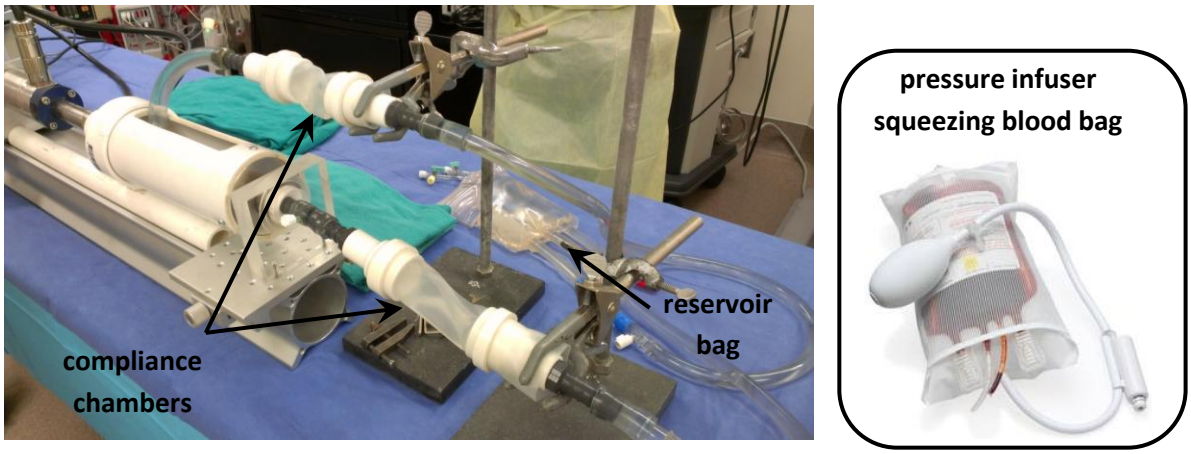

Figure 25: Compliance chambers (first hemolysis test configuration) and pressure infusion bag

The pressure levels shown in the right panel of Figure 24 are close to normal, healthy levels (see Figure 26 for comparison; right panel of Figure 26 adapted from Wiggers_Diagram.png on the WikiMedia Commons). The hemolysis loop's inlet pressure is higher than its left atrium-analogue partly because it is being measured before the compliance

element, while the left atrial pressure is measured within a compliance element—the left atrium. The spike in the hemolysis loop's outlet pressure occurs where the shuttle changes direction and the valves snap open/closed, which is comparable to the dichrotic notch seen in the aortic pressure when the aortic valve closes. The ringing in the flow loop is due mostly to the rigid tubing.

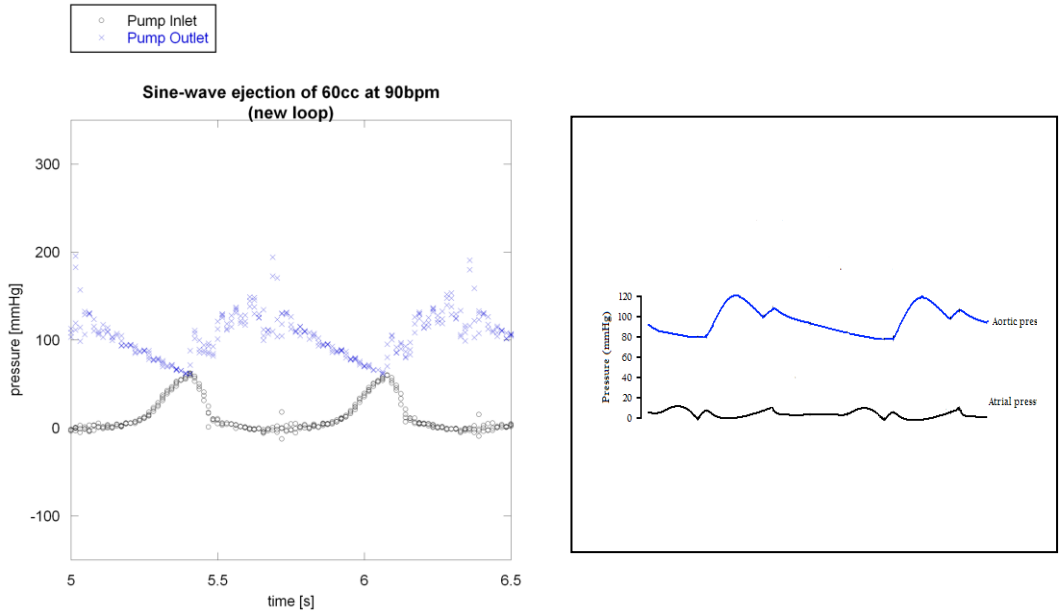

Figure 26: Comparison of hemolysis loop and healthy human pressure levels

If one aligns multiple cycles of the LAPP pressure rise (LAPP outlet pressure minus LAPP inlet pressure), as shown in Figure 27 (a), it becomes clear that the ringing is a real and very repeatable part of the pressure signal—though not necessarily desirable, it should not be considered noise or filtered out. The data in Figure 27 (a) were taken from ten consecutive cycles. The same agreement is seen over much longer times, too. The curves in Figure 27 (b) are an overlay of two cycles roughly five hours apart. In preparation for the six hour hemolysis tests, the LAPP was run for several hours to check the steady state temperature and to verify the hardware could operate for that long a time. The pressures in Figure 27 (b) were recorded at the beginning and end of one of these "stress" tests. The conditions differ from those in Figure 27 (a), but the same degree of repeatability from cycle to cycle is observed.

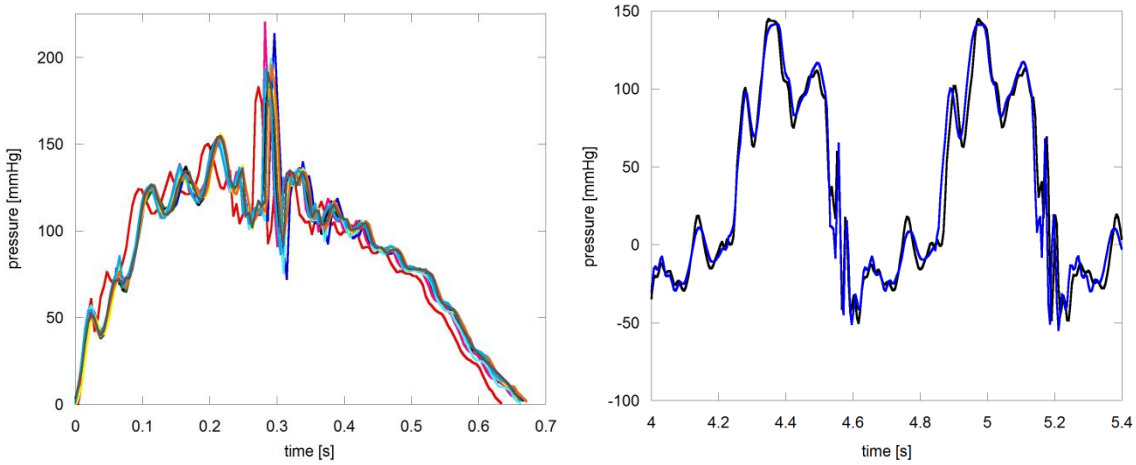

Figure 27: Multiple cycles of the LAPP pressure rise overlaid

The consistency in the pressure data from the Hemolysis Testing Loop indicates that the LAPP runs reliably from beat to beat and over several hours. Looking at the details of the waveforms, the loop and LAPP are able to produce pressures in a physiological range. These two factors—the consistency in ejection and the overall pressure waveform—indicate that the Hemolysis Testing Loop is suitable for conducting experiments to quantify blood damage.

FLUENT Model

The verification process for the numerical models is somewhat different than for the bench-top flow loops. The FLUENT model should still be compared to physiological pressures, but its solutions must also be checked for time step and grid independence to ensure that model is giving results that are based on the physics of the problem and not functions of the computational parameters. Just as a solution at a given time point is said to be "converged" when its value no longer changes with successive iterations, the time step size or mesh spacing can be said to be converged when successive refinements no longer change the results. It is possible to refine the grid or time step size too much in which case precision errors become appreciable, but this is not usually an issue in most problems—certainly not for the models considered below.

In a problem where there is deformation or rigid body motion of one region relative to another, the combination of time step size and mesh spacing cannot be made arbitrarily. If the

mesh spacing is too small relative to the time step, the grid will become inverted and the finite volume solution cannot proceed. Thus to check for time step and grid independence in the FLUENT, the dynamic mesh option was de-selected, so the shuttle would not move. The shuttle velocity is specified by a user defined function that depends on the current flow-time alone, so it is not anticipated that the grid or time step would have any effect on the motion profile.

Time Step Convergence

The FLUENT simulation was run (without the dynamic mesh motion) at three time step sizes: 5×10^{-4} *sec*, 1×10^{-3} *sec*, and 5×10^{-3} *sec*. Plots of the average temperature and the outlet pressure are shown in Figure 28. The pressures are reported at each time step, but the temperatures are only written to a file every 0.1 *sec*. For both quantities, only six digits are kept. There is excellent agreement between the temperatures and outlet pressures; the left panels show the data generated with the three time step sizes, and the right panels show the difference between the larger or smaller time steps and the medium step normalized by the amplitude of the waveform. In the case of the temperature, the amplitude was taken as the difference between the starting temperature and the final average temperature (322.55 *K*) obtained from long run simulations.

As seen in the lower right panel of Figure 28, the smaller time step slightly, though consistently, under-estimates the outlet pressure relative to the medium step size, while the larger step over-estimates the same. In this case, since there is no shuttle motion pumping fluid, the flow is caused by the compliance element discharging through the gap. Therefore the positive pressure difference between the solutions at small and medium size time steps indicates more fluid has left the compliance chamber. At the smaller time step, the temporal gradients are being resolved better, so it makes sense that this step size predicts are slightly faster discharge. By the same argument, the larger time step size predicts a slower discharge. The larger time step is five times greater than the medium time step, while the medium time step is twice as large as the

small time step; this explains why the magnitude of the normalized error is larger for the larger step than the smaller.

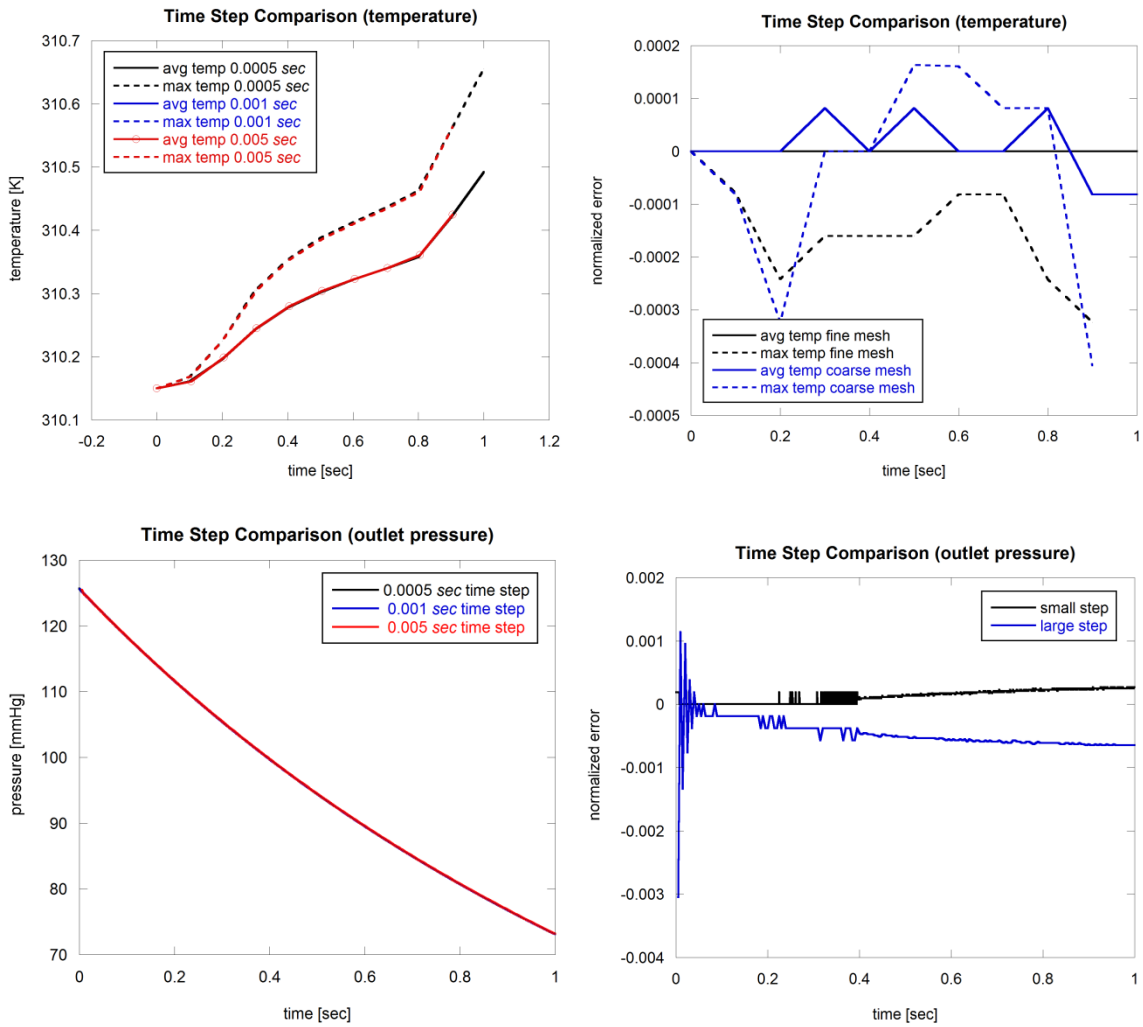

Figure 28: FLUENT data appears independent of time step size

These time step comparison plots show that choosing a time step between 0.0005 *sec* and 0.005 *sec* should have negligible effect on the results. The time step in the full FLUENT simulations (with dynamic mesh) for the heat transfer was 0.001 *sec*; the temperature development is presented in the next chapter.

Mesh Convergence

As discussed above, the dynamic mesh capability was de-activated to perform the grid convergence check. The mesh motion causes cells to grow and shrink from one time step to another, so comparisons from one mesh to another are not as clean because the element sizes are varying as the solution variables are developing in time. Instead three meshes (each of roughly uniform elements) were created that represent the range of sizes expected if the dynamic mesh was active. Screenshots of the mesh near the shuttle and a table of mesh statistics are shown below (Figure 29). The coarse and fine meshes were made by doubling and halving, respectively, the node interval relative to the base mesh (i.e., the starting mesh used when the dynamic motion is enabled). The equisize skewness, a measure of an element's area relative to the smallest circumscribing circle, is reported below; smaller values reflect better meshes with triangular elements closer to equilateral than oblique.

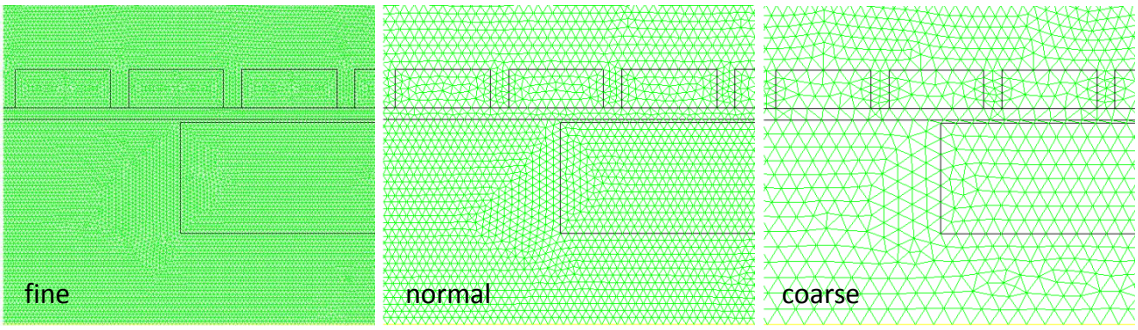

Figure 29: Meshes used in FLUENT grid convergence study

Table 2: FLUENT Mesh Statistics

PARAMETER	**Fine Mesh**	**Normal Mesh**	**Coarse Mesh**
Number of Elements	189466	45148	17398
Maximum Skewness	0.522856	0.519186	0.797827

Using each of the three meshes shown above, the same FLUENT case was run with the dynamic mesh motion disabled. The pressure adjust-function and heat sources were able to compute as normal. Plots of the temperature at the titanium-blood interface and of the outlet pressure are shown in the plot group below (Figure 30).

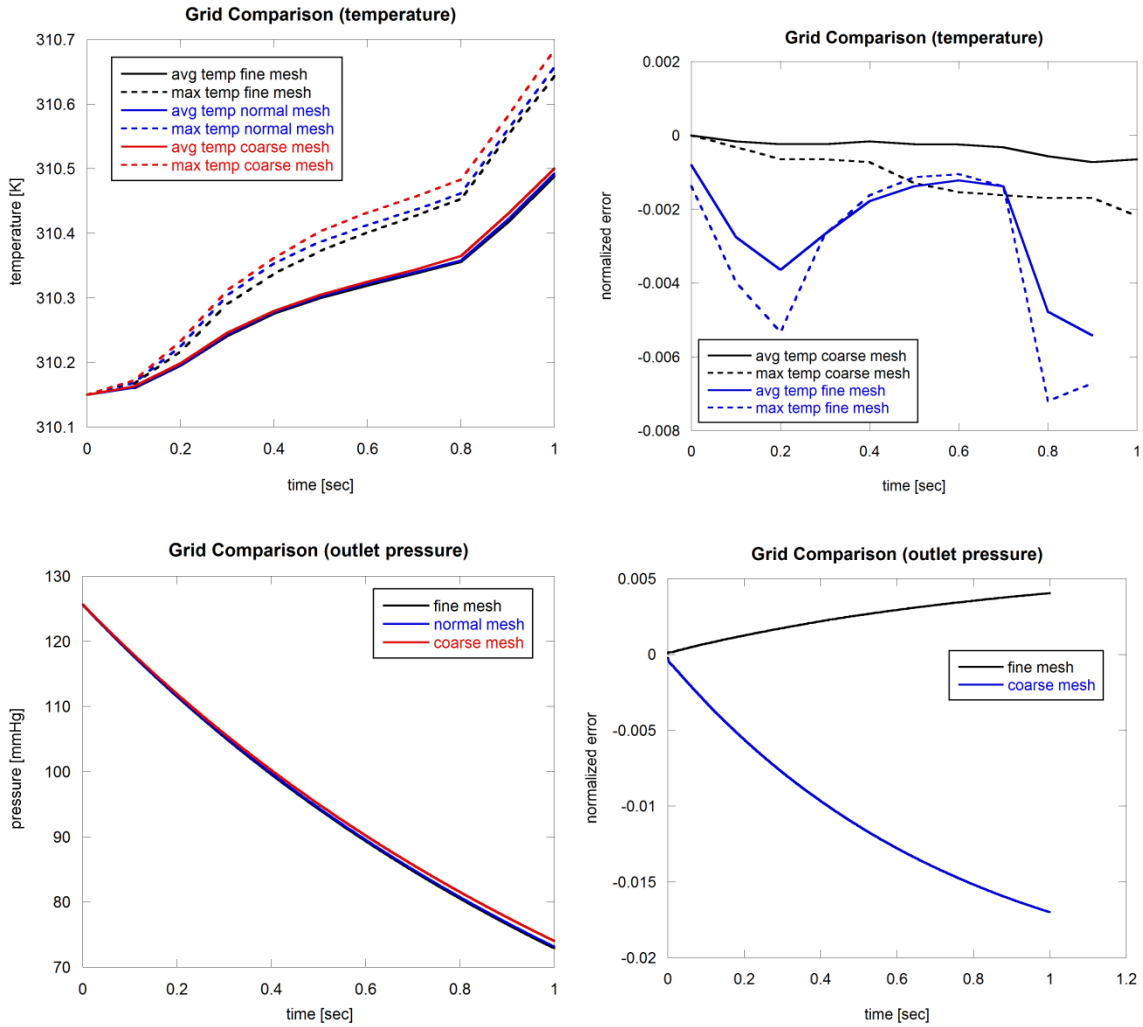

Figure 30: FLUENT data appears to be independent of grid spacing

There is more variability in the pressure and temperature data for the different meshes than seen in the time step comparison cases. With the dynamic mesh disabled, the shuttle remains in one location, and all of the flow must go through the gap. The coarser meshes do not resolve the gap fully, and the velocity is underestimated, which slows the rate at which the compliance chamber pressure bleeds down. The reduction in velocity also means less heat is convected away from the titanium by the blood, leading to slightly higher temperature values.

The differences in value obtained on the different grids are very slight, and so it can be assumed that results obtained using grids with spacings between those tested above will not have

any appreciable effect on the solution. This is especially encouraging because the dynamic mesh can be set to remesh cells that fall outside a user specified minimum and maximum size. From casual observation, these size bounds are not strictly enforced, but the sizes should still fall within the range of sizes studied here.

Pressure Comparison

The pressure computed in the FLUENT model should be compared to the pressure from the flow loops to verify that the resistance and compliance values are properly calibrated, especially since these parameters adjust the LAPP outlet pressure via a user defined function,. As discussed in detail in the 2009 Thesis *Hydrodynamic Effects of Left Ventricular Assist Device Implantation: a numerical and experimental approach* (Holley Love, University of Houston), the systemic resistance can be approximated by analogy to Ohm's law as the quotient of mean aortic pressure and average flow rate (Nichols and O'Rourke, 2005),

$$R_s = \frac{P_{mean}}{Q}, \qquad \text{Eq. 1}$$

where R_s is the systemic resistance, P_{mean} is the average aortic pressure, and Q is the average flow rate. With a value for systemic resistance, systemic compliance can also be estimated by analogy to electric circuits (Li, 2000):

$$C = \frac{t_d}{R_s \ln(P_{\max} / P_{\min})}, \qquad \text{Eq. 2}$$

where t_d is the time over which the decay in aortic pressure occurs, R_s is the systemic resistance, P_{max} is the maximum aortic pressure, and P_{min} is the minimum aortic pressure. Neither of these estimates is appropriate for a real patient (Nichols and O'Rourke, 2005 and Battegay et al., 2005), but they are representative for the Mock Circulatory Loop and FLUENT model where the body's distributed resistance and compliance have been captured in two discrete elements.

A plot of the outlet pressure is shown in Figure 31 below. The shape is similar to the data collected in the flow loops, but the curve is smooth with no ringing because the fluid inertia is not

included in the FLUENT model. The amplitude is smaller, partly because of the missing inertia and partly because the *requested* ejection volume in the Mock Circulatory Loop is 50 *mL* per beat and the FLUENT simulation was made for an ejection volume of 45 *mL* per beat. Also, the locations at which the pressure is being measured differ slightly—the experimental pressure is measured within the compliance chamber, the FLUENT pressure is measured after the compliance.

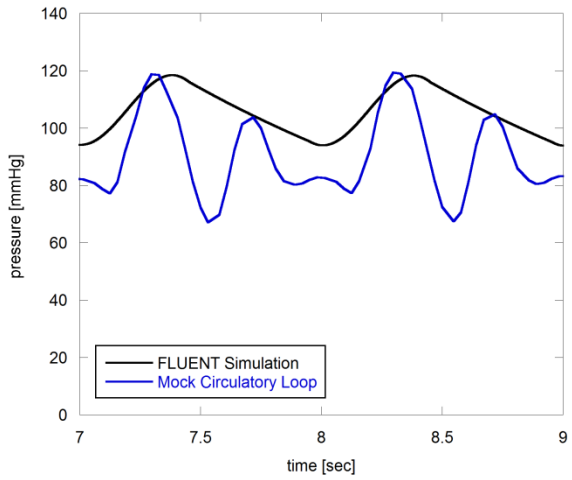

Figure 31: Comparison of aortic pressure in FLUENT and the Mock Circulatory Loop

It should be noted that the choice to compare to the Mock Circulatory Loop rather than the Hemolysis Testing Loop was a purposeful one. The Mock Circulatory Loop has been designed to mimic the characteristics of heart failure patients and allows better control over systemic resistance and compliance; it also has a mock-ventricle that beats similarly to an ailing heart, so the interaction between the LAPP and native heart can be studied. The Hemolysis Testing Loop has none of these features—it was designed to be comparable to the standardized loop for continuous flow ventricular assist device testing. Therefore, the FLUENT model was honed to match the former loop, since there is more utility in comparing to a patient's conditions than to a somewhat arbitrary standard. It is possible, nevertheless, to adjust the resistance and compliance values in the FLUENT model to match the Hemolysis Testing Loop, if desired.

The agreement between the experimental and simulated aortic pressures, though not exact, is acceptable for the level of study being attempted. The true purpose of the FLUENT model is to study the heat transfer aspects of the LAPP. The grid and time step convergence data relating to temperature indicate that the model is capable of resolving these fields and values.

COMSOL Model

As in the FLUENT model, the COMSOL solutions must be checked for grid and time step independence. However, instead of also comparing to pressure data, the COMSOL model should be compared to electromagnetic data. As described in detail below, magnetic field data was collected from a permanent magnet, and force data was collected from the electronic LAPP.

Magnet Comparison

A Hall Effect sensor (or Hall probe) can be used to measure components of the magnetic flux density (also called the **B** field) and verify that the magnetism has been applied properly in the COMSOL model. The Hall Effect refers to the production of a voltage across a conductor in a direction orthogonal to both an applied magnetic field and the current flowing through the conductor. In many sensing applications the voltage is calibrated so that magnetic flux density, and ultimately distance (or relative velocity) between the sensor and magnet, can be calculated.

For the present work, a Hall probe attached to a traverse system was held approximately 0.25 *inches* away from the annular face of a magnet. The probe was moved in a grid pattern, the voltage recorded, and the magnetic flux density calculated for each point. Since the magnet is axisymmetric, the axial and radial components of the magnetic fields are of interest. To get the second component, the probe orientation was then rotated 90˚, and the magnetic flux density was again sampled in a grid.

The resulting axial and radial **B** fields are shown in Figure 32 for an axially poled grade 42 neodymium iron boron magnet with 0.75 *inch* inner radius, 1 *inch* outer radius, and .5 *inch* length; the colorbar has units in Gauss, while the floor is gridded in inches. These compare with values predicted in COMSOL using a magnet of the same geometry with magnetic properties

obtained from the magnet manufacturer (K&J Magnetics, Philadelphia, PA). The axial and radial components of computed magnetic flux density at a distance of 0.25 *inches* from the magnet is shown in the plot in Figure 33; the colorbar has units of Gauss as in the preceding plot, but the lengths are given in millimeters. Note that the sign is switched for the radial solution relative to the data due to alignment of the Hall probe.

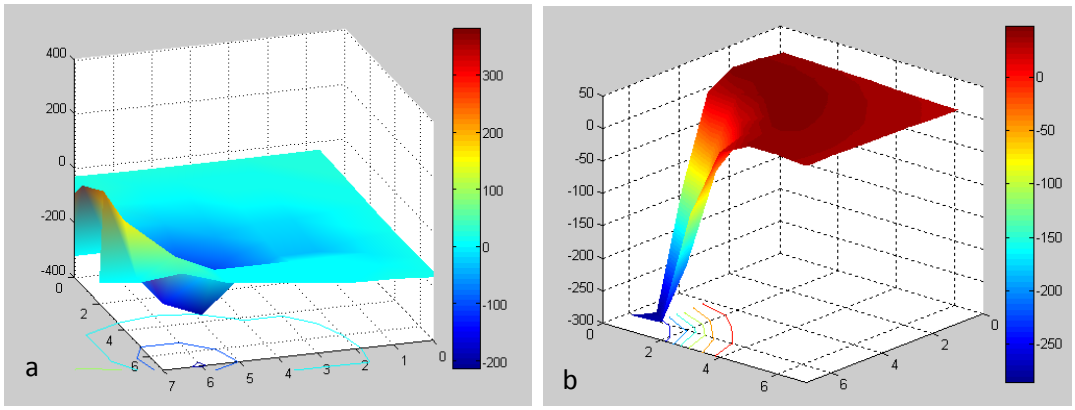

Figure 32: axial (a) and radial (b) magnetic flux density fields from Hall probe

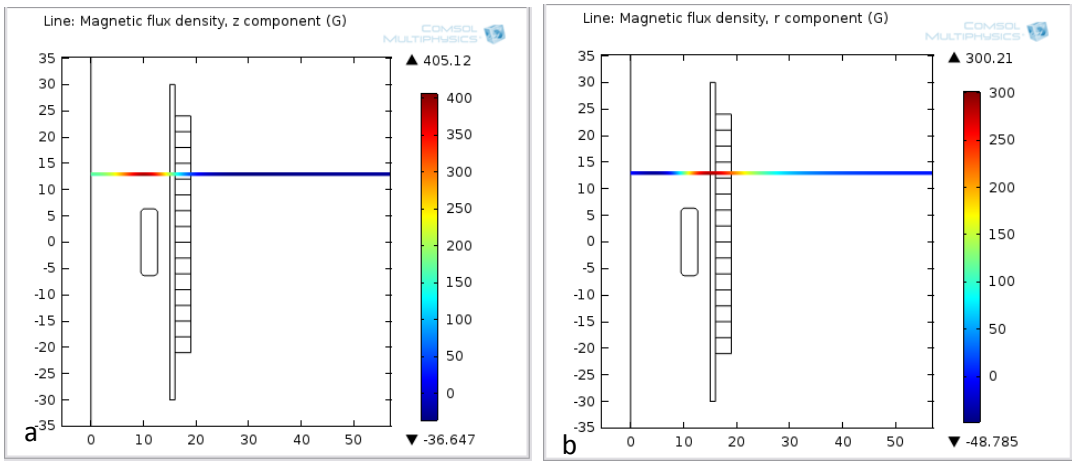

Figure 33: axial (a) and radial (b) magnetic flux density fields from COMSOL

Force Comparison

Related to the magnet strength, another aspect of the COMSOL model that needs verification is the amount of force that is generated by the windings when electrical current is

passed through them. This requires a special testing rig to obtain data from the LAPP to compare against.

A simple, though useful, method to gauge the coil force is to measure the deflection of a cantilever beam attached to the LAPP windings using a proximity probe. A photograph of the setup is shown in Figure 34. A specially made shuttle is screwed onto the thrust tube of a linear actuator; the long piece of Delrin™ is used to ensure that the metal thrust tube remains outside the LAPP coils and hence will not alter the magnetic field. Not only does the linear actuator keep the shuttle held firmly in place, it allows precise positioning of the shuttle within the coils, so that a series of readings can be taken along the length of the LAPP. After the shuttle is attached to the actuator, the LAPP field windings can be slid over the shuttle. To couple the LAPP body to the aluminum cantilever beam, the outlet pressure tap fitting was inserted into a hole in the beam. Care was taken to position and angle the beam so that the LAPP body would be able to move as freely as possible. In this horizontal orientation, some friction and torque (binding) is unavoidable, which will alter the beam deflection. A vertical arrangement or pivot would reduce these undesirable secondary forces, but the increased complexity of such a system did not seem justified by the anticipated improvement in the data.

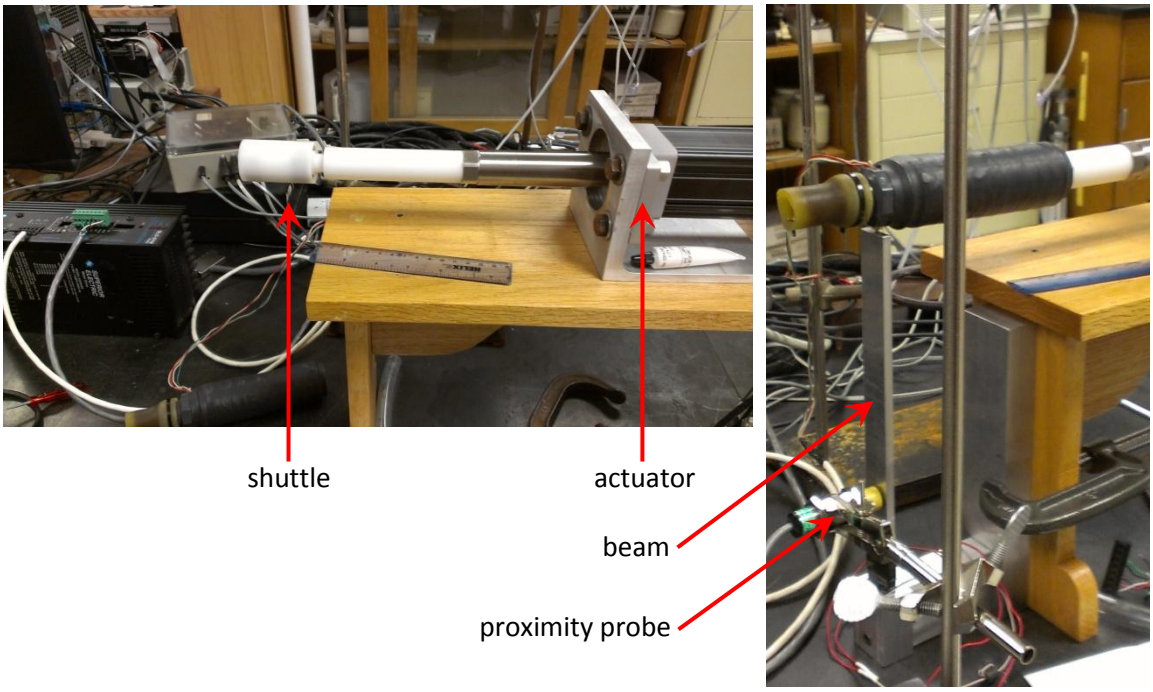

Figure 34: (a) a shuttle is attached to an actuator, while (b) the LAPP is coupled to a cantilever beam

The length of beam and placement of the proximity probe were adjusted so that the deflection seen by the probe remained within the probe's nominal sensing range. The probe was positioned roughly 2 *mm* from the face of the beam with the flat face of the probe parallel to the beam. A proximity probe was selected as a measurement device since it is able measure displacement with high resolution over relatively short distances without contacting what it's measuring, its "target." The sensor type used in the LAPP testing is an eddy current model. An oscillator within the probe body creates eddy currents (and hence magnetic flux) on the surface of the probe tip. When a metallic target near the probe tip is moved, the magnetic flux density seen by the probe changes. The probe is able to sense and convert these changes to an output voltage signal. The probe was calibrated so its output voltage could be converted from a displacement measure to a measure of the force causing the deflection.

With the shuttle inside the LAPP body, current was run through the windings just as if the shuttle were being used in one of the flow loops. If it could have moved freely, the shuttle's position would have mapped the sine wave

$$x(t) = \frac{stroke}{2}\left(1 - \sin\left(2\pi\frac{t}{hr} - \frac{\pi}{2}\right)\right), \qquad \text{Eq. 3}$$

where t is time and hr is the heart rate in Hertz. As it was, however, the shuttle remained stationary, and the coils were allowed to move slightly in response to the interaction of the shuttle and windings magnetic fields. This motion deflected the aluminum cantilever beam and was converted into an estimate of the axial force between the shuttle magnets and the LAPP field windings. A series of data taken at different positions within the LAPP is shown below in Figure 35. Each curve represents the average of five complete cycles at a given starting point measured relative to the end of the winding closest to the LAPP outlet. The heart rate was set to ten beats per minute to minimize any dynamic complications (like friction and back EMF) that might alter the force measurement.

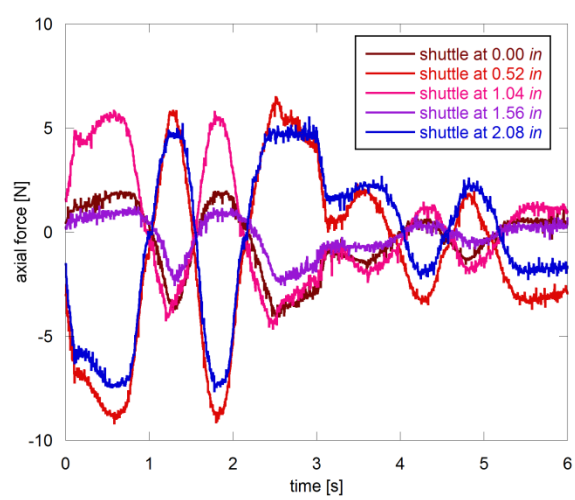

Figure 35: Axial force for several shuttle positions

The amplitude of the force changes from one curve to another depending on where the magnets are located relative to the windings, while the shape remains the same because the current waveform is unchanged. Two peaks occur in the first half of the cycle and two with

smaller magnitude occur in the second half. There are two peaks because the stroke length requested was 2.6 *inches*, which means the current wave-front will pass through one complete set of windings and half of another (each set of four windings is ~1.48 *inches*). The peaks are smaller in the second half of the curves because the current is reduced in this part of the cycle; when the LAPP is pumping, less force is required on the return stroke, so the driving current can be decreased. A sharp jump is seen at 3 *sec* where the current is reduced and the wave direction changes. The sign of the force in Figure 35 indicates whether the interaction between the shuttle and magnets is attractive or repulsive, and the magnitude indicates how far out of phase the magnets are relative to the current wave-front with larger magnitudes meaning more lagging (or leading).

The COMSOL model was adjusted to mimic conditions of the force experiment. The Moving Mesh physics interface was disabled, so the shuttle would be unable to move, but the current waveform and force calculations were the same as in the complete model wherein the shuttle moves in response to the magnetic field it experiences. A comparison of the axial forces when the shuttle is aligned with the last outlet winding is shown in Figure 36.

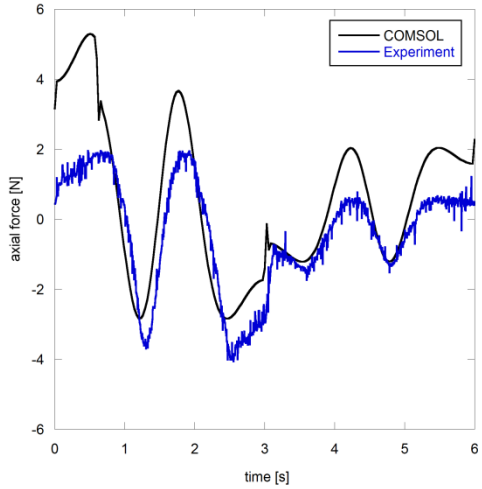

Figure 36: Comparison of the COMSOL model force and the experimental data

The data and simulations show close agreement except for a slightly increased in magnitude in the COMSOL result. This may be due to the fact that the coils are able to move slightly as the beam deflects; there is absolutely no motion in the COMSOL case. Additionally, as mentioned above, the cantilever setup did have some friction and torque, which might contribute to the smaller forces recorded. To achieve the match shown in Figure 36, the stroke was set to 2.6 *inches* and the shuttle location was aligned in the same way as the experiment. The other important parameter one needs is the starting phase of the current waveform. The current waveform equation can be written

$$I(t) = I_{set}\, c\, \frac{stroke}{2}\left(sin\left(offset + eq + \varphi + 1 - \frac{stroke}{\lambda} sin\left(2\pi t_{sin} - \frac{\pi}{2}\right)\right)\right), \qquad \text{Eq. 4}$$

where I_{set} is the normal current level (1 *Amp*), c is a factor controlling whether or not the current is boosted or reduced $\left(c = \begin{Bmatrix} 1.5\ if\ \frac{t}{hr} < \frac{1}{10} \\ 0.5\ if\ \frac{t}{hr} > \frac{1}{2} \\ 1\ otherwise \end{Bmatrix}\right)$, *offset* is the starting phase of the current waveform, *eq* is a phase shift accounting for the starting position of the shuttle, φ is the phase shift between a winding and its neighbors (φ=nπ/2, with n=0, 1, 2, or 3), λ is the wavelength of the windings (λ=1.48 *inches*), t_{sin} is a time such that $t_{sin} = \begin{Bmatrix} (t - int(t))\ if\ t \times hr \leq 0.5 \\ (hr - (t - int(t)))\ otherwise \end{Bmatrix}$ with t being simulation time and *int( )* designating the floor (or integer part) of *t*, and *hr* is the heart rate.

The current, boost/reduction, and stroke are specified when the LAPP is called to run, and the winding wavelength is fixed for a given LAPP. The offset was determined by measuring the voltage across the windings when the controller is powered on but before the LAPP begins to pump. Both phases showed the same voltage drop at initialization, indicating the same current was flowing through all the windings. A (2n+1)π/4 offset in the outer sine wave would give this behavior. A plot showing the variation in the force for different offsets—in addition to the (2n+1)π/4 values mentioned above—is shown below in Figure 37. The effect of the offset parameter is to change the spacing between the extrema in the force vs. time curve. Comparing

to the data, the $-\pi\lambda/4$ offset seems to give the closest match to the inter-peak spacing observed in the cantilever beam experiments. Smaller offsets tend to bring the peaks too close together, while larger offsets move the peaks too far apart. Because the offset is operating within a sine wave, symmetry is observed—for a given offset value, adding $\pi/2$ will reproduce the force curve's magnitude but the sign will be opposite (*cf*. the black and purple curves in Figure 37).

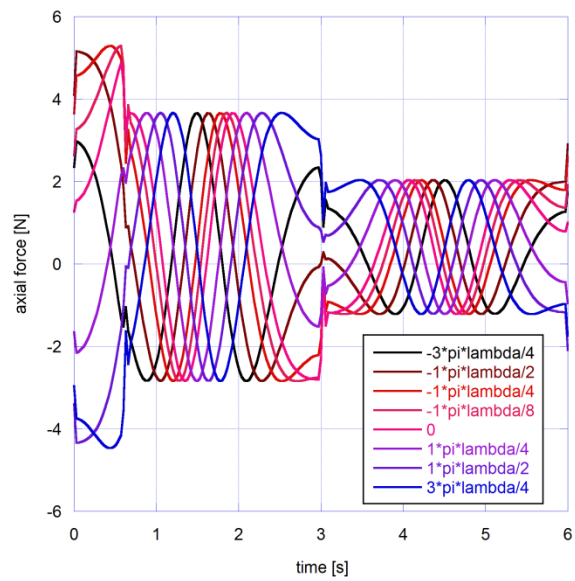

Figure 37: The offset parameter controls the peak force timing in the COMSOL model

The final parameter in the current waveform to be set is *eq*, the phase shift required for the shuttle to be initially at equilibrium. Without this shift, the simulated shuttle will tend to move rapidly towards its "lock in" point, where the force it experiences from the coils and pressure is minimized (a potential energy well). If the shuttle location is not near enough to this optimal starting position, it can move too rapidly for the mesh to adjust or the solution can become unstable. To find the value of *eq*, the full model is run with the current and pressure kept constant at their initial values. The shuttle will move in response and will settle into an equilibrium position. This position can be interpreted as a spatial phase shift in the travelling sine wave, so the new position normalized by $\lambda/2\pi$ is the value of *eq* in the current equation above. A

plot of the position during this procedure is shown in Figure 38. Changing the physical starting point of the shuttle or the pressure waveform will change the value of *eq*.

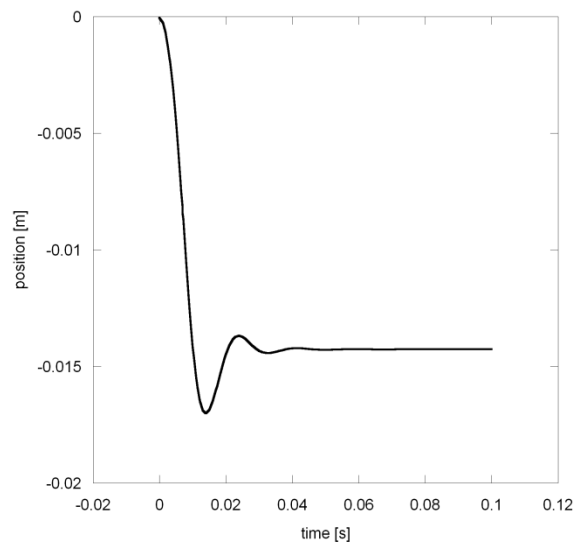

Figure 38: After a few time steps, the shuttle comes to an equilibrium position

The match between the forces generated in the COMSOL simulation and experimental test rig indicate strongly that the COMSOL model is correctly setup in regards to the magnet properties, the geometry of the coils and magnets, and the description of the winding current. The numerical model must still be recomputed using different time steps and grid spacing to ensure that the agreement is true in general and not just for the particular conditions chosen above.

Time Step Convergence

With the moving mesh disabled, time step convergence can be easily evaluated. Successful moving mesh models must carefully balance the time step and grid size to avoid running over node points and creating inverted mesh elements. This is, however, a separate issue from determining whether a given time step (or mesh spacing) is small enough to resolve the physics of the problem. Therefore, when the shuttle is held stationary, the computed velocity is a non-physical quantity but still must be checked for convergence, since it is calculated by the ODE Interface. To call attention to the fact that the shuttle is not actually moving, the term pseudo-velocity will be used in these convergence tests.

The model was run with a 1×10^{-4} *sec* time step and a 1×10^{-3} *sec* time step; the computed pseudo-velocity and force data were compared. Figure 39 shows the agreement between the pseudo-velocity and pressure and coil forces; the left panels show the data generated at the two time step sizes, and the right panels show the difference between the larger and smaller time steps normalized by the amplitude of the waveform. Those time points whose values are more different occur near the points where the current boost and reduction take effect, at 0.1 *sec*, 0.5 *sec*, and 1.0 *sec*.

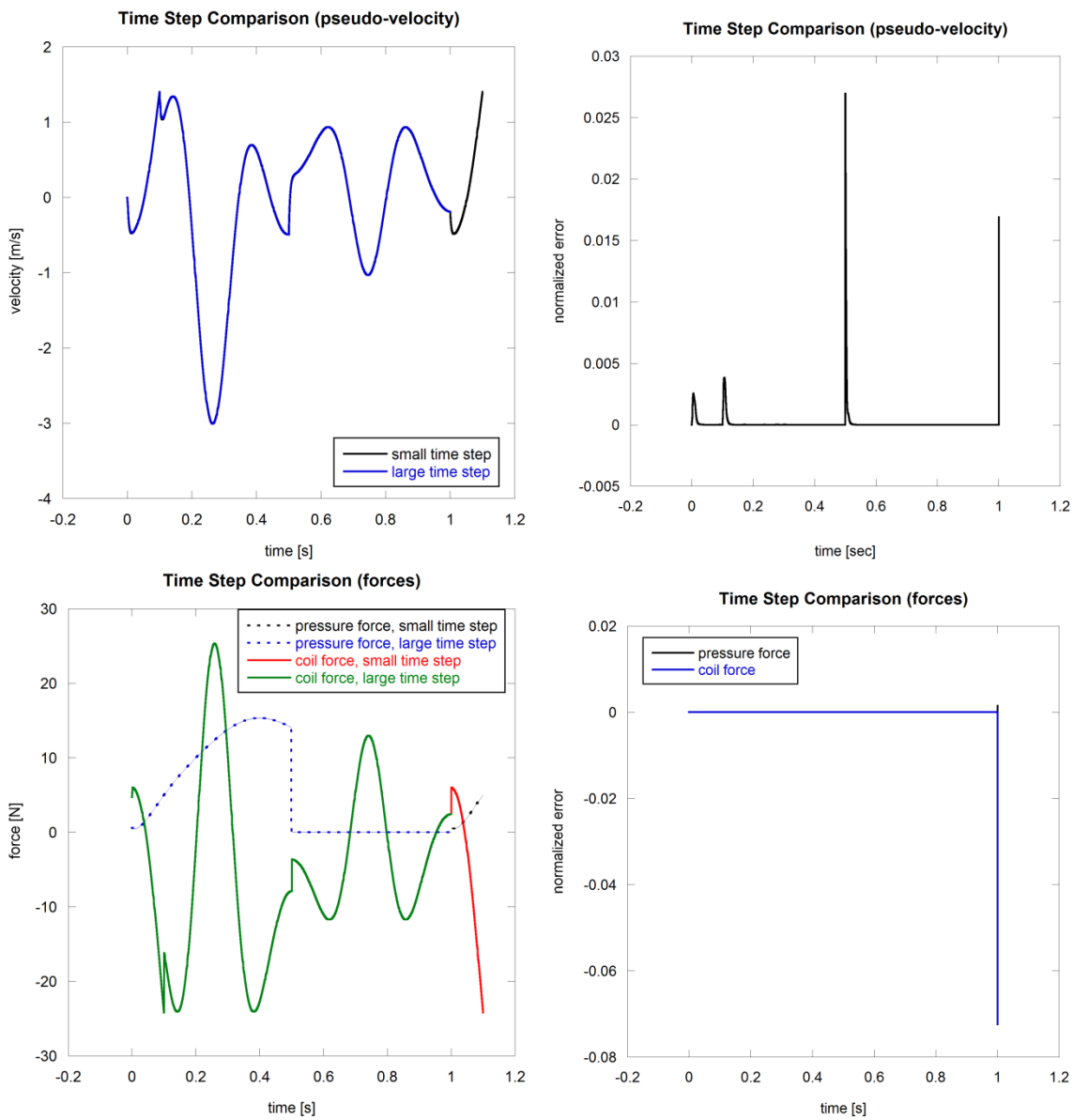

Figure 39: COMSOL data appears independent of time step size

This variation in pseudo-velocity is probably a result of the way the step change in current and pressure are implemented—slight errors in the time could cause the switch to happen a step late. For instance, if the computation time is 0.0099999 instead of 0.0100000, the current will not switch off of the boosted level until the next time step, which might be 0.0199999. The accordance of the forces and pseudo-velocity at the large and small time steps is however, quite good and implies that the solution is independent of the time step over this range of sizes, namely 0.0001 to 0.001 *sec*.

Mesh Convergence

Again disabling the Moving Mesh Interface, the effect of the computational grid spacing was verified. Three grids were generated: one that works with the moving mesh (US), one with all those mesh spacings cut in half (HS), and one with the mesh spacings doubled (DS). The three grids are shown in Figure 40. Mesh statistics for each are given in the table below.

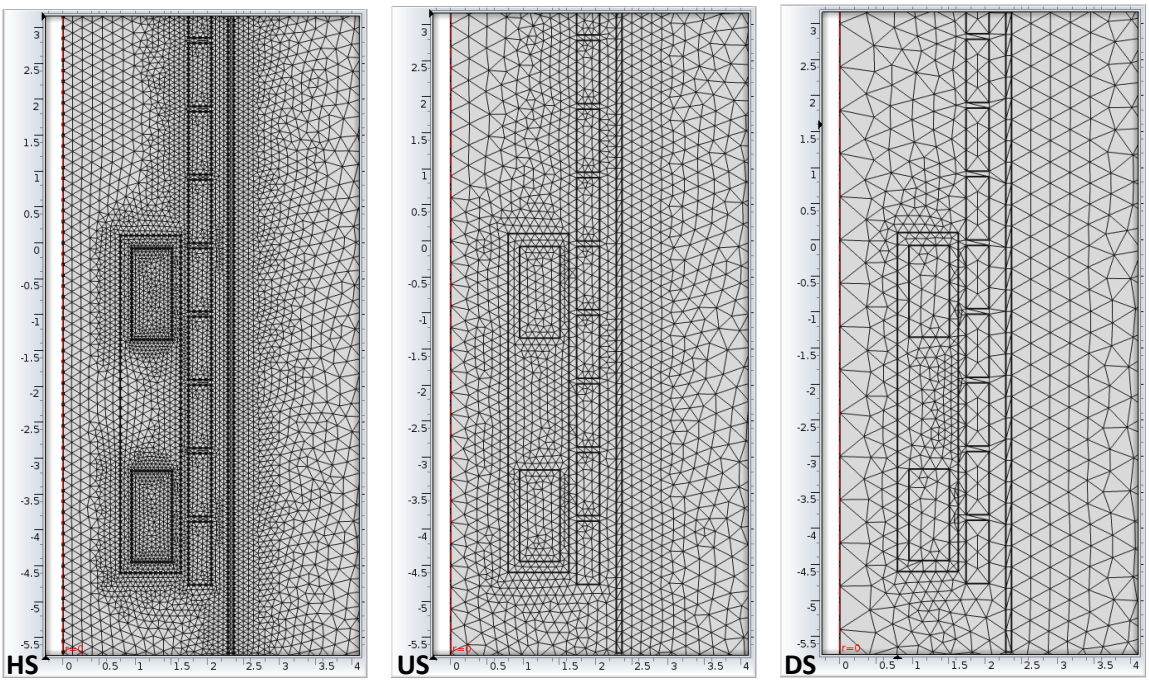

Figure 40: Three computational meshes used to check for grid independence

Table 3: COMSOL Mesh Statistics

PARAMETER	**HS Mesh**	**US Mesh**	**DS Mesh**
Number of Elements	19543	7372	3039
Minimum Quality	0.6942	0.5728	0.1381
Average Quality	0.9644	0.9476	0.9093

Using a time step of 1×10^{-4} *sec*, the COMSOL model was run with the mesh motion disabled. Pseudo-velocity and pressure and coil force for the three grids are plotted in the left panels of Figure 41, and the difference relative to the US grid normalized by the amplitude of the curve is shown in the right panels. As with the time step, there is close agreement between all three grids (values for the HS and DS meshes are within five percent of the US case normalized by the amplitude of the curve).

Also as before, most of the variation in the velocity occurs where the current or pressure make a step change in value. There is a larger variation overall, however, due to the resolution of the gradients. When more mesh nodes are available, spatial changes of a given parameter can be computed more accurately because the finite difference formulation approaches the true derivative as the node spacing tends toward zero. As mentioned above, computationally there is a lower bound in mesh size past which truncation errors dominate, but the grid spacings used here are well above that. The magnitude of the forces computed from the coarse mesh is smaller than that from the fine mesh (relative to the US mesh) because the sharp gradients in the magnetic flux density are smeared out as the grid spacing increases. The steep gradients are responsible for keeping the magnets locked in phase with the magnetic field generated by the coils.

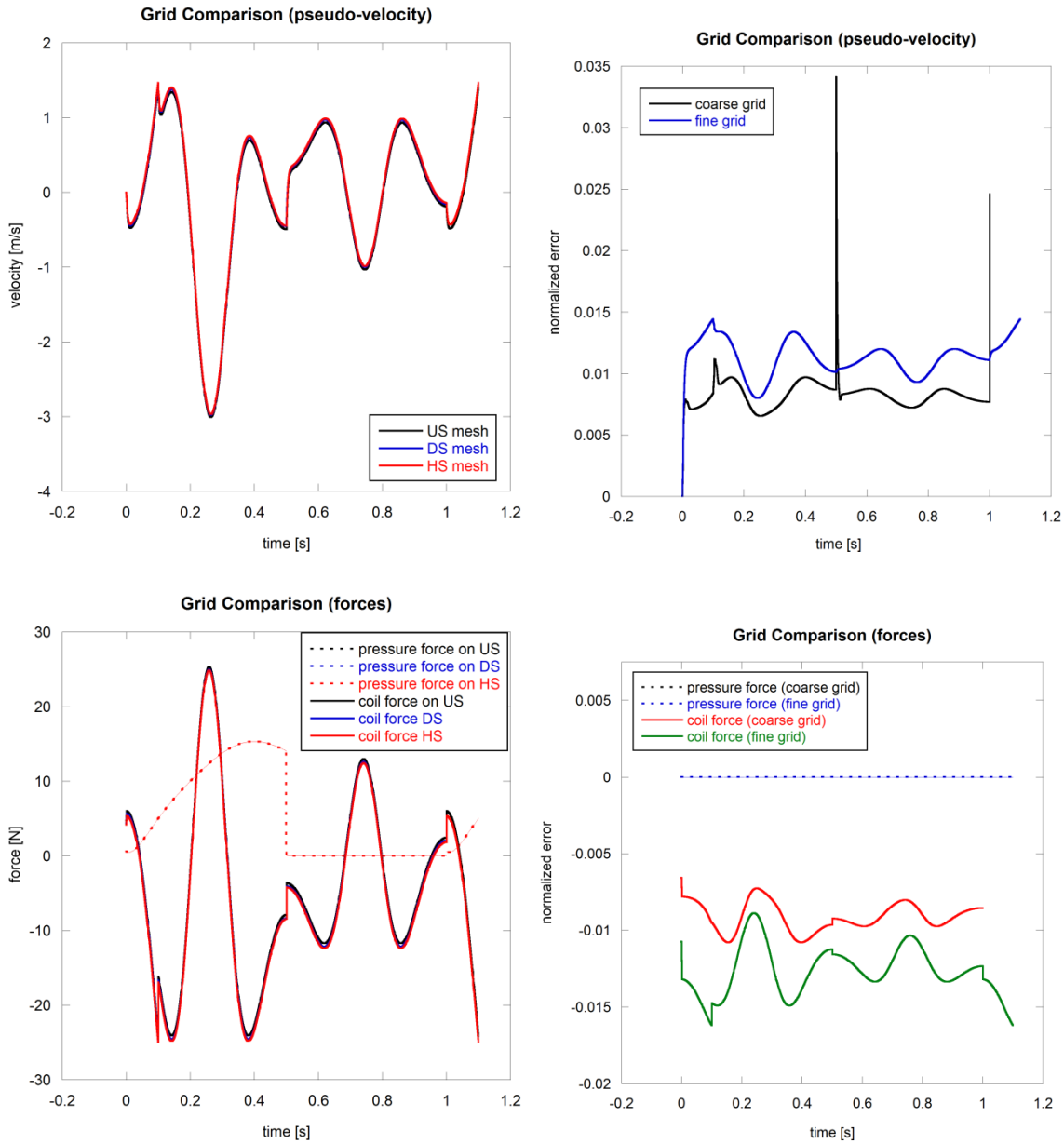

Figure 41: COMSOL data appears to be independent of grid spacing

The mesh and time step convergence results taken with the comparison to the experimental magnetic flux density and force data make a compelling case that the COMSOL model is an accurate tool for guiding the LAPP's development and for investigating topics that may be difficult to delve into experimentally, like testing new magnet and coil geometries.

CHAPTER 4: Numerical Results and Discussion

The goal of this dissertation work was to design, craft, and test a functional linear pump suitable for use as a heart assist device; the FLUENT and COMSOL models were developed alongside to meet this goal by identifying ways to improve functionality, often by means of a parametric study. The results from the numerical models presented below were chosen to highlight the capabilities of those models as predictors of overall trends—guides for the general changes one would expect from varying parameters of interest. The models have not been refined to the degree that they are replacements for performing physical testing, but they are useful in determining whether or not a given parameter change would enhance LAPP performance.

Fluid Mechanics and Heat Transfer

Gap Estimation

Flow through the gap between the outer surface of the shuttle and the inner surface of the titanium tube can be approximated by a Poiseuille-Couette flow—flow between long parallel plates driven by both a pressure gradient and wall motion, respectively. The height of the gap is small relative to the radius of the shuttle so that the geometry can be approximated as flat. Also, the length of the shuttle is long relative to the gap height, so edge effects at the gap inlet and outlet can be neglected. With these assumptions, one can write the flowrate through the gap as

$$Q \approx \pi\left(r_o^2 - r_i^2\right)\left(u_s\left(1 - \frac{y}{h}\right) + \frac{h^2}{2\mu}\left(\frac{dp}{dx}\right)\left(\frac{y^2}{h^2} - \frac{y}{h}\right)\right), \qquad \text{Eq. 1}$$

where r_o is the inner radius of the titanium tube, r_i is the outer radius of the shuttle, u_s is the velocity of the shuttle, , h is the height of the gap, μ is the dynamic viscosity, dp/dx is the pressure gradient across the length of the shuttle, and y varies from 0 to h.

If one is interested in the average flowrate through the gap, the above equation can be simplified. The cross-sectional area can be approximated by $2\pi r_o h$. The average velocity in the

gap over a complete cycle is zero because the shuttle moves sinusoidally between two fixed points. So, evaluating the expression above at the mid-point of the gap ($y=h/2$), one obtains

$$Q \approx 2\pi r_o h\left(\frac{h^2}{2\mu}\left(\frac{dP}{dx}\right)\left(\frac{1}{2}\right)\right) = \frac{\pi r_o h^3}{2\mu}\left(\frac{dP}{dx}\right). \qquad \text{Eq. 2}$$

The inner diameter of the titanium tube is 1.32 *inches* (0.0335 *m*), and the outer diameter of the shuttle used in the second electronic LAPP hemolysis test is 1.3145 *inches*; the gap is therefore 0.00275 *inches* (7×10^{-5} *m*). A representative average pressure difference across the shuttle running at 60 beats per minute in the Mock Circulatory Loop is 61 *mmHg*, so for a shuttle 2.1875 *inches* long, the average pressure gradient is 1.46×10^{5} *Pa*. With these parameter values and a blood viscosity estimate of 0.004 *Pa·s*, using the formula noted above, the predicted average flowrate through the gap should be roughly 0.02 *L/min* (3.29×10^{-7} m^3/s). This leakage value is less than one percent of the total flow through the LAPP, if operating at 5 *L/min*.

Such a low level of leakage is acceptable and desirable because fluid in the gap will tend to keep the shuttle centered in the titanium tube, and the shear stress is less than if the shuttle were to fit tightly in the tube; lower shear translates to lower blood damage. Additionally, since the coefficient of linear thermal expansion of Delrin™ is much larger than that of titanium (~68×10^{-6} *in/in/°F* [DuPont literature] versus ~4.8×10^{-6} *in/in/°F* [Engineering Toolbox]), the gap gives some margin for expansion if the blood temperature increases, reducing the chance that the shuttle may seize if the windings are generating too much heat.

Shape of Shuttle

Because the shuttle must travel in both directions along the axis of the titanium tube, one could argue that the ideal shuttle shape would be symmetric, since the leading and trailing edges of the shuttle are reversed as the shuttle completes each half ejection-cycle. Though using a streamlined edge at both ends of the shuttle would reduce the form drag experienced by the shuttle, the added length required to elongate and shape the shuttle ends would either necessitate a shorter stroke or a longer device. Therefore, in order to reduce the overall dimension and to have

the largest possible stroke, the shuttle was made symmetric with only a slight easing of the shuttle edges around the inner and outer surfaces. Photographs of the shuttle are shown in Figure 42; each of the two pieces of the shuttle in the left panel contains a magnet.

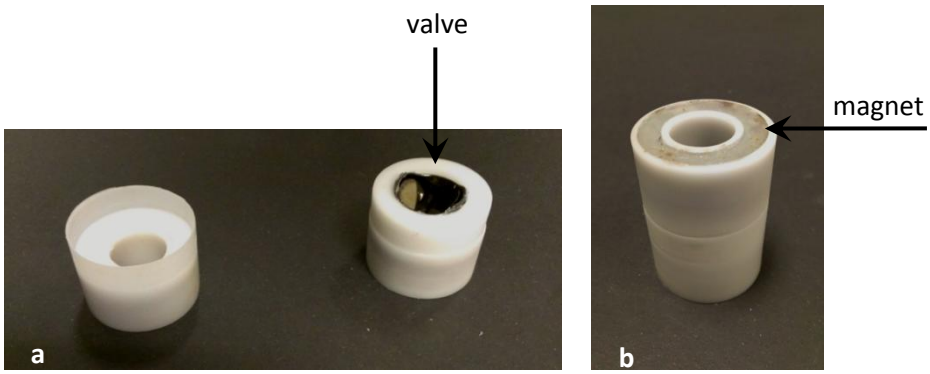

Figure 42: Photographs of the prototype shuttle (a) before and (b) after assembly

Heating

FLUENT was used to estimate the heat transfer from the coils to the blood flowing through the LAPP. As a worst-case boundary condition, the domain outside the LAPP was filled with stagnant air. If the LAPP were to be implanted, the body tissue would help distribute the heat much more effectively than stagnant air. Even if the LAPP were used extracorporally, a patient's movements and drafts in the room would enhance the heat transfer beyond this case. Thus the stagnant case can be used to define an upper bound for the temperature of the coils.

The inlet temperature of the blood was kept at 37.0 $^{\circ}C$ (310.15 K), which is the value specified in the Hemolysis Testing Standard. It is acceptable to use a constant inlet temperature, because this represents a condition where the heat lost through the tubing in the hemolysis loop balances the heat gained by the blood while passing through the LAPP. Such an arrangement is possible in the experimental flow loop by using a water bath and forced air cooling. The mechanism by which the blood cooling happens is not of interest, and so the inlet temperature is specified in lieu of modeling the entire flow loop.

The windings are heated in the FLUENT simulations by a Joule heating model, which describes the heat generated in terms of the electrical current and resistivity. Specifically,

$$\frac{Q}{\forall} = \left(c \times I_{set} sin\left(\varphi - \frac{stroke}{2\lambda}\pi sin\,(2\pi t * hr)\right)\right)^2 \frac{R_w}{\forall}, \qquad \text{Eq. 3}$$

where $Q/\forall$ is the volumetric heat generated per winding, c is the factor controlling whether or not the current is boosted or reduced $\left(c = \begin{Bmatrix} 1.5\ if\ \frac{t}{hr} < \frac{1}{10} \\ 0.5\ if\ \frac{t}{hr} > \frac{1}{2} \\ 1\ otherwise \end{Bmatrix}\right)$, I_{set} is the normal current level, φ is the phase shift between a winding and its neighbors (φ=nπ/2, with n=0, 1, 2, or 3), λ is the wavelength of the windings (λ=1.48 *inches*), t is the flow time, hr is the heart rate, R_w is the resistance of a winding, and $\forall$ is the volume of that winding. The material properties are kept constant; there are no density, viscosity or resistivity changes with temperature. The temperature field is initialized to 310.15 K (37 $^{\circ}C$) over the entire domain.

The initial heating solution was computed for a slightly smaller LAPP than the final prototype. The winding wavelength was 1.25 *inches*; the overall length of the titanium and shuttle was also shorter. Additionally, the current was not boosted or reduced (c=1 for all times). The average, minimum, and maximum temperature on the blood contacting surface of the titanium tube is presented in Figure 43 below.

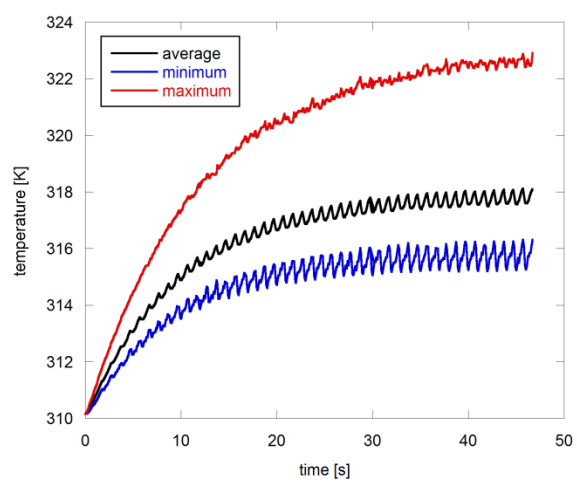

Figure 43: Temperatures increase in time on the titanium surface

As the windings heat, the temperature of the titanium increases in an exponential way. Because of the flow field within the shuttle, however, the rise is not steady. As the shuttle is ejecting fluid, the titanium temperature increases. After the valve switch halfway through the cycle, the titanium cools. At early times, the rise in the first part of the cycle in greater than the cooling, but after long times the rise and fall are balanced so that the temperature oscillates about a fixed point. The final average temperature for the small LAPP with constant c value and stagnant air behind the coils is 322.55 K (49.4 $^{\circ}C$; 120.9 $^{\circ}F$). This value would be lower if the stagnant air were circulated, or better yet replaced with a medium with higher heat conductivity. Because of the body's high water content and fluid circulation, it is expected that a patient's body would be able to dissipate much of the winding heat.

Still, the temperature rise at constant current is undesirable. To reduce the heat generation, schemes to reduce the current over parts of the pumping cycle were explored. Since current boosting and reduction are both available on the motor control unit, it was decided to boost the current during the initial acceleration phase of the pumping cycle, maintain normal current for the remaining ejection phase, and use reduced current for the shuttle return stroke, where the pressure across the shuttle is small. If one models the final LAPP prototype geometry with the boosted and reduced current, the temperature is lower than in the above case, as shown in Figure 44. This behavior is expected because the heat generation depends upon the square of the current. The boosted current (c=1.5) increases the heat generation 2.25 times but lasts over only one tenth of the cycle; the reduced current (c=0.5), in contrast, will reduce the heat generation by a factor of four during half of the cycle. It should also be noted that the use of current boost increases the maximum pressure rise the pump can produce by about 50%.

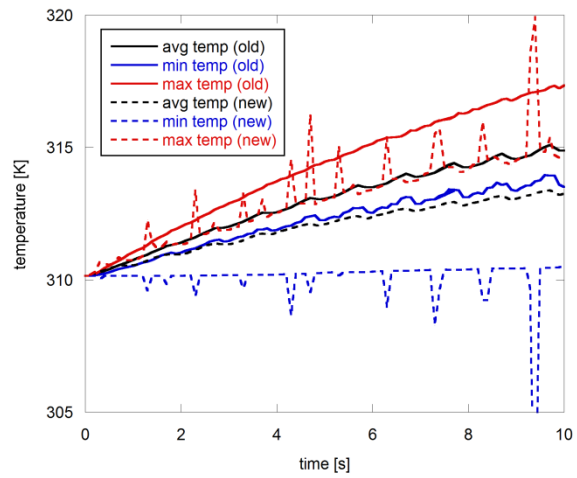

Figure 44: Temperature rise comparison for old and new LAPP geometries and currents

Spikes are apparent in the minimum and maximum temperature curves and probably result from a low quality mesh point. The average temperature, however, appears unaffected by these spurious points. The projected final average temperature on the titanium surface is a couple of degrees cooler in the new case relative to the old, and its oscillation amplitude is also expected to be smaller. The longer LAPP with the boosted and reduced current is clearly an improvement over the earlier prototype in terms of the operating temperature.

A final interesting result from the FLUENT model is that the windings do not heat evenly. This was particularly noticeable in the original model with a (constant c=1) when a 2.0 *inch* stroke was used. Partly because of the fluid mechanics and partly because of the way the current varies, in windings at the inlet end became hotter than those at the outlet end. A contour plot made at 46.75 *sec* is shown below (Figure 45). Every other winding is hotter than its neighbors because the square of the current remains at higher values longer in these windings. A plot of the square of the current in the windings is shown in Figure 46. If the windings are numbered sequentially starting from the left most, the odd numbered windings will have the same heat generation rate. The even numbered windings will also have the same heat generation rate,

but the average value will be lower, so they rise to a lower temperature than the odd windings (*cf.* Figure 45).

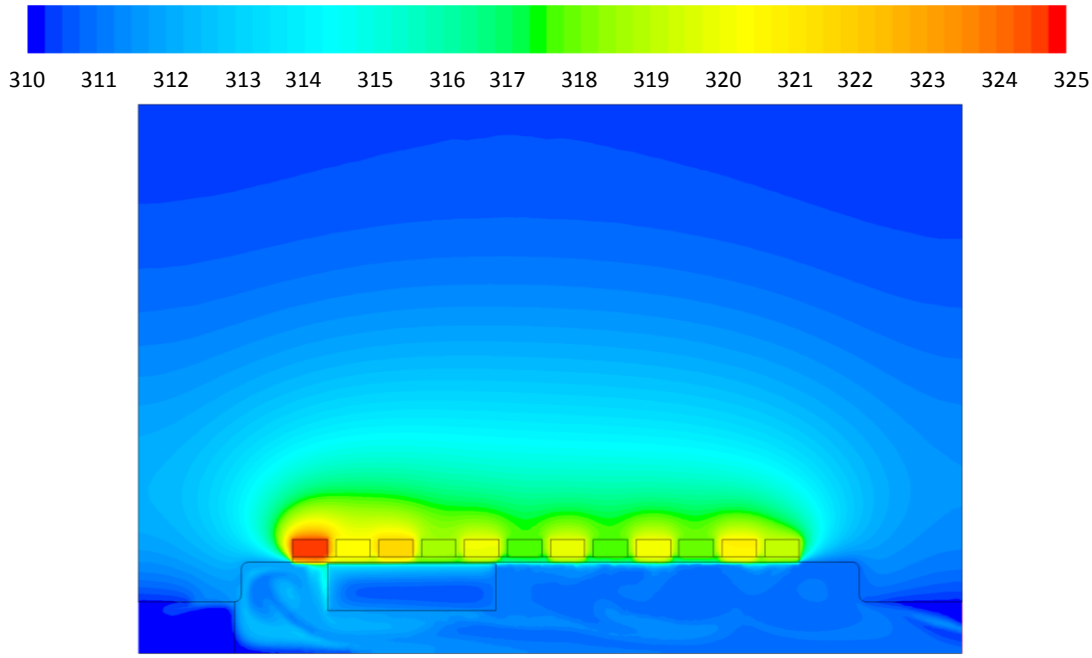

Figure 45: Contours of static temperature at 46.75 *sec*

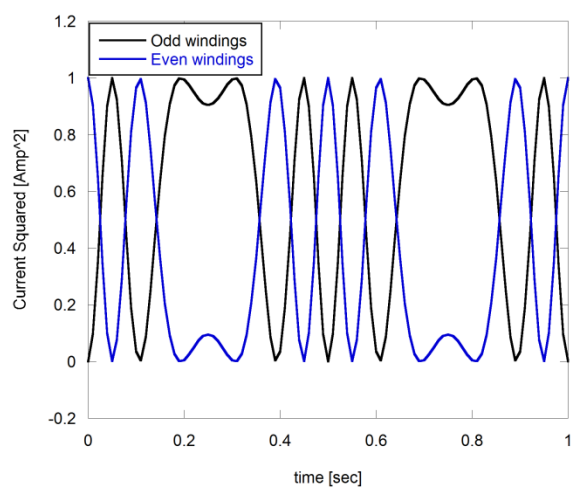

Figure 46: The square of the current is higher overall in the odd windings

Looking back again at Figure 45, one sees the first winding is significantly hotter than all the others and the twelfth winding is a bit hotter than the tenth. These windings are located above

regions in the LAPP that are prone to separation. Fluid dwells next to the titanium longer in these corner regions with a low velocity, so the convective heat transfer is less here. The shuttle also has a slight insulating effect, which is visible by comparing the windings directly above the shuttle in Figure 45 to their counter parts further to the right. Because of the sinusoidal motion, the shuttle velocity is low at the ends of the stroke, so the first few and last few windings end up being covered for relatively longer times, which increases their temperature slightly.

It is important to be aware that the certain combinations of stroke and winding length can produce uneven temperature distributions in the windings. When possible, the average heat generation rate should be the same for all of the windings to reduce thermal stresses on the blood as it travels through the LAPP.

Electromagnetics

Full COMSOL Model

When the Moving Mesh Module is enabled in the COMSOL model, the shuttle and magnets will move in an effort to balance the electromagnetic interaction of the magnets and the coils, the fluid pressure force acting against the shuttle, and a viscosity-like damping term. The position and velocity of the shuttle for 1.1 cycles are shown in Figure 47. Overall, the shuttle position follows the requested cosine profile. The shuttle takes a jump at $0.5\,sec$ when the pressure force is removed. In the experimental case, the LAPP valves switch at this point, and the pressure difference across the shuttle is negligible throughout the rest of the cycle. Therefore, in the COMSOL simulation, the pressure force is set to zero for $0.5 \leq t \leq 1.0$. When the retarding pressure is suddenly removed, the shuttle rapidly advances toward (and slightly overshoots) the new balance point.

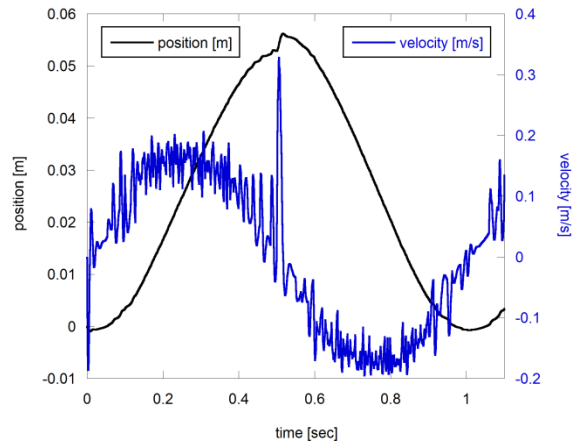

Figure 47: Shuttle position and velocity computed by COMSOL

The position vs time trace is much smoother than the velocity vs time trace because some of the noise is integrated out in the computation of the position. The velocity curve is jagged because the magnetic force curve used in its calculation is jagged. The shuttle force is shown below with the negative of the coil force and the negative of the pressure force. The negatives of the pressure and coil force have been plotted to facilitate comparison of the magnitudes of the forces.

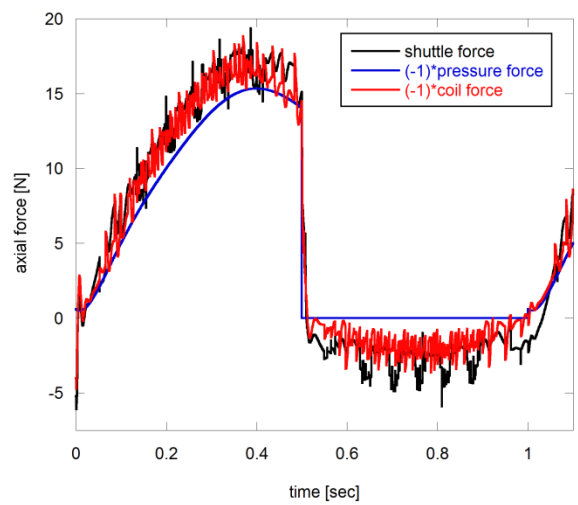

Figure 48: Forces in the COMSOL model with Moving Mesh

The pressure force is smooth because it is calculated from a polynomial fit to experimental pressure data collected in the Mock Circulatory Loop. The value drops to zero at 0.5 *sec* as mentioned above. Even though the LAPP pressure gradient is non-zero, the pressure gradient across the shuttle is very close to zero because the shuttle valve is open. At 1.0 *sec* the pressure picks up again. In the flow loop, the pressure peaks slightly after the maximum velocity due to inertia and begins to drop as the shuttle decelerates.

The coil and shuttle forces are very spikey. Within the shuttle force curve, large peaks occur when the magnets reach a new winding. The reasons for the underlying oscillations in the coil and shuttle forces are unknown. These results might be a dynamic instability in the problem or it could be numerical in nature. The shuttle and coil force were smooth in the simulations where the shuttle was not allowed to move. The magnitude of the forces in these stationary force studies closely matched the data taken using the cantilever beam. However, when the shuttle is allowed to move, the forces become unstable. The model results presented here had to be run at a 10 *Amp* current (rather than the 1.0 or 1.5 *Amp* current used in the hemolysis testing loop) because if the shuttle force dropped below the pressure force, the shuttle would be driven back. This phenomenon where the shuttle drops back a winding is observed experimentally, but the pressure difference required to cause a skip is higher.

Despite the instabilities in the forces, the motion of the shuttle is correct, and the underlying shapes of the forces seem correct. For these reasons, plus the close agreement to testable parameters (force when shuttle is stationary, shape of the back EMF curve (see below), etc), the COMSOL model can be considered a useful predictor in gauging the trends in force and displacement when the geometry or driving current waveforms are changed. The ability to quickly assess whether an adjustment will enhance LAPP performance is helpful when optimizing device operation and for performing extension studies like the two presented below.

Back EMF Estimation

The back (or counter) electromotive force (EMF) is an important quantity in electric motor operation. As a magnet moves near a conductor, eddy currents are induced in the conductor. These currents set up a magnetic field opposing the changes wrought by the motion of the magnet. The currents in turn generate a voltage, or EMF. This type of EMF is called counter or back EMF because it is acting against the changes induced by the changing magnetic field. The back EMF is calculable by a combination of Faraday's and Lenz's Laws. It can be shown that

$$EMF = \frac{-L}{A} \int E_{\varphi} \boldsymbol{dA}, \qquad \text{Eq. 4}$$

where E_{φ} is the azimuthal component of the electric field, A is the cross-sectional area of the winding, and L is the length of the wire in the winding. Back EMF can be used to estimate the speed at which the shuttle is moving, so understanding and predicting the EMF is important for controller design.

For the LAPP, the EMF can be measured directly. The coils (with no current imposed) were held in place and the specially made shuttle was moved through the LAPP body (photograph reproduced from Figure 34 (a) as Figure 49 below). The same motion profile was used to move the actuator as is used to move the shuttle, since the back EMF is produced in proportion to the velocity.

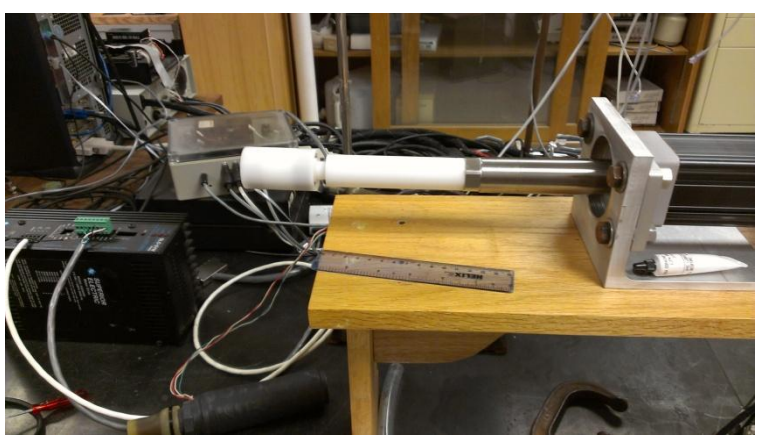

Figure 49: Specially made shuttle is attached to the linear actuator to gather EMF data

The EMF can be calculated in the COMSOL model using the formula given above. The magnets are moved dynamically in a sinusoidal motion. In the experimental system, the LAPP's windings are all wound in the same direction, so every other winding block is connected in series head-to-head and tail-to-tail. A schematic of the connections is shown below. Note that the LAPP has an additional four windings—these would be labeled 3A-3D and connected in the same manner; 3C and 3D go to the Controller). The letters indicate the phase shift: A-0˚, B-90˚, C-180˚, and D-270˚. Due to the way they are wound, the back EMF measured in the LAPP is for six windings. In the COMSOL model, the EMF is calculated for each winding—the A's, B's, C's, and D's, to use the convention of the schematic. The value for the C's and D's are then subtracted from the A's and B's, respectively, to account for the alternating connection direction in the LAPP. This value is the total EMF generated by all six of the windings that are connected together.

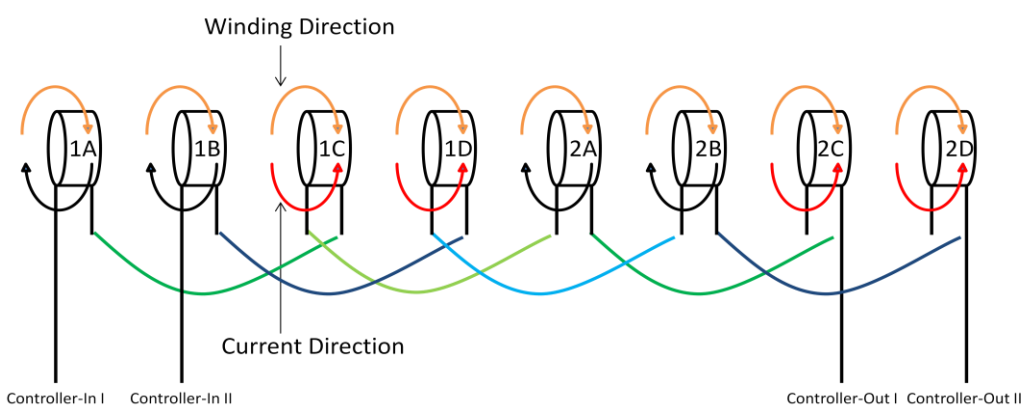

Figure 50: Schematic illustrating the LAPP winding diagram

A plot comparing the measured EMF and the simulation-predicted EMF is shown below versus time and velocity for the A-C winding set (Figure 51). Because the shuttle begins with zero velocity, the EMF at point **A** is zero. The shuttle begins to accelerate, so the EMF magnitude increases up to point **B**. The shuttle continues to accelerate in the same direction, but the EMF

begins to decrease as the shuttle magnets pass their first winding. At point **C** the magnets have reached their second winding and are travelling roughly twice as fast as they were at **B**, hence the magnitude of the EMF is twice as great. The shuttle continues to accelerate in the forward direction until the point halfway between **C** and **D**. Due to the geometry, the EMF happens to be zero at this point. The shuttle has begun to decelerate by the time it reaches **D**. The speed at **C** and **D** is the same, but the EMF sign is different because the magnets are aligned differently relative to the windings. The shuttle continues to decelerate to point **E**, where the velocity is equal to that at point **B**, but the winding-magnet orientation is again reversed. At point **F** the shuttle velocity is instantaneously zero before it begins to reverse direction and return to the starting point. Thus the second half of the waveform is the same as the first but with opposite sign because the shuttle is executing the same motion profile in the opposite direction.

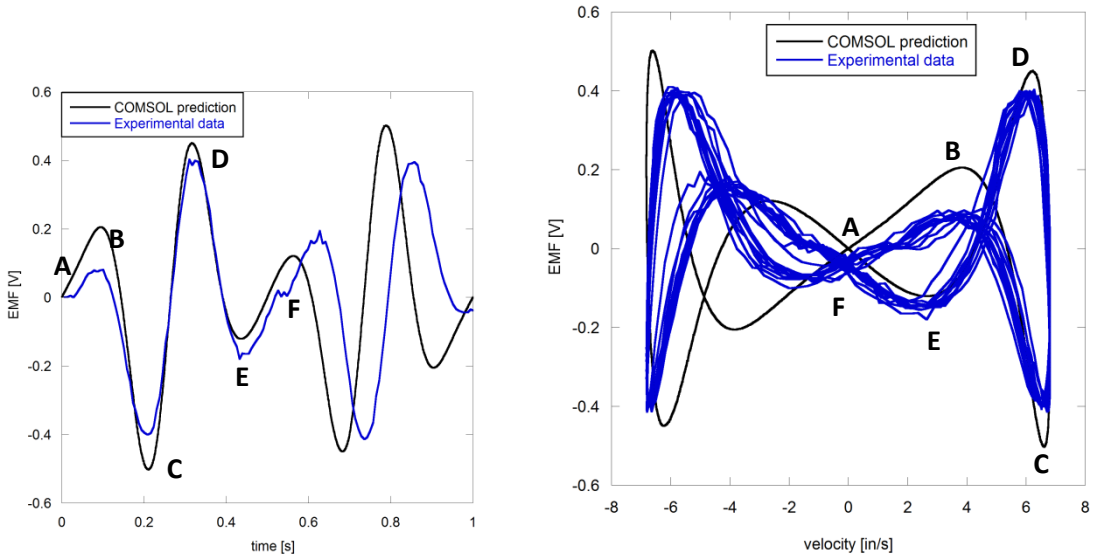

Figure 51: Comparison of EMF vs time (a) and vs velocity (b) for COMSOL simulated and experimental data

The discrepancies in the shape of the curves are most likely due to unevenness in the winding spacing. The briefly extended stay at zero EMF in the experimental data is probably due

to a combination of hesitation in the actuator as the direction changes and the location of the magnets relative to the windings.

High Permeability Shielding

A material with a very high magnetic permeability can be added to the outside of the LAPP to shield it from undesirable external magnetic fields. High permeability magnetic shields, often called μ-metals, are frequently made from blends of nickel and iron with proprietary proportions of copper, chromium, and/or molybdenum. The shield is effective because it is able to provide a low reluctance pathway for magnetic flux much like a ground wire provides a low resistance pathway for electrical flux. As a consequence of the shield's geometry and low reluctance, tends to straighten lines of magnetic flux density. If a thin tube of this material was added to the outside of the LAPP, it could make the surfaces of magnetic flux density have a stronger radial component and thus increase the interaction of the coils and magnets.

A μ-metal shield with a relative magnetic permeability of 8×10^4 was added to the force simulations with the stationary shuttle (*cf.* the Force Comparison subsection in Chapter Three for details). Plots of the force on the shuttle with and without the shield are shown in Figure 52. In the presence of this material, the forces were increased by up to eighteen percent. As commented above, this increase is due to the redirection of the magnetic flux lines. The force is calculated as

$$\boldsymbol{F} = \boldsymbol{i} \times \boldsymbol{B}, \qquad \text{Eq. 5}$$

where $\boldsymbol{F}$ is the magnetic force, $\boldsymbol{i}$ is the current in the wire, × represents the vector cross product, and $\boldsymbol{B}$ is the magnetic flux density. To get a force in the axial direction in the LAPP geometry, the magnetic flux density must be in the radial direction because the current in flowing the azimuthal direction.

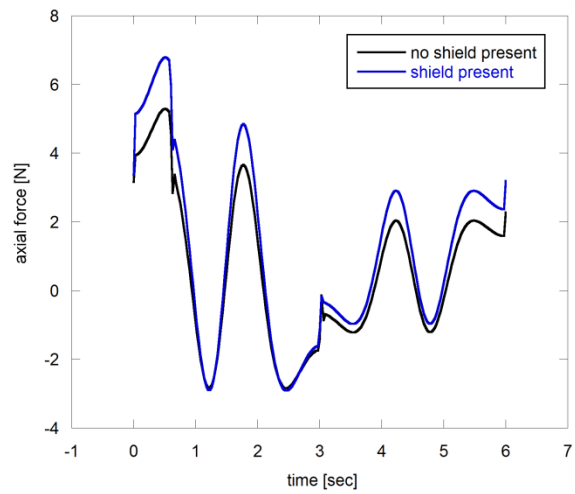

Figure 52: Addition of shielding can increase the shuttle force

When iso-contours of the magnetic flux density are examined (see Figure 53), the lines are indeed flattened more into the radial direction in the presence of the μ-metal. It should be pointed out that the geometry of the shield appears in both contour plots. In the case "without μ-metal," the material in the shield region is specified as air. Keeping the μ-metal geometry and changing the material property instead eliminates confusion about whether the changes being observed were caused by using a different computational mesh.

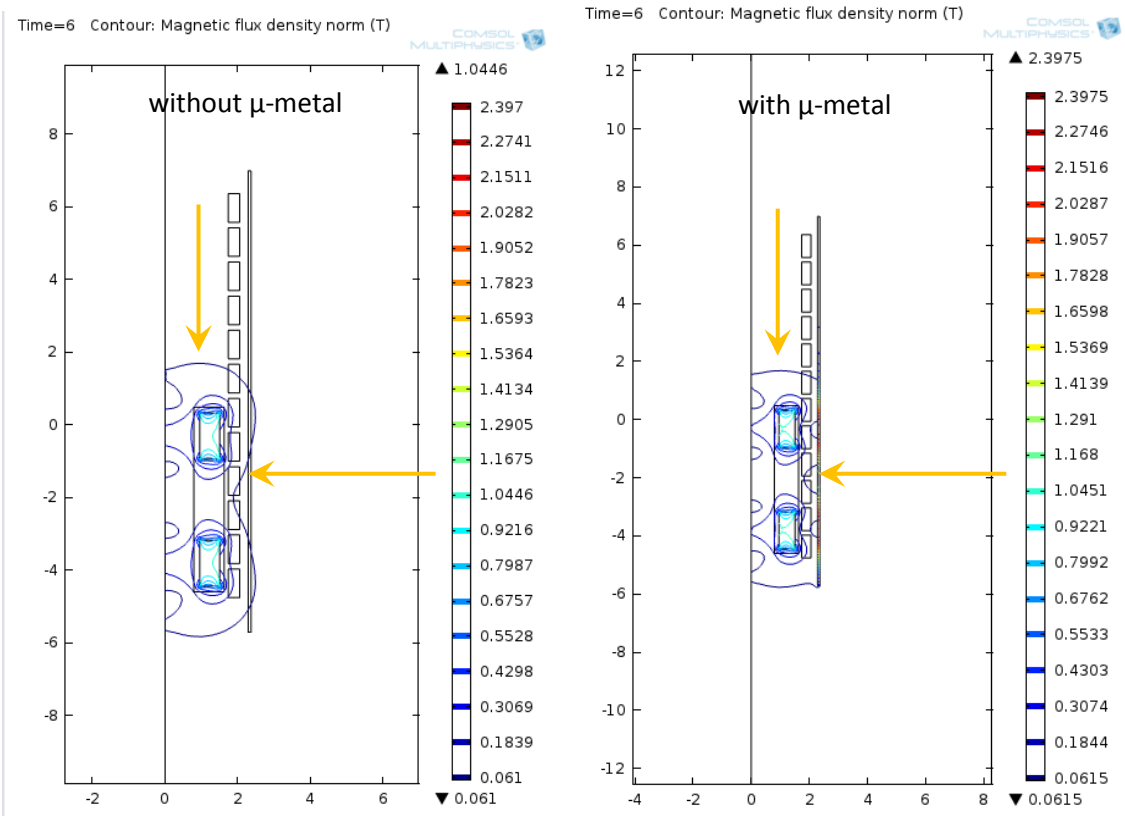

Figure 53: μ-metal causes the magnetic flux density to be flattened into the radial direction (note arrows)

The μ-metal's ability to increase the magnetic force felt by the shuttle should allow a lower level of current to produce the minimum force required to accelerate the shuttle against the retarding fluid forces. Being able to operate at a lower current is very desirable because the windings will produce less heat.

CHAPTER 5: Hemolysis Testing

Bench-top and numerical simulations have been performed to verify the pressure-flow relationship for the LAPP, but assessing its impact on cells requires using biological products. *In vitro* studies using whole blood, typically of bovine origin, and *in vivo* studies, typically using Corriente cross calves, are the most common ways to estimate hematological effects of vascular devices before human trials. Some researchers use ovine, porcine, and canine animal models, however, the Texas Heart Institute's Cardiovascular Research Labs prefer bovine models.

In order to be an effective ventricular assist device, the LAPP must harmonize with the body: it must provide adequate flow at physiological pressure levels and not damage the cells which it contacts. The LAPP can disrupt a patient's anatomy and physiology in three main ways: by causing an immune response, by displacing organs, and by damaging blood cells. Immune response is reducible by making all body-contacting surfaces from bio- and hemo-compatible materials and ensuring the surface finishes are appropriate. For example, the inner surface of the LAPP could be made of highly polished titanium, a material that is accepted by the body and a finish that will discourage cells from attaching and causing fouling of the tube. By carefully selecting an implantation orientation and anastomosis locations, disturbance of neighboring organs can be minimized. One possibility for implantation is to place the LAPP axis parallel to and above the diaphragm; the inlet would be connected to the apex of the left ventricle, while the outlet would be sewn to the ascending aorta.

A common way to quantify assess the damage done to blood cells is to perform a hemolysis test, which quantifies the amount of cells that have been ruptured by measuring the extracellular concentration of hemoglobin; hemoglobin is an iron-based oxygen carrying molecule that should only be found inside red blood cells, so its presence in blood plasma indicates that the cell membranes have been compromised. Severe levels of hemolysis can lead

to hemolytic anemia and renal failure accompanied by dizziness, shortness of breath, and coldness in the extremities. In ventricular assist devices, the most common cause of hemolysis is high levels of shear stress.

To measure hemolysis in the LAPP, the hemolysis testing loop (described in Chapter 2) was used. Tests were run for six hours with one to three samples drawn at the start of the test and again at the top of each hour. One milliliter is drawn and wasted to remove any stagnant (non-circulating) blood from the sample port before the 14 *mL* samples are drawn for analysis. Ideally, three samples would be drawn at each time point, but this depletes the circuit volume too much, causing the inlet compliance chamber to pinch closed; the standard does not allow fresh blood to be added to the flow loop once testing has begun. Hematocrit and free plasma hemoglobin values are obtained for each sample. Using these numbers a dimensionless Modified Index of Hemolysis (MIH) can be calculated as

$$MIH = (\Delta freeHB)\forall\left(\frac{100-HT}{100}\right)\left(\frac{10^6}{QtHB}\right), \qquad \text{Eq. 1}$$

where *ΔfreeHB* is the change in free hemoglobin concentration relative to the baseline level in *mg/dL*, $\forall$ is the circuit volume in liters, *HT* is the hematocrit measured in percent, *Q* is the flow rate in *L/min*, *t* is the sample time in minutes, and *HB* is the total blood hemoglobin concentration at time zero in *mg/dL*. The MIH is a measure of the mass of hemoglobin released into the blood plasma normalized by the total amount of hemoglobin being pumped through the flow loop. For LVAD applications, an "acceptable" MIH value is less than twenty with lower values being better.

Three hemolysis tests were performed with the LAPP (one using the mechanically actuated device and two using the electrically actuated version) and one was performed with a "gold-standard" control—the HeartMate Internal Pneumatic (IP). The Thoratec (formerly Thermo Cardiosystems, Inc.) HeartMate IP was used successfully in patients for short-term support roughly twenty years ago. As discussed in Chapter 1, this LVAD was quite large and

early models required the patient to pull along a small cart with the pneumatic driver and control unit, but the pumping mechanism was very gentle and well tolerated. Surprisingly, few hemolysis studies were performed with the HeartMate IP (or any other pulsatile LVADs), but its record of performance in patients make it an ideal choice for direct comparison to the LAPP. Data from the hemolysis tests is presented in the Appendix.

Before the electronic LAPP was ready for testing, the mechanically actuated version was used to see whether the LAPP pumping concept would be gentle on blood cells. There was concern that the high shear in the gap between the shuttle and inner surface of the titanium would cause high levels of hemolysis. The test loop and results for this first hemolysis test are shown in Figure 54 below. The external magnets were moved in a sine wave with an amplitude of ~6.67 *cm* (2.6 *inches*) at a rate of 95 beats per minute.

The blood for the test arrived at the Texas Heart Institute with a high degree of hemolysis, indicating it may have been stressed during shipping or been drawn from the animal improperly. Thus the hemolysis study had a questionable beginning. Additional factors leading to the high hemolysis values obtained during the test were also identified. The shuttle may have been a bit too large for the titanium tubing, and the actuator, LAPP, and magnets may not have been precisely aligned leading to the shuttle being dragged along the inside of the titanium. There was also a “squeeze” point at the ends of the compliance chambers where the silicone and PVC framework overlapped (see Figure 55). When the volume of the compliance chamber decreased each beat, blood remained trapped in this region and may be been damaged.

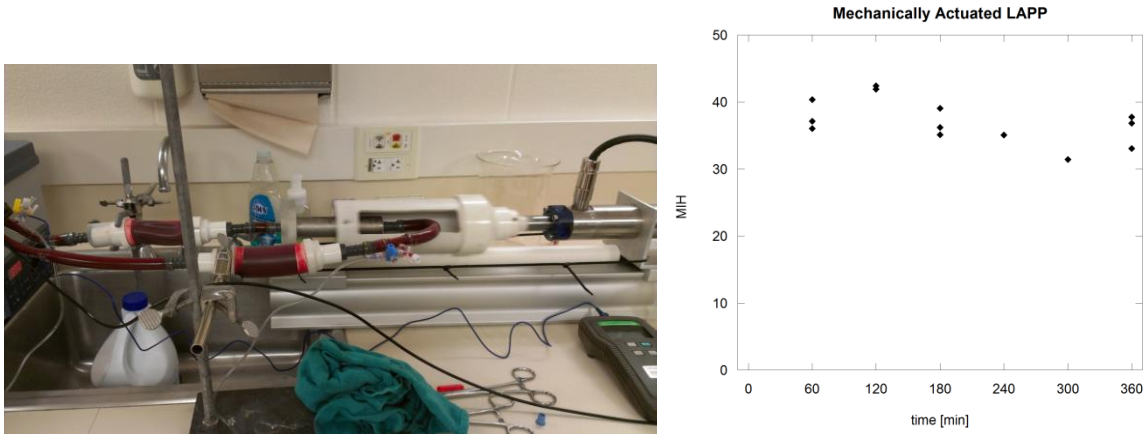

Figure 54: Flowloop and MIH data for the mechanically actuated LAPP

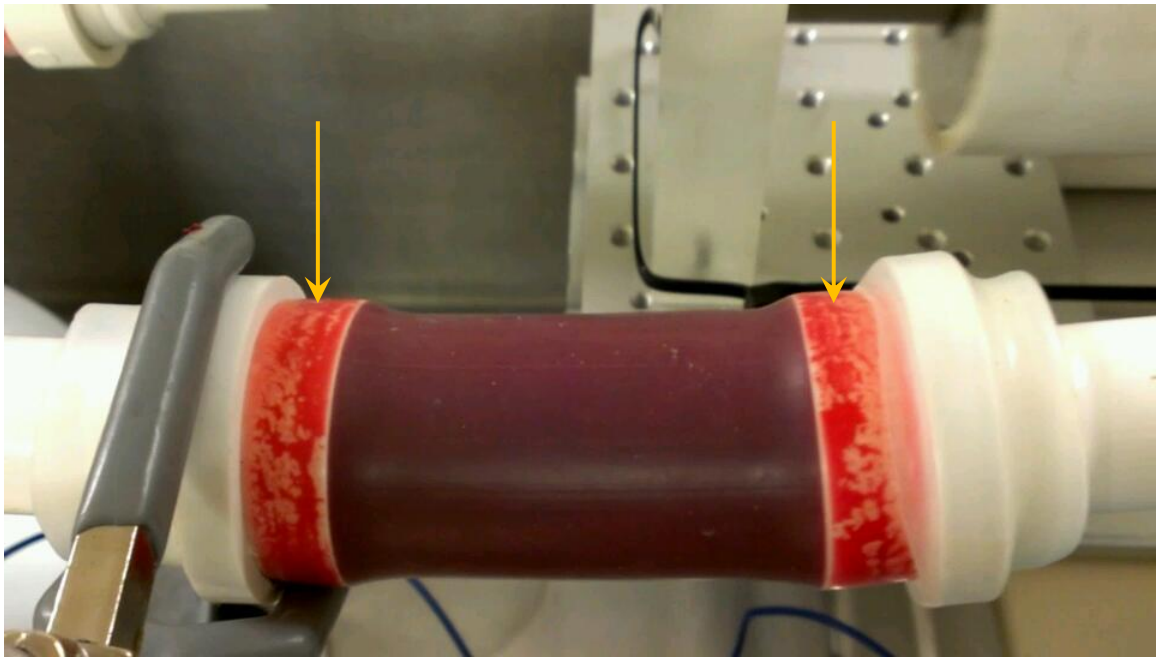

Figure 55: Blood is cyclically squeezed between the silicone tubing and the PVC framework

The results from the first test were encouraging and several areas for improvement were noted. In order to verify that the Hemolysis Testing Loop itself was not contributing significantly to the blood damage, a control study was run using the aforementioned HeartMate-IP after reworking the compliance chambers to reduce the squeeze area.

Because the HeartMate-IP draws air from the room to move the diaphragm and pump, heat is lost from the blood across the membrane surface. The water bath temperature was raised

and an electric air blanket was placed over the loop during the test. Even with these measures, the blood temperature failed to rise above 35 $^{\circ}C$. The data obtained, however, was within the acceptable limits. The loop and MIH data for the HeartMate-IP study are shown in Figure 56. The HeartMate control unit was set to 65 beats per minute, and ejection varied from 70 to 75 mL per beat.

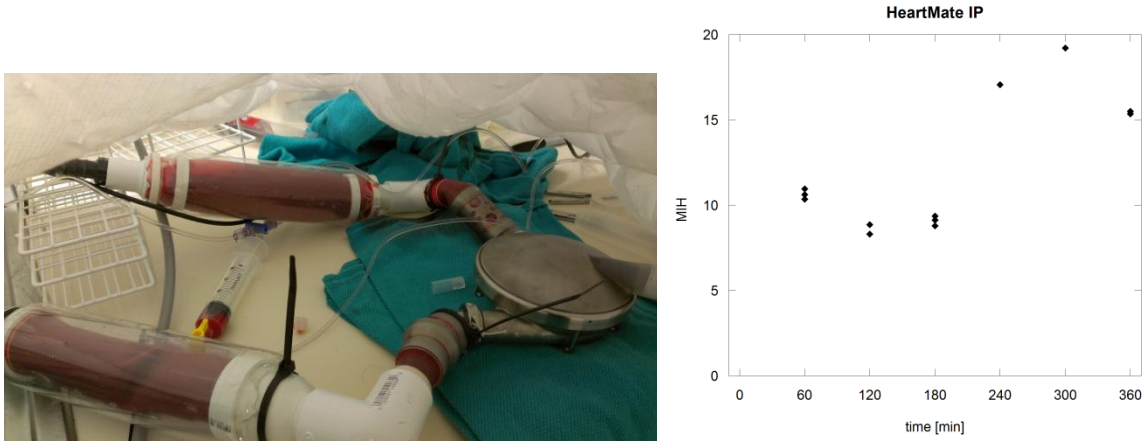

Figure 56: Flowloop and MIH data for the HeartMate-IP

The low level of hemolysis observed in the HeartMate-IP test indicated that the flow loop and experimental procedures were adequately gentle on the test blood. One possible source for hemolysis unique to the HeartMate-IP involves its inlet and outlet valves. An inflow and outflow conduit—each containing a bioprosthetic trileaflet valve (porcine origin)—must be mounted to the HeartMate-IP body containing the diaphragm. These inflow and outflow pieces are stored in a glutaraldehyde solution to prevent the tissue valves from decomposing. When these pumps were implanted in patients, the conduits were soaked and rinsed at least three times in sterile saline to thoroughly wash the fixation solution from the Dacron® graft material. In the hemolysis study, this procedure was a bit less effective. Dacron® will weep fluid, which is undesirable during a bench-top blood study. To keep the blood contained, silicone tubing was stretched tightly over the titanium cages of the conduits. This tubing, however, reduced the effectiveness

of the wash steps—diffusion was responsible for diluting the solution between the outside of the Dacron® and inside of the silicone tubing. It is possible that some glutaraldehyde remained and damaged the blood. The hemolysis levels were so low ($MIH_{HM\text{-}IP}$=12.2±7.44) that this seems to have been a small effect, but it is a point to improve upon in future studies.

Once the HeartMate study showed the loop was suited to hemolysis testing, it was time to perform another study with the LAPP. By this point a two-magnet shuttle had been constructed, and the electronic LAPP was deemed to be strong enough to pump at the desired rate. A PVC housing was built to allow forced air cooling driven by a small DC fan. The level of cooling provided by the fan was insufficient, however, to keep the blood temperature below 37 ˚*C*. The water bath temperature was reduced by regular additions of ice, but still the blood temperature reached 42 ˚*C*. This temperature is not only potentially damaging to the blood in itself, but it causes the Delrin™ shuttle to expand, narrowing the gap, and damaging the blood by increasing the shear and decreasing the clearance. A photograph of this hemolysis loop and data is shown in Figure 57. Clear plastic supports were slipped over the compliance chambers to help keep the soft tubing from twisting and collapsing during the test.

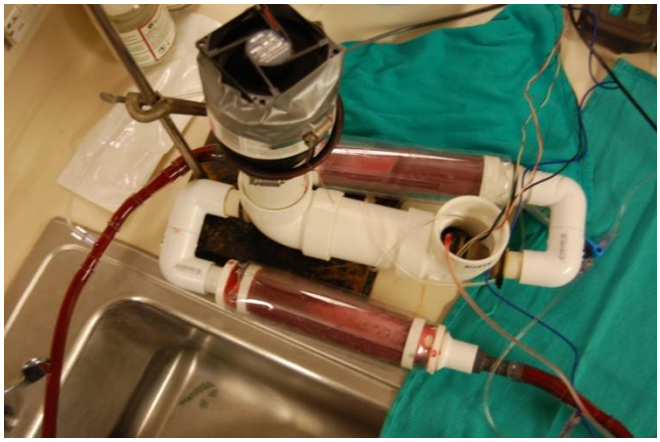

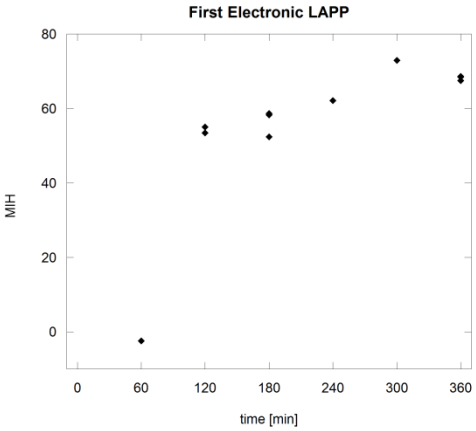

Figure 57: Flow loop and MIH data for the first electrically actuated LAPP

Oddly, the samples processed from the sixty minute time point exhibited a free plasma hemoglobin concentration below the baseline level (resulting in a negative MIH). It is believed that some saline from the pre-test wash remained in the sample port and diluted the blood. The dramatically higher MIH values for the fan-cooled LAPP relative to the mechanically actuated LAPP lead one to conclude that the increased temperature was to blame for the increased hemolysis, though whether it was a direct effect of the high temperature or a secondary effect (shrinking the gap) cannot be stated positively. Thus in the next test, both the LAPP cooling and the initial gap height were increased. Though in most experiments one variable is changed at a time to show causation, the time and expense involved in the hemolysis testing made it more prudent to make any potential improvements that could be identified.

A final hemolysis test was conducted using the electronic LAPP with forced air cooling provided by a vacuum cleaner (Stinger 2.5 Gallon Wet/Dry Vac, WD2025; Emerson Tool Company, St. Loius, MO). Figure 58 shows the flow loop nestled in the sink and the MIH data. This time the temperature stayed between 34 and 38 $^{\circ}C$ during all but the first hour of the test when the blood was coming up to temperature. Unfortunately, the LAPP was unable to pump the requested 2.6 *inch* stroke at 90 beats per minute; the actual flowrate was ~2.76 *L/min*. It was discovered after the test that the controller current was set to 1 *Amp*, instead of 1.5 *Amp*. This reduces both the pumping force and the heat generation.

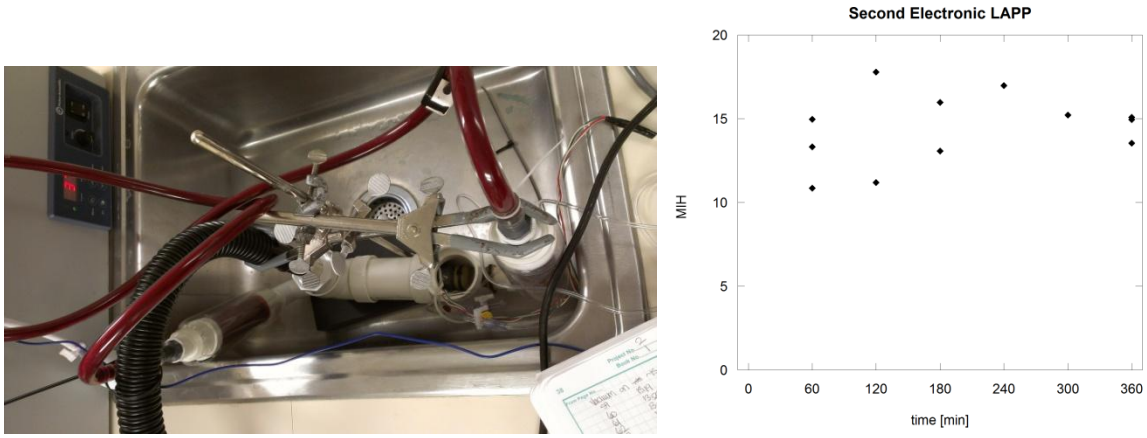

Figure 58: Flow loop and MIH data for the second electrically actuated LAPP

The hemolysis levels were very close to those for the HeartMate-IP (MIH_{HM-IP}=12.2±7.44; MIH_{LAPP2}=14.4±4.21). The MIH formula does account for the reduced flowrate, but it is unclear if the formula is applicable outside the range of flowrates requested by the ASTM standard. The results are, however, very encouraging. They indicate that the LAPP, after modifications, performed at a level only slightly worse than the HeartMate-IP, which itself is a proven pulsatile pump with low levels of hemolysis. Plans are being made to repeat both the HeartMate-IP and air cooled LAPP experiments to verify the MIH data.

CHAPTER 6: Future Work and Conclusions

Though it is not yet ready for animal testing, the basic concept of the LAPP as an assist device seems sound. Several additional studies based on the models described above can be performed, ranging from characterizing the existing LAPP to trying out new designs

Linearly Actuated Pulsatile Pump

In order to be used for ventricular assist, the LAPP efficiency must be improved. At the present stage of development, the heat generation in the windings is still too great. One obvious strategy is to use a commutator and switch windings off when they are not being used. With the two magnet shuttle and present winding geometry, this would allow four windings to be fully switched off at a time, giving about a thirty percent reduction in heating.

Also, the addition of a μ-metal shield might allow the driving current level to be reduced, thereby reducing the heat generated. If the optimal shield thickness and radius were found in COMSOL, it would be of interest to construct such a shield around the prototype LAPP. Adjusting the direction of the magnetic field lines in the simulation was shown to increase the axial force on the shuttle. Thus with the shield present, a lower current should be able to generate the same minimum force needed to move the shuttle. Because the heat generation depends upon the square of the current, even a small reduction in amperage could bring the system temperature down appreciably.

More long-term, after the heating issue is resolved, the LAPP's controller and power supply can be miniaturized and packaged for maximal patient comfort. Ultimately, an interface based on pacemaker technology could be integrated into the LAPP control system to have the LAPP ejection volume and rate adjust to signals sent from the brain. Additionally, the LAPP materials must be checked for long-term wear and hemocompatibility. The LAPP is being designed to replace previous models of pulsatile pumps that tended to fail within eighteen

months, so it is important to show the LAPP has better durability and can compete with continuous flow devices for reliability.

Mock Circulatory Loop

The Mock Circulatory Loop was employed to make early assessments of the LAPP and to have a standard to compare and calibrate the numerical models. However, its real purpose has not yet been fulfilled. As alluded to in the Model Verification (Chapter 3), this loop will be used to study the phasing between the LAPP and native heart, as well as measure dye washout times.

The question of optimal phasing is important because when the LAPP is operating as an assist device, it should increase blood flow to the body without increasing the workload of the heart. For instance, if the LAPP is ejecting at the same time as the heart, the aortic pressure will be increased; the heart would then be working against an even higher pressure than it would normally and could cause further damage to the cardiac tissue. If the LAPP filled while the heart ejected, the volume to be ejected by the ventricle would be reduced, so the ventricular walls would be less stretched, have lower tension, and may be able to repair themselves. Such a mode of operation is referred to as counter pulsation. It is possible that there is a point between perfect co-pulsation and counter-pulsation that is more favorable to the pressure-flow relationship. A parametric study measuring the ventricular and aortic pressures and the instantaneous aortic flowrate at different phase angles would help select this optimal operating point.

Dye washout can be interesting to ensure that there are no stagnant regions within the ventricle or at the aortic valve. If blood remains stationary, it will begin to clot. In some patients with continuous flow pumps, clots have been found behind the aortic valve. This valve is made up of three triangular cups, called cusps. Two of these feed the coronary arteries, but the third has no outlet; a photograph of an aortic root casting (crafted by Jesse Rios) is shown below (Figure 59). When a continuous flow pump dominates the native heart, the aortic pressure can be such that the ventricle is unable to open the aortic valve. Some patients in this flow regime develop clots in the non-coronary cusp that can break loose and lead to strokes. A dye washout

study, where dye in introduced into a region and its residence time is measured, can assess fluid dwell time and determine if such a problem may exist for the LAPP. The pulsatile nature of the LAPP makes this scenario unlikely, but it is important to verify.

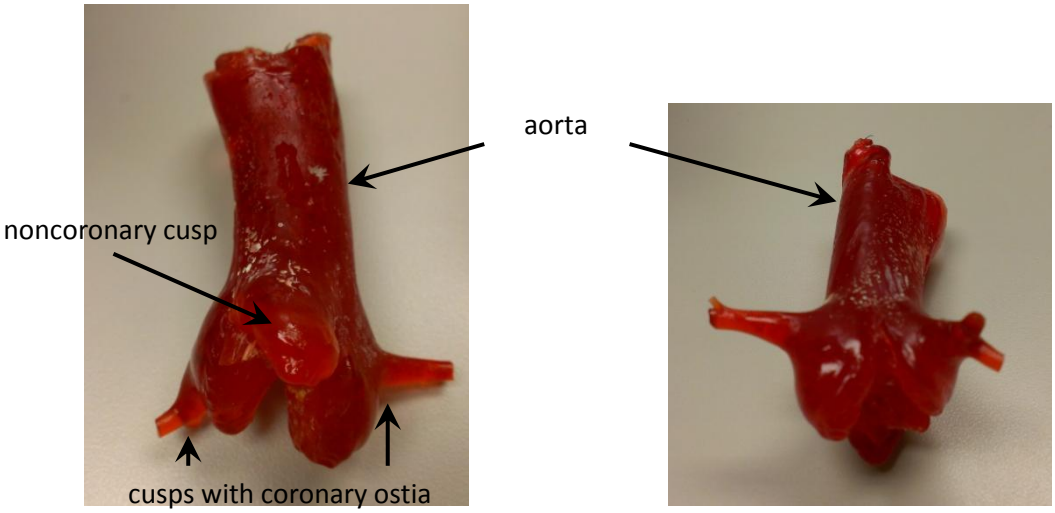

Figure 59: Two views of a cast of the aortic root showing the cusps and coronary arteries

Hemolysis Testing Loop

At least two additional hemolysis tests are planned. One to verify the final LAPP test and one to verify the HeartMate-IP test. If possible the LAPP will be run with a 2.6 *inch* stroke at 95 beats per minutes. This should get the flowrate up to match that of the HeartMate-IP and thus eliminate the major difference between the two tests. It is important to be able to compare the hemolysis results for two systems operating as nearly as possible under the same conditions. As mentioned in the Hemolysis Testing chapter, the derivation of the MIH formula was not disclosed, so there is some concern that conducting the test at a flowrate outside the recommended range may not be comparable to tests run with the requested value.

FLEUNT Model

Future studies in the FLUENT model will replace the stagnant air with other conditions to compare the heat transfer. First, a velocity can be imparted to the air to simulate the forced air

cooling used in the hemolysis studies. This should reduce the final temperature of the system, but it will be interesting to see how much. Further, the air can be replaced with a material whose properties approximate the body's internal environment. This would give an estimate for the temperature distribution that may occur inside a patient. Establishing the correct material properties (heat capacity, thermal conductivity) will not be easy, however.

COMSOL Model

The COMSOL model can be used to test out new LAPP designs. Specifically, it would be interesting to see how the electromagnetic forces change if the LAPP diameter is increased. Other parameters to change include the size and aspect ratio of the coils and the number and shape of the magnets. The placement and thickness of μ-metal shields can be optimized to generate the maximum increase in force. Radically new ideas can be tested, too, like solid magnet shuttles or annular shuttles with a internal and external coaxial of windings. Before these extensions are performed, however, the cause of the coil and shuttle force instability must be found and eliminated.

Conclusion

Overall, the LAPP presents itself as a unique tool for studying the effects of pulsatility and has potential for use clinically in heart failure treatment. The numerical models and bench-top flow loops described in the preceding document can be used refine the LAPP design. These models, though simple, have been shown to capture the behavior of the LAPP remarkably well. Further development of the Linearly Actuated Pulsatile Pump may one day give ailing patients a second chance at comfort and a normal lifestyle.

REFERENCES

Battegay E, Bakris GL, and Lip GYH. *Hypertension: Principles and Practice*. London: Informa HealthCare. 79-81. 2005.

Baughman KL and Jarcho JA. "Bridge to Life — Cardiac Mechanical Support." *New England Journal of Medicine*, 357:9 (Aug) 846-849. 2007.

Birks EJ. "The Comparative Use of Ventricular Assist Devices: Differences between Europe and the United States." *Texas Heart Institute Journal*. 37(5): 565–567. 2010.

Bozkurt B and Mann DL. "The Treatment of Heart Failure in the 21st Century: is the Glass Half Empty or Half Full?" *Methodist Debakey Cardiovascular Journal*. 9(1):3-5. January 2013.

Go AS, Mozaffarian D, Roger VL, Benjamin EJ, Berry JD, Borden WB, Bravata DM, Dai S, Ford ES, Fox CS, Franco S, Fullerton HJ, Gillespie C, Hailpern SM, Heit JA, Howard VJ, Huffman MD, Kissela BM, Kittner SJ, Lackland DT, Lichtman JH, Lisabeth LD, Magid D, Marcus GM, Marelli A, Matchar DB, McGuire DK, Mohler ER, Moy CS, Mussolino ME, Nichol G, Paynter NP, Schreiner PJ, Sorlie PD, Stein J, Turan TN, Virani SS, Wong ND, Woo D, and Turner MB. "Executive Summary: Heart Disease and Stroke Statistics--2013 Update: a Report from the American Heart Association." *Circulation*. 127(1):143-152. 1 January 2013.

Guyton AC and Hall JE. *Textbook of Medical Physiology*. Eleventh Edition. Philadelphia, PA: Elsevier Saunders. 107. 2006.

Helman DN and Rose EA. "History of Mechanical Circulatory Support." *Progress in Cardiovascular Disease*, 43:1 (Jul/Aug) 1-4. 2000.

Hunt SA, Baker DW, Chin MH, Cinquegrani MP, Feldman AM, Francis GS, Ganiats TG, Goldstein S, Gregoratos G, Jessup ML, Noble RJ, Packer M, Silver MA, Stevenson LW, Gibbons RJ, Antman EM, Alpert JS, Faxon DP, Fuster V, Jacobs AK, Hiratzka LF,

Russell RO, and Smith SC Jr. "ACC/AHA Guidelines for the Evaluation and Management of Chronic Heart Failure in the Adult: Executive Summary. A Report of the American College of Cardiology/American Heart Association Task Force on Practice Guidelines (Committee to revise the 1995 Guidelines for the Evaluation and Management of Heart Failure)." *Journal of the American College of Cardiology*. 38(7):2101-13. December 2001.

Li JKJ. *The Arterial Circulation: Physical Principles and Clinical Applications.* New York, NY: Humana Press. 36-37; 208. 2000.

Nichols WW and O'Rourke MF. *McDonald's Blood Flow in Arteries: Theoretical, Experimental, and Clinical Principles.* Fifth Edition. New York, NY: Oxford University Press. 29-30. 2005.

Renlund DG and Kfoury AG. "When the Failing, End-Stage Heart Is Not End-Stage." *New England Journal of Medicine*, 355:18 (Nov) 1922-1925. November 2006.

Rizzieri AG, Verheijde JL, Rady MY, and McGregor JL. "Ethical Challenges with the Left Ventricular Assist Device as a Destination Therapy." *Philosophy, Ethics, and Humanities in Medicine.* 3:20. 11 August 2008.

Taylor DO, Stehlik J, Edwards LB, Aurora P, Christie JD, Dobbels F, Kirk R, Kucheryavaya AY, Rahmel AO, and Hertz MI. "Registry of the International Society for Heart and Lung Transplantation: Twenty-sixth Official Adult Heart Transplant Report—2009." *The Journal of Heart and Lung Transplantation*. 28(10): 1007–1022. October 2009.

Wampler RK, Moise JC, Frazier OH, and Olsen DB. "*In vivo* Evaluation of a Peripheral Vascular Access Axial Flow Blood Pump." *ASAIO Transactions*. 34(3):450-4. July-September 1988.

APPENDIX

Below are the data collected during the hemolysis tests. The formula for calculating MIH is given in Chapter 5. In the data, the total blood hemoglobin is calculated (rather than measured) by taking an average of the hematocrit for all times points in a given experiment and dividing that average by 3. The average starting plasma free hemoglobin is computed from the baseline plasma free hemoglobin values. "Static" refers to the static control bag, a bag of blood which is kept in the water bath (but not circulated) for the duration of the test; the "pre" and "post" designation indicates whether the sample was drawn the minute before of after the test, respectively. The "baseline" samples were taken after the blood circulated for five minutes. Plasma free hemoglobin, "pfHb," with units of *mg/dL* was obtained from analysts at Equine Laboratories (7575 North Sam Houston Parkway West, Houston, Texas 77064). Hematocrit ("Ht") was measured by spin crit at the Texas Heart Institute animal lab. The change in plasma free hemoglobin ("ΔpfHb") is measured relative to the average starting value (computed from the baseline). Lastly, the MIH is calculated from the formula given in Chapter 5:

$$MIH = (\Delta freeHB)\forall\left(\frac{100-HT}{100}\right)\left(\frac{10^6}{QtHB}\right),$$

where *ΔfreeHB* is the change in free hemoglobin concentration relative to the baseline level in *mg/dL*, $\forall$ is the circuit volume in liters, *HT* is the hematocrit measured in percent, *Q* is the flow rate in *L/min*, *t* is the sample time in minutes, and *HB* is the total blood hemoglobin concentration at time zero in *mg/dL*. The MIH is a measure of the mass of hemoglobin released into the blood plasma normalized by the total amount of hemoglobin being pumped through the flow loop. For LVAD applications, an "acceptable" MIH value is less than twenty with lower values being better.

Mechanically Actuated LAPP (1 November 2012)

circuit volume (approx)	1.1886	L
flow rate	4.75	L/min
total blood hemoglobin ((avg Ht)/3)	10.42857	g/dL
average starting pfHb	49.767	

	pfHb (mg/dL)	pfHb (g/dL)	Ht (%)	t (min)	ΔpfHb	MIH
static pre	36.856	0.036856	32	0	-0.012911	
static pre	36.026	0.036026	32	0	-0.013741	
static pre	36.899	0.036899	32	0	-0.012868	
baseline	49.738	0.049738	32	5	-2.9E-05	
baseline	49.345	0.049345	32	5	-0.000422	
baseline	50.218	0.050218	32	5	0.000451	
60 min	196.075	0.196075	31	60	0.146308	40.37227
60 min	184.311	0.184311	31	60	0.134544	37.12611
60 min	180.389	0.180389	31	60	0.130622	36.04387
120 min	352.935	0.352935	30	120	0.303168	42.43434
120 min	349.041	0.349041	30	120	0.299274	41.8893
180 min	443.129	0.443129	31	180	0.393362	36.18148
180 min	474.502	0.474502	31	180	0.424735	39.06717
180 min	431.365	0.431365	31	180	0.381598	35.09942
240 min	558.225	0.558225	31	240	0.508458	35.07601
300 min	619.597	0.619597	31	300	0.56983	31.44781
360 min	768.614	0.768614	31	360	0.718847	33.05981
360 min	850.966	0.850966	31	360	0.801199	36.84718
360 min	870.573	0.870573	31	360	0.820806	37.74891
static post	36.637	0.036637	32	360	-0.01313	-0.5951
static post	41.485	0.041485	32	360	-0.008282	-0.37537

average MIH	37.10721
2σ	6.449376

HeartMate-IP (31 January 2013)

circuit volume (approx)	1.37865	L
flow rate	4.7125	L/min
total blood hemoglobin ((avg Ht)/3)	10.52381	g/dL
average starting pfHb	9.600667	

	pfHb (mg/dL)	pfHb (g/dL)	Ht (%)	t (min)	ΔpfHb	MIH
static pre	9.671	0.009671	32	0	7.03333E-05	
static pre	7.806	0.007806	32	0	-0.00179467	
static pre	7.184	0.007184	32	0	-0.00241667	
baseline	9.963	0.009963	32	5	0.000362333	
baseline	9.963	0.009963	32	5	0.000362333	
baseline	8.876	0.008876	32	5	-0.00072467	
60 min	44.384	0.044384	32	60	0.034783333	10.95869
60 min	42.45	0.04245	32	60	0.032849333	10.34937
60 min	43.327	0.043327	32	60	0.033726333	10.62567
120 min	62.31	0.06231	32	120	0.052709333	8.303188
120 min	65.875	0.065875	32	120	0.056274333	8.864775
180 min	97.54	0.09754	31	180	0.087939333	9.371076
180 min	95.33	0.09533	31	180	0.085729333	9.135571
180 min	92.152	0.092152	31	180	0.082551333	8.796914
240 min	220.128	0.220128	30	240	0.210527333	17.06966
300 min	310.04	0.31004	31	300	0.300439333	19.20942
360 min	297.638	0.297638	31	360	0.288037333	15.34706
360 min	300.738	0.300738	31	360	0.291137333	15.51223
360 min	297.638	0.297638	31	360	0.288037333	15.34706
static post	21.392	0.021392	32	360	0.011791333	0.619154
static post	10.222	0.010222	32	360	0.000621333	0.032626

average MIH	12.22236
2σ	7.446375

First Electronic LAPP (1 February 2013)

circuit volume (approx)	1.1886	L
flow rate	4.75	L/min
total blood hemoglobin ((avg Ht)/3)	10.5873	g/dL
average starting pfHb	29.14333	

	pfHb (mg/dL)	pfHb (g/dL)	Ht (%)	t (min)	ΔpfHb	MIH
static pre	33.096	0.033096	32	0	0.003953	
static pre	39.452	0.039452	32	0	0.010309	
static pre	31.624	0.031624	32	0	0.002481	
baseline	30.073	0.030073	32	5	0.00093	
baseline	30.073	0.030073	32	5	0.00093	
baseline	27.284	0.027284	32	5	-0.00186	
60 min	19.843	0.019843	33	60	-0.0093	-2.45459
60 min	19.998	0.019998	33	60	-0.00915	-2.41368
60 min	19.998	0.019998	33	60	-0.00915	-2.41368
120 min	446.458	0.446458	33	120	0.417315	55.06987
120 min	434.056	0.434056	33	120	0.404913	53.43327
180 min	696.04	0.69604	33	180	0.666897	58.67021
180 min	624.731	0.624731	33	180	0.595588	52.39681
180 min	691.389	0.691389	33	180	0.662246	58.26104
240 min	930.12	0.93012	30	240	0.900977	62.10938
300 min	1351.775	1.351775	30	300	1.322632	72.94114
360 min	1500.594	1.500594	29	360	1.471451	68.58962
360 min	1477.341	1.477341	29	360	1.448198	67.50571
360 min	1497.493	1.497493	29	360	1.46835	68.44507
static post	32.244	0.032244	32	360	0.003101	0.138426
static post	36.894	0.036894	32	360	0.007751	0.346021

average MIH (without 60min)	61.74221
2σ (without 60 min)	14.49958

Second Electronic LAPP (6 March 2013)

circuit volume (approx)	1.30095	L
flow rate	2.76	L/min
total blood hemoglobin ((avg Ht)/3)	10.58333	g/dL
average starting pfHb	7.906333	

	pfHb (mg/dL)	pfHb (g/dL)	Ht (%)	t (min)	ΔpfHb	MIH
static pre	9.593	0.009593	32	0	0.001686667	
static pre	9.078	0.009078	32	0	0.001171667	
static pre	9.864	0.009864	32	0	0.001957667	
baseline	8.298	0.008298	32	5	0.000391667	
baseline	7.972	0.007972	32	5	6.56667E-05	
baseline	7.449	0.007449	32	5	-0.00045733	
60 min	29.403	0.029403	32	60	0.021496667	10.8507
60 min	34.304	0.034304	32	60	0.026397667	13.32454
60 min	37.571	0.037571	32	60	0.029664667	14.9736
120 min	52.272	0.052272	32	120	0.044365667	11.19705
120 min	78.408	0.078408	32	120	0.070501667	17.79328
180 min	85.579	0.085579	32	180	0.077672667	13.06874
180 min	102.91	0.10291	32	180	0.095003667	15.98475
240 min	140.481	0.140481	31	240	0.132574667	16.97569
300 min	156.45	0.15645	31	300	0.148543667	15.21637
360 min	182.952	0.182952	31	360	0.175045667	14.94263
360 min	184.6586	0.1846586	31	360	0.176752267	15.08831
360 min	166.617	0.166617	31	360	0.158710667	13.5482
static post	10.716	0.010716	32	360	0.002809667	0.236369
static post	11.565	0.011565	32	360	0.003658667	0.307793

average MIH	14.41366
2σ	4.21824